Nutrient-sensitizing drug repurposing screen identifies lomerizine as a mitochondrial metabolism inhibitor of chronic myeloid leukemia

Authors: Ahmed Khalaf[1], Lucie de Beauchamp[1], Eric Kalkman[1], Kevin Rattigan[1], Ekaterini Himonas[1], Joe Jones[1], Daniel James[2], Engy Shokry Abd Shokry[2], Mary T. Scott[1], Karen Dunn[3], Saverio Tardito[1,2], Mhairi Copland[3], David Sumpton[2], Emma Shanks[2], G. Vignir Helgason[1]*

Affiliations:

[1]Wolfson Wohl Cancer Research Centre, School of Cancer Sciences, University of Glasgow, Glasgow, G61 1QH, UK.

[2]Cancer Research UK Scotland Institute, Glasgow, G61 1BD, UK.

[3]Paul O'Gorman Leukaemia Research Centre, School of Cancer Sciences, University of Glasgow, Glasgow, G12 0ZD, UK.

*Corresponding author: E-mail: Vignir.Helgason@glasgow.ac.uk

One Sentence Summary:

Lomerizine inhibits Ca^{2+} uptake, mitochondrial metabolism and eradicates leukemic stem cells when combined with tyrosine kinase inhibitors.

Abstract:

In chronic myeloid leukemia (CML), the persistence of leukemic stem cells (LSCs) following treatment with tyrosine kinase inhibitors (TKIs) such as imatinib, can lead to disease relapse. It is known that therapy-resistant LSCs rely on oxidative phosphorylation (OXPHOS) for their survival and that targeting mitochondrial respiration sensitizes CML LSCs to imatinib treatment. However, current OXPHOS inhibitors have demonstrated limited efficacy or have shown adverse effects in clinical trials, highlighting that identification of clinically safe oxidative pathway inhibitors is warranted. We performed a high-throughput drug repurposing screen, designed to identify mitochondrial metabolism inhibitors in myeloid leukemia cells. This identified lomerizine, an FDA approved voltage-gated Ca^{2+} channel blocker currently used for the treatment of migraines, as one of the top hits. Transcriptome analysis revealed increased expression of voltage-gated *CACNA1D* and receptor-activated *TRPC6* Ca^{2+} channels in CML LSCs ($CD34^{+}CD38^{-}$) compared to normal counterparts. This correlated with increased endoplasmic reticulum (ER) mass, and increased ER and mitochondrial Ca^{2+} content in CML stem/progenitor cells. We demonstrate that lomerizine mediated inhibition of Ca^{2+} uptake leads to ER and mitochondrial Ca^{2+} depletion, with similar effects seen following *CACNA1D* and *TRPC6* knockdown. Through stable isotope-assisted metabolomics and functional assays, we observe that lomerizine treatment inhibits mitochondrial isocitrate dehydrogenase activity, mitochondrial oxidative metabolism, and selectively sensitizes CML LSCs to imatinib treatment. In addition, combination treatment with imatinib and lomerizine reduced CML tumor burden, targeted CML LSCs and extends survival in xenotransplantation model of human CML, suggesting this as a potential therapeutic strategy to prevent disease relapse in patients.

INTRODUCTION

Chronic myeloid leukemia CML is a myeloproliferative malignancy, which arises following the chromosomal t(9;22) (q34;q11) translocation in a single hematopoietic stem cell (HSC). The Philadelphia chromosome carries the fusion BCR::ABL1 oncogene that encodes for a constitutively active tyrosine kinase which drives malignant transformation. Tyrosine kinase inhibitors (TKIs) such as imatinib have revolutionized the management of CML in the clinic, with 10-year survival from diagnosis achieved by over 80% of patients (*1-3*). However, more than half of individuals with CML who attempt treatment-free remission (TFR), experience molecular recurrence within 12 months of stopping treatment, despite showing the sustained deep molecular response (DMR) that qualifies for TKI cessation (*4*). Indeed, only 10% of individuals with CML will successfully achieve and maintain TFR (*5*). Furthermore, around 20-30% of patients with CML encounter drug resistance or progress to the blast phase, where therapeutic options are limited and outcomes are dismal (*5*).

The primary resistance of leukemic stem cells (LSCs) to TKI treatment has been previously reported (*6, 7*). This is also evident by the fact that LSCs are still detectable in every CML patient treated with TKIs, even those who exhibit DMR (*8*). LSCs have been shown to play a similar role in acute myeloid leukemia (AML), also driving therapy resistance or relapse (*9, 10*). Metabolic rewiring has been shown to be critical for CML and AML LSCs, which acquire reliance on mitochondrial oxidative phosphorylation (OXPHOS) (*11, 12*). This may be driven by high tricarboxylic acid (TCA) cycle activity in leukemic cells, which contrasts with primary solid tumors that have lower TCA cycle flux compared with heathy tissues (*13*). Consistently, targeting OXPHOS has been shown to be a promising strategy for the selective elimination of therapy-resistant leukemic cells, including LSCs, in preclinical studies (*11, 12, 14-17*). However, the

drawbacks of currently available OXPHOS inhibitors have reduced their use in preclinical studies and restricted their application in clinical trials (*18-20*). For example, off target effect or dose limiting toxicities of rotenone (*21, 22*), BAY 87-2243 (*20*) and ASP4132 (*23*), poor potency of biguanides (*24-26*) and relatively short half-life (~10 hours) of the protein translation inhibitor tigecycline (*27*) have been of concern. Additionally, treatment with the mitochondrial electron transport chain (ETC) complex I inhibitor IACS-010759, which showed promising results in preclinical studies (*28*) and was subsequently tested in two phase I trials, showed dose-limiting toxicities, including increased serum lactate concentrations (leading to lactate acidosis) and neurotoxicity in most patients, raising safety concerns for potent ETC inhibition in humans (*29*).

Mitochondria play an important role in the response to cellular calcium ion (Ca^{2+}) perturbations. It is known that mitochondria buffer Ca^{2+} content to catalyze TCA cycle dehydrogenase activities (*30*). Moreover, Ca^{2+} overload in the mitochondria leads to oxidative stress-induced apoptosis (*31, 32*). Ligand stimulation of inositol triphosphate receptor (IP3R) results in mitochondrial activation, with mitochondrial Ca^{2+} concentrations spiking to 10-20-fold higher than the cytosolic concentrations (*33, 34*). This activation, which may require sustained release of Ca^{2+} from the endoplasmic reticulum (ER), primarily works through the concurrent activation of the dehydrogenase enzymes pyruvate dehydrogenase (PDH), isocitrate dehydrogenase (IDH) and α-ketoglutarate dehydrogenase (α-KGDH, or oxoglutarate dehydrogenase), and also due to the spatial proximity between the mitochondria and the ER (*35*). Several plasma membrane Ca^{2+} channels can load cellular organelles with Ca^{2+}. Voltage-gated Ca^{2+} channels (VGCCs; CACN) are localized in the plasma membrane and made up of distinct subunits: α1, α2δ, β1-4, and γ. The ion-conducting pore is formed by one of the α1 subunits, such as CACNA1D (*36*). Other plasma

membrane Ca^{2+} channels, such as transient receptor potential channels (TRPCs), are activated by phospholipase C stimulation or when ER Ca^{2+} content is depleted (*37*).

Here, we present findings on the role of Ca^{2+} in mitochondrial metabolism in CML. Through nutrient-sensitized drug repurposing screening, we identified the FDA-approved drug lomerizine as a potential mitochondrial respiration inhibitor. Mechanistically, we subsequently showed that *CACNA1D*, *TRPC6*, and ER gene sets are enriched in $CD34^+CD38^-$ LSCs when compared to normal counterparts. Additionally, ER and mitochondrial Ca^{2+} content was higher in primary $CD34^+$ CML cells ex vivo, when compared to normal $CD34^+$ cells. We demonstrated that lomerizine inhibited CACNA1D and TRPC6 mediated Ca^{2+} influx and depleted ER and mitochondrial Ca^{2+} content in CML cells.

Of clinical relevance, lomerizine reduced proliferation and survival of CML $CD34^+$ CML cells, without affecting $CD34^+$ normal cells, and sensitized imatinib-resistant CML cells to ponatinib and asciminib treatment. Finally, combined imatinib and lomerizine treatment reduced CML tumor burden and targeted LSCs in robust CML xenograft models. Thus, our findings provide a rationale for targeting mitochondrial metabolism in CML through repurposing of lomerizine, highlighting a potential approach for treating individuals with therapy resistance in the clinic.

RESULTS

Drug repurposing screening identifies lomerizine as a potent mitochondrial metabolism inhibitor in CML cells

To identify clinically applicable compounds that target cells dependent on mitochondrial respiration, we used a nutrient-sensitized repurposing screening strategy. Upon replacement of glucose with galactose as the only sugar source in cell culture media, there is a shift in cellular

metabolism towards OXPHOS, as cells are unable to effectively use galactose for glycolysis (*38-40*). Therefore, cells grown in galactose-containing media are more sensitive to inhibition of mitochondrial metabolism than glucose-grown cells. To validate this approach, extracellular acidification rate (ECAR) and oxygen consumption rate (OCR) were quantified as proxies of glycolysis and mitochondrial respiration, respectively. K562 and KCL22 CML cell lines were cultured in glucose or galactose containing media before analysis. As expected, cells cultured in glucose media utilized both glycolysis and mitochondrial respiration, whereas culturing cells in galactose media significantly shifted their metabolism towards OXPHOS, due to an inhibition of glycolysis (Fig. 1A, fig. S1A and S1B). Validating our approach, cells grown in galactose were more sensitive to the mitochondrial complex I inhibitor rotenone compared to glucose cultured cells (Fig. 1B and D). In contrast, treatment with TKIs or the non-metabolic compound omacetaxine was equally potent in glucose or galactose media (Fig. 1C and D).

Subsequently, K562 and KCL22 cells were cultured in glucose or galactose media for 3 days with 1,274 Food and Drug Administration (FDA)-approved compounds. Cell viability was then measured using the resazurin assay, which measures the reduction of non-fluorescent resazurin to a red fluorescent dye by the mitochondrial respiratory chain in live cells (Fig. 1D). Compounds that decreased cell viability significantly more in galactose media compared to glucose media were considered potential mitochondrial metabolism inhibitors. The screen identified several compounds that preferentially decreased the viability of cells grown in galactose media. Those candidate compounds were scored, and top hits were selected for further study (fig. S1C). One of the top hits, lomerizine, is an L-type VGCC inhibitor, currently used in the clinic for migraine treatment (*41-43*). Although variable effects were seen with other calcium channel blockers (fig.

S1D), this suggests that Ca^{2+} homeostasis may be important for mitochondrial metabolism in leukemic cells.

To explore the connection between Ca^{2+} and mitochondrial respiration in CML cells, K562 cells were cultured for 24 hours in media supplemented with an additional 2 mM $CaCl_2$ or low concentration (200 nM) EGTA, a Ca^{2+} chelator. $CaCl_2$ supplementation increased *(P=0.05)* maximal OCR, whereas EGTA treatment reduced *(P=0.01)* maximal OCR (Fig. 1E), indicating that Ca^{2+} content can influence mitochondrial respiration. 3 days of EGTA treatment caused a reduction *(P<0.01)* in cell expansion and modest induction *(P=0.001)* of apoptosis when compared to either control or $CaCl_2$ treated cells, suggesting Ca^{2+} alteration may be an approach for targeting CML cells (Fig. 1F and G).

ER mass and Ca^{2+} signaling is increased in CML LSCs

To explore the potential role for calcium signaling in CML development, we moved to transcriptome analysis. Analysis of human primary CML LSCs ($CD34^+CD38^-$) and their normal counterparts (*44*) demonstrated that voltage-gated Ca^{2+} influx activity, mitochondrial Ca^{2+} homeostasis and ER-related gene signatures were enriched in LSCs (Fig. 2A). Of relevance, it is known that Ca^{2+} within the ER lumen is maintained at concentrations >100 times greater than the cytoplasm, mediated by the sarco/endoplasmic reticulum calcium ATPase (SERCA) pump. ER mass and ER function are also critical for mitochondrial Ca^{2+} homeostasis, as mitochondrial Ca^{2+} uptake requires sustained Ca^{2+} release from the ER (*34*).This could potentially indicate unique ER attributes in CML cells compared to normal cells.

Next, we validated the transcriptome analysis using human $CD34^+$ CML cells, isolated from three individuals with chronic phase CML at diagnosis (table S1). Consistently, primary $CD34^+$ CML cells had significantly higher *(P=0.0027)* ER mass than normal counterparts, as determined by ER

tracker staining (Fig. 2B). Next, the cytosolic and mitochondrial Ca^{2+} concentrations in $CD34^+$ CML cells were determined by staining cells with Indo-1 AM and Rhod-2 AM fluorescent Ca^{2+} sensor dyes, respectively (Fig. 2C). Whereas basal cytosolic Ca^{2+} content was lower *(P=0.005)*, mitochondrial Ca^{2+} content was higher *(P=0.002)* in $CD34^+$ CML cells compared to $CD34^+$ normal cells (Fig. 2D and E). Additionally, $CD34^+$ CML cells transferred more ER-derived Ca^{2+} to the mitochondria *(P=0.001)* and cytosol *(P=0.003)* upon stimulation with the SERCA inhibitor/ER Ca^{2+} mobiliser thapsigargin (*45*) (Fig. 2F and G). Together, this data indicates that enhanced ER Ca^{2+} buffering and Ca^{2+} transfer to the mitochondria are unique attributes of $CD34^+$ CML cells when compared to normal counterparts, likely due to their higher ER mass.

Lomerizine treatment suppresses oxidative mitochondrial metabolism in CML cells, including CML LSCs

Next, we measured metabolic changes in CML cells following lomerizine treatment by measuring metabolite abundance by liquid chromatography-mass spectrometry (LC-MS). Culturing CML cells in the presence of uniformly labelled ($^{13}C_6$) glucose for 24 hours allows quantification of ^{13}C isotope enrichment in metabolites central to glucose, nucleotides, amino acids, and mitochondrial energy metabolism. Initially, metabolic changes in TCA cycle intermediates were analyzed in the presence of 5 μM lomerizine, with the ETC complex I inhibitor IACS-010759 (*28, 29*) included as a reference inhibitor. Whereas lomerizine treatment did not affect glucose uptake it modestly reduced ($P<0.01$) abundance of glucose-derived carbons in pyruvate without significant changes in lactate. However, IACS-010759 treatment caused an increase *(P<0.01)* in intracellular lactate and lactate secretion (Fig. 3A and fig. S2A), similar to what has been observed in the clinic with IACS-010759 and other complex I inhibitors (*26, 29, 46, 47*). As expected, both lomerizine and IACS-010759 treatment reduced *(P<0.01)* abundance and labelling of TCA cycle intermediates

citrate, α-ketoglutarate (α-KG; catalyzed from isocitrate by IDH) and succinate. Using labelling of citrate and succinate as a proxy for PDH and α-KGDH activity, respectively, indicated decreased enzymatic activity following lomerizine treatment. Lomerizine treatment also reduced *(P<0.01)* the abundance and labelling of aspartate, which is required for nucleotide synthesis and cell proliferation (*48*). A significant decrease *(P<0.01)* in purine (ATP) and pyrimidine (CTP and UPT) "energy molecule" abundance was also observed following lomerizine treatment (Fig. 3A and fig S2A).

Encouraged by the inhibitory effect of lomerizine on TCA cycle activity in K562 cells we cultured primary $CD34^+$ cells in $^{13}C_6$ glucose in the presence of lomerizine. Again, this revealed similar effect on incorporation of glucose derived carbons into the TCA cycle metabolites, including citrate, α-KG and malate (fig. S2B). Additionally, a reduction in aspartate and energy nucleotides, including ATP, CTP and UTP was observed. Similarly, using uniformly labelled ($^{13}C_{16}$) palmitate we observed a reduction in labelling of citrate, α-KG and malate in lomerizine treated $CD34^+$ CML cells, indicating that lomerizine treatment had a similar effect on fatty acid oxidation and that its impact was not limited to glucose oxidation (fig. S2C). Consequently, we assessed whether lomerizine, alone or in combination with TKI-meditated BCR::ABL1 inhibition, affected the incorporation of glucose derived carbons in TCA cycle metabolites in primitive CML LSCs. Although the amount of labelling was reduced in this slowly growing population when compared with K562 cells, a decrease *(P≤0.01)* was observed in abundance and labelling in the TCA cycle intermediates citrate, α-KG and malate following lomerizine and/or combination treatment (Fig. 3B).

Ca^{2+} is required as a cofactor for the catalytic activity of mitochondrial dehydrogenases, which may affect TCA cycle activity (*49*). Therefore, we investigated whether lomerizine-mediated

reduction in Ca^{2+} would inhibit mitochondrial dehydrogenase activity in CML cells, in the presence or absence of BCR::ABL1 inhibition. Whereas imatinib treatment did not alter isocitrate dehydrogenase 3 (IDH3) activity, lomerizine treatment inhibited IDH3 in control *(P<0.01)* and imatinib treated *(P=0.01)* cells (Fig. 3C), reflecting the effect on its product, α-KG (Fig. 3B, middle). In addition, inhibition of dehydrogenase and TCA cycle activity by lomerizine may indirectly impact mitochondrial respiration. To test this, a mitochondrial stress test was performed following 12 hours treatment with lomerizine alone, imatinib, or the combination of lomerizine and imatinib in CML cells. Whereas imatinib caused a modest reduction in OCR, lomerizine significantly *(P=0.05)* inhibited maximal mitochondrial respiration, with the combination treatment resulting in almost complete inhibition in OCR (Fig. 3D). To assess the effect on glycolysis we treated CML cells as before and measured ECAR. This revealed that lomerizine treatment did not affect ECAR, whereas imatinib treatment alone and in combination with lomerizine inhibited maximal glycolytic activity (Fig. S3A; *P≤0.01*). In contrast, IACS-010759 significantly *(P=0.03)* increased ECAR (consistent with increased lactate secretion; Fig 3A) and reversed the imatinib-induced inhibition of glycolysis (fig. S3B).

We next examined whether short-term lomerizine treatment was sufficient to inhibit mitochondrial respiration in CML cells. This uncovered that 60 minutes lomerizine treatment reduced OCR in a concentration-dependent manner (fig. S3C). Additionally, the inhibitory effect of 12 hours lomerizine treatment repressed $CaCl_2$ induced OCR (fig. S3D). To investigate the effect of lomerizine treatment on individual ETC complex activity, we exposed CML cell mitochondria to respiration complex-specific substrates following membrane permeabilization. As expected, the ETC complex I specific inhibitor IACS-010759 blocked complex I linked OCR but not complex II or IV linked OCR (fig. S3E). In contrast, neither imatinib nor lomerizine significantly inhibited

the OCR mediated by complexes I, II or IV, suggesting that the effect of lomerizine on mitochondrial respiration may be primarily through inhibition of TCA cycle dehydrogenases.

Lomerizine depletes mitochondrial Ca^{2+} through CACNA1D and TRPC6 inhibition

Next, we aimed to uncover the downstream target of lomerizine. Further interrogation of the transcriptomic dataset (E-MTAB-2581 (*44*)), generated from CML LSCs ($CD34^+CD38^-$) and normal hematopoietic stem cell HSCs enriched samples, revealed that calcium channel, voltage-dependent, L type, alpha 1D subunit (*CACNA1D*) and the Ca^{2+} channel gene transient receptor potential channel 6 (*TRPC6*) were highly expressed in LSCs compared to their normal counterparts (Fig. 4A and B). *CACNA1D* expression was also increased in LSCs when compared with leukaemic progenitor cells (Fig. 4A). Transcriptomic analysis of $CD34^+$ CML samples treated with 2 µM imatinib for up to 7 days ex vivo (E-MTAB-2594 (*50*) and GSE216837(*51*)), demonstrated that neither *CACNA1D* nor *TRPC6* transcripts were significantly altered upon imatinib treatment (Fig. 4A and B). Together, this implied a possible role of *CACNA1D* and *TRPC6* in Ca^{2+} influx and ER-mediated Ca^{2+} transfer to the mitochondria in CML LSCs. Consistent with these findings, Ca^{2+} influx to the cytosol was higher *(P=0.011)* in CML when compared with normal cells, as measured by the instant response of cells to 1,2-dioctanoyl-sn-glycerol (DOG), the diacylglycerol (DAG) analogue that activates the Ca^{2+} channels CACNA1D and TRPC6 (*52*) (Fig. 4C), although the effect on uptake in the mitochondria was not statistically significant (Fig. 4D).

Lomerizine has been reported to target different types of VGCC, including CACNA1D, in solid cancer stem cells (*53*), but it is not known if lomerizine affects TRPC6 activity. To test if lomerizine treatment inhibits CACNA1D and TRPC6 mediated Ca^{2+} influx in CML, K562 cells were pre-treated with lomerizine for 24 hours prior to stimulation with DOG. Lomerizine significantly reduced *(P<0.01)* DOG-induced Ca^{2+} uptake in the cytosol and mitochondria (Fig.

4E). Next, specific stimulators, FPL64176 and hyperforin, were applied to activate CACNA1D and TRPC6, respectively (*54*, *55*). Reassuringly, lomerizine treatment prevented CACNA1D mediated Ca^{2+} uptake in cytosol and mitochondria, although the influx to cytosol only reached significance *(P=0.04)* in the presence of imatinib (Fig. 4F). Similarly, lomerizine reduced *(P<0.01)* TRPC6 mediated Ca^{2+} uptake in cytosol and mitochondria (Fig. 4G). In contrast, imatinib did not alter CACNA1D or TRPC6 mediated cytosolic Ca^{2+} influx (Fig. 4F and G). Moreover, FPL64176-stimulated Ca^{2+} uptake in mitochondria could be blocked with the CACNA1D inhibitor nicardipine (*56*), and hyperforin-stimulated Ca^{2+} influx to cytosol and mitochondria could be blocked with the TRPC6 inhibitor BI-749327 (*57*), further validating the specificity of the assay and the role of CACNA1D and TRPC6 in the regulation of Ca^{2+} uptake in CML cells (Fig. 4F and G).

Having determined that lomerizine blocks CACNA1D and TRPC6 mediated Ca^{2+} uptake, we next sought to examine the effect of lomerizine on Ca^{2+} mobilization from the ER by measuring thapsigargin-induced Ca^{2+} release from the ER. (Fig. 4H). Lomerizine significantly reduced *(P≤0.01)* thapsigargin-induced Ca^{2+} efflux from the ER to the cytosol and mitochondria. In contrast, imatinib slightly increased *(P≤0.01)* thapsigargin-induced Ca^{2+} mobilization to the cytosol, indicating that imatinib may cause a retention of Ca^{2+} in the ER (Fig. 4H).

Next, we asked if the reduction in ER Ca^{2+} mobilization by lomerizine is due to an inhibition of ER Ca^{2+} release or a reduction in ER Ca^{2+} content. To address this, we generated K562 cells, stably expressing the fluorescent ER Ca^{2+} reporter GCaMPer, which allows measurement of ER Ca^{2+} in living cells (*58*). In the absence of extracellular Ca^{2+}, m-3M3FBS stimulates IP3R-mediated ER Ca^{2+} mobilization to either the cytosol or mitochondria without interference from plasma membrane Ca^{2+} influx (*59*). Lomerizine alone, or when combined with imatinib, inhibited Ca^{2+}

mobilization from the ER in response to IP3R stimulation with m-3M3FBS (Fig. 4I, K). In order to examine the effect on ER Ca^{2+} content, GCaMPer expressing cells were pre-treated for 24 hours with 10 µM 2-Aminoethoxydiphenyl borate (2APB), a membrane-permeable IP3R inhibitor, leading to an inhibition of ER Ca^{2+} release (*60*). To measure the maximum Ca^{2+} storage capacity of ER, the 2APB-mediated Ca^{2+} retention was followed by acute Ca^{2+} mobilization with high concentration of m3-M3FBS (that can reverse 2APB mediated IP3R inhibition) (*61*). These cells were simultaneously treated with lomerizine or imatinib, to measure the effect on ER Ca^{2+} content. This revealed that lomerizine, but not imatinib, significantly reduced *($P<0.01$)* ER Ca^{2+} mobilization upon IP3R stimulation, suggesting that the ER Ca^{2+} content is lower in lomerizine treated CML cells (Fig. 4J and K).

Whilst imatinib did not alter the cytosolic Ca^{2+} influx in response to CACNA1D or TRPC6 stimulation, it did reduce *($P\leq0.01$)* mitochondrial Ca^{2+} content (Fig. 4F, G). We hypothesized that this was caused by a reduction in mitochondrial volume. To address this, we generated CML cells, stably overexpressing the fluorescent form of the outer mitochondrial membrane protein TOM20. Whereas lomerizine had no effect, imatinib treatment reduced *($P=0.03$)* fluorescence, suggesting a decrease in mitochondrial TOM20 amount following BCR::ABL1 inhibition (fig. S4A). Similarly, imatinib treatment reduced *($P=0.0093$)* mitochondria mass in $CD34^+$ CML cells stained with Mito Tracker dye (fig. S4B). Consistently, imatinib treatment reduced mitochondrial membrane potential (measured by TMRM; *$P<0.01$*) and cellular *($P=0.02$)* reactive oxygen species (ROS)amount, indicating decreased mitochondrial activity (Fig. S4C). As imatinib treatment has been found to induce autophagy in CML cells (*62*, *63*), we speculated that the reduction in mitochondrial mass observed in imatinib-treated CML cells resulted from autophagy-mediated mitochondrial degradation (mitophagy). To test this, mitochondrial-targeting mKeima (mito-

mKeima) expressing CML cells were generated (*64*). Unlike antimycin A/oligomycin A treatment (known to induce mitophagy (*65*)), imatinib treatment had no effect on mitophagy in mito-mKeima expressing cells, indicating that the reduction in mitochondrial mass upon imatinib treatment in this context is mainly mitophagy independent (Fig. S4D). To confirm this, we treated autophagy deficient ATG7 knockout (KO) cells with imatinib, which revealed a significant reduction (P=0.0085) in mitochondrial content (fig. S4E). This explained reduced mitochondrial Ca^{2+} response to the Ca^{2+} ionophore ionomycin (*66*) when ATG7 KO K562 cells were pre-treated with imatinib, further excluding a major role for canonical autophagy in imatinib-induced reduction in mitochondria content (fig. S4F).

To assess if the imatinib-induced mitochondria mass reduction was caused by a reduction in de novo synthesis (rather than degradation by mitophagy), we generated K562 cells expressing a doxycycline-inducible mitochondrial-targeted maturation marker (MitoTimer); a green fluorescent protein when newly synthesized, which shifts irreversibly to red fluorescence when it matures (gets oxidized). This enables measurements of "new" (green) and "old" (red) mitochondria and estimation of mitochondrial biogenesis and the rate of mitochondrial turnover (*67*, *68*). Using this system, autophagy inhibitor bafilomycin (inhibits autophagosome-lysosome fusion (*69*)) prevented the degradation of old mitochondrial as would be expected following autophagy inhibition (*70*). Whereas imatinib single treatment did not affect old mitochondria content it reduced *(P=0.03)* new mitochondria amount, suggesting a reduction in mitochondrial biogenesis (fig. S4G). Lomerizine treatment had a similar effect on mitochondrial biogenesis, with the combination of imatinib and lomerizine leading to reduction in green signal. Furthermore, mitochondrial biogenesis gene sets were significantly downregulated *(P=0.005)* upon imatinib treatment in $CD34^{+}CD38^{-}$ CML cells compared to untreated cells (fig. S4H), further suggesting

that the reduction in mitochondrial content following imatinib treatment is more likely to be driven by a reduction in biogenesis than an increase in mitophagy. Together with reduction in mitochondrial channel uniporter (MCU) amount following imatinib treatment, we also observed a decreased phosphorylation of transcription factors involved in mitobiogenesis, such as cAMP response element-binding protein (CREB), which may be a contributing factor to the decreased mitochondrial Ca^{2+} content observed in imatinib treated cells (fig. S4I) (*71*).

Taken together, these findings indicate that lomerizine, but not imatinib, depletes intracellular Ca^{2+} ions in the cytosol, ER and mitochondria through inhibition of CACNA1D and TRPC6 mediated Ca^{2+} uptake. In addition, imatinib altered the amount of mitochondrial Ca^{2+}, likely through an autophagy independent reduction in de novo mitochondrial biogenesis.

CACNA1D and TRPC6 deletion depletes Ca^{2+} and inhibits mitochondrial metabolism

To further address the role of CACNA1D and TRPC6 in mitochondrial metabolism and survival of CML cells, stable KO of CACNA1D and TRPC6 were created in K562 cells using CRISPR-Cas9 technology. We verified genetic editing within *CACNA1D* or *TRPC6* using genomic DNA sequencing with further validation of successful sequence aberration within the whole amplicon using the Tide online platform (fig. S5A and B). The generated cell lines were used to confirm the specificity of FPL64176 or hyperforin stimulation towards either CACNA1D or TRPC6, respectively. As expected, CACNA1D KO cells did not respond to FPL64176-mediated CACNA1D stimulation (fig. S6A). Similarly, TRPC6 KO cells did not respond to hyperforin-mediated TRPC6 stimulation (fig. S6B). Reassuringly, hyperforin was able to induce Ca^{2+} uptake in CACNA1D KO cells to similar amounts as control cells (fig. S6C) and FPL64176 induced Ca^{2+} uptake in control and TRPC6 KO cells (fig. S6D), indicating specificity of these stimulators towards their respective Ca^{2+} channels. Further, we investigated if deleting CACNA1D or TRPC6

affects cellular response to various Ca^{2+} stimulations. Consistently, CACNA1D or TRPC6 KO cells subsequently reduced *(P≤0.05)* Ca^{2+} uptake in cytosol or mitochondria as compared to control cells, both in the presence and absence of imatinib (Fig. 5A and B). Further, CACNA1D and TRPC6 KO cells showed reduction *(p≤0.01)* in thapsigargin-mediated ER Ca^{2+} mobilization to cytosol and mitochondria despite the presence of imatinib (Fig. 5C and D). However, the effect of thapsigargin on mobilization of ER Ca^{2+} to cytosol was enhanced by imatinib despite CACNA1D or TRPC6 KO, suggesting that imatinib enhanced ER Ca^{2+} retention independently of CACNA1D or TRPC6 expression (Fig. 5C). Both CACNA1D and TRPC6 deletion consistently reduced *(P<0.01)* ER Ca^{2+} mobilization to mitochondria despite the presence or absence of imatinib (Fig. 5D). These findings point to an essential role of CACNA1D and TRPC6 in replenishing ER Ca^{2+} stores in CML cells.

Similar to lomerizine treatment, CACNA1D or TRPC6 depletion led to an inhibition of mitochondrial respiration in CML cells, that was further decreased when combined with imatinib treatment (Fig. 5E and F). Consistently, CACNA1D or TRPC6 depletion significantly inhibited *(P<0.01)* IDH3 activity, and this effect was enhanced following imatinib treatment (Fig. 5G). WhereasCACNA1D or TRPC6 KO alone caused a minimal increase in apoptosis, combinatorial treatment with imatinib led to a substantial increase *(P<0.01)* in cell death (Fig. 5H). Similarly, CACNA1D or TRPCP6 KO led to a reduction *(P<0.01)* in cell proliferation that was further inhibited upon imatinib treatment (Fig. 5I and J). These results highlight the essential role of CACNA1D and TRPC6 mediated Ca^{2+} influx for ER to mitochondrion Ca^{2+} transfer, which is critical for mitochondrial respiration and survival of CML cells.

To further confirm that lomerizine mediates its effect mainly by inhibiting CACNA1D and TRPC6-mediated Ca^{2+} uptake, double knockout (DKO) cells were generated. As expected, (and

in line with fig S6A-D), CACNA1D and TRPC6 DKO prevented Ca^{2+} uptake in response to FPL64176 (CACNA1D) and hyperforin (TRPC6), with similar effect seen following lomerizine treatment (fig. S6E-H), although it was noticed that lomerizine further prevented hyperforin-induced uptake to mitochondria in DKO cells (fig. S6H). We next stimulated single KO and DKO cells with DOG to promote dual CACNA1D and TRPC6 activation and measured Ca^{2+} uptake to cytosol and mitochondria in control and lomerizine treated cells. This revealed an additive effect in DKO compared to single KO cells, which was in line with lomerizine treatment, highlighting the importance of inhibiting both calcium channels for maximal effect (fig. S6I-J).

Lomerizine treatment selectively targets CML LSCs ex vivo

To increase the clinical relevance of our work, we aimed to further verify our findings using primary $CD34^+$ cells, isolated from individuals with CML. Lomerizine treatment consistently inhibited *($P \leq 0.04$)* cytosolic and mitochondrial Ca^{2+} content in control and imatinib treated $CD34^+$ CML cells (Fig. 6A). In contrast, lomerizine did not significantly reduce cytosolic nor mitochondrial Ca^{2+} amounts in $CD34^+$ normal counterparts when used as a single agent, whereas a modest reduction *($P=0.08$)* was observed in cytosolic Ca^{2+} content when lomerizine was combined with imatinib treatment (Fig. 6B). Similarly, lomerizine alone or in combination with imatinib decreased *($P=0.03$)* OCR in $CD34^+$ CML cells (Fig. 6C). We then assessed the effect of single or combination treatment on proliferation and apoptosis of $CD34^+$ CML and normal cells. Reduced cell growth and survival was observed following combination of lomerizine and imatinib treatment in $CD34^+$ CML cells (Fig. 6D, E), with similar effect seen in the $CD45^+CD11b^+$ myeloid population (fig. S7A). This was not observed with $CD34^+$ or mature myeloid normal cells, in contrast to cells treated with omacetaxine mepesuccinate (Oma), an FDA-approved inhibitor of protein synthesis, used on occasion for treatment of advanced phases of CML (Fig. 6F, G and fig

S7B). Colony-forming cells (CFC) assay revealed similar effects, suggesting selective targeting of CML stem/progenitor cells by lomerizine (Fig. 6H and I). Additionally, treatment with the tool Ca^{2+} channel inhibitors 2APB, BI-749327 and nicardipine (a clinical Ca^{2+} channel blocker used to treat hypertension and angina) had similar effects on $CD34^+$ CML cell number and CFC potential (fig. S7C and D).

We also tested the survival of a phenotypically primitive stem cell population, labelled with CD34 and CD133 surface markers (*72*), after exposure to lomerizine and imatinib. Lomerizine reduced *($P \leq 0.014$)* the fraction $CD34^+CD133^+$ CML cells when combined with imatinib compared to untreated or single treated cells (Fig. 6J). The same treatments had no effect on normal $CD34^+CD133^+$ cells (Fig 6K). Next, $CD34^+$ CML cells were stained with Cell Trace Violet (CTV) to track cell division over 72 hours of treatment (Fig. 6L). As previously reported (*12*), the anti-proliferative effect of imatinib treatment enriched for the undivided population of $CD34^+$ CML cells when compared to untreated cells, in line with the concept that primitive CML cells are not eradicated upon imatinib treatment. Combination of lomerizine with imatinib reduced absolute cell counts in every cell division, including the undivided cell population *($P<0.01$)*, as compared to single treatment, suggesting that the combination of lomerizine with imatinib may be effective in targeting primitive CML cells. Furthermore, we performed a long-term culture-initiating cell (LTC-IC) assays using $CD34^+$ CML cells. This most stringent ex vivo stem cell assay demonstrated that lomerizine or imatinib treatment reduced the long-term colony formation capacity of CML $CD34^+$ cells, with a further significant reduction *($P<0.001$)* upon combinational treatment (Fig. 6M). Together, our findings demonstrate that inhibiting Ca^{2+} channels with lomerizine reduces survival of phenotypically and functionally defined CML LSC ex vivo.

Moreover, we investigated whether lomerizine sensitizes CML cells with acquired imatinib resistance to third generation TKIs. Imatinib-resistant cell lines are often sensitive to third generation TKIs such as ponatinib (*73*) and asciminib (*74*). We therefore treated KCL22 cells, carrying the T315I mutation ($KCL22^{T315I}$) with lomerizine alone and in combination with third generation TKIs. In line with imatinib-sensitive K562 cells (Fig. 4F and G) lomerizine, when used alone or in combination with ponatinib and asciminib, reduced *($P<0.01$)* cytosolic and mitochondrial Ca^{2+} content following stimulation with ionomycin in $KCL22^{T315I}$ cells (fig. S8A and B). Furthermore, lomerizine sensitized $KCL22^{T315I}$ cells to TKI-induced death (fig. S6C). A similar effect was observed when imatinib-resistant K562 cells ($K562^{IM\text{-}Res}$), that developed BCR::ABL1 independent mechanism of resistance (*75*), were treated with lomerizine and third generation TKIs (fig. S8D-F), suggesting that lomerizine may enhance the efficacy of ponatinib and asciminib against CML cells with acquired drug resistance.

It is accepted that the bone marrow microenvironment can protect leukaemic cells from drug-induced death, with leukemia-stroma crosstalk and mitochondria transfer to leukemic cells being highlighted as a protective mechanism (*76, 77*). To explore whether lomerizine maintains activity against CML cells cocultured with stromal cells, we cultured fluorescent labelled K562 cells with human bone marrow HS-5 stromal cells (*78*) in the absence or presence of lomerizine and imatinib treatment. This revealed that whereas monocultured cells were sensitive to imatinib, HS-5 coculture protected K562 cells from imatinib-induced death (fig. S8G and H) in agreement with previous work (*77*). However, combination of imatinib and lomerizine significantly *($P=0.0061$)* induced K562 cell death in coculture, although not to the same degree as monocultured K562 cells (21% vs 29%). No effect was seen on survival of HS-5 cells (fig. S8I). Similarly, compared with untreated or single treatments, the combination of imatinib and lomerizine caused increased

(P<0.01) cell death in primary $CD34^+$ CML cells, when cocultured with fluorescent HS-5 cells (fig. S8J and K). To test whether mitochondrial transfer could be partly responsible for protecting CML cells when grown on stromal cells, mitochondria transfer was measured between K562 (overexpressing TOM20-GFP) and HS-5 cells (overexpressing Mito-DSRed (*79*)). This revealed bi-directional transfer of mitochondria between K562 and HS-5 cells, which was inhibited by treatment with the tunnelling nanotube inhibitor cytochalasin-D (fig. S8L). This resulted in a modest net reduction in mitochondrial content *(P=0.0002)* in cocultured K562 cells when compared with monoculture, suggesting that mitochondria transfer is unlikely to be responsible for the increased resistance of CML cells when cocultured with stromal cells (fig. S8M).

Lomerizine treatment reduces tumor burden and CML LSC engraftment in vivo

Next, we investigated the effect of lomerizine in vivo. An initial dose escalation study in $NRGW^{41}$ ($NOD.Cg\text{-}Rag1^{tm1Mom}Kit^{W\text{-}41}JIl2rg^{tm1Wjl}$) mice (*80*) was performed, where mice were treated with increasing daily doses (10-80 mg/kg) of lomerizine (Fig. 7A). The dose escalation study demonstrated good tolerability at 80 mg/kg QD, with lomerizine plasma concentration of around 1 μM after 24 hours (Fig. 7B). Therefore, 80 mg/kg QD was selected for the subsequent in vivo studies, albeit this dose exceeds the concentration previously determined in human plasma (~0.1 μM) of individuals administrated with 10-40 mg daily dose (*81*).

A tail vein injection of KCL22 cells causes extramedullary tumors in immunocompromised mice, making this model appropriate for target evaluation assessment (*63*). Tumor-forming KCL22 cells expressing firefly luciferase were transplanted into non-irradiated $NRGW^{41}$ mice and tumour burden monitored weekly (Fig. 8C). The transplanted mice were left untreated for two weeks to allow tumors to develop. Vehicle, lomerizine (80 mg/kg, QD, IP injection), imatinib (50 mg/kg, BID, oral gavage), or a combination of lomerizine and imatinib were then administered for four

weeks. Lomerizine treatment reduced *(P<0.01)* tumor burden considerably when administered alone or in combination with imatinib, when compared with vehicle or imatinib only treated mice (Fig. 7D). Encouragingly, overall survival of transplanted mice was also enhanced *(P≤0.027)* following lomerizine and imatinib combination, when compared to untreated or imatinib monotherapy (Fig. 7E).

We next asked if lomerizine would target bone marrow located human CML LSCs. To investigate this, $CD34^+$ CML cells were transplanted into sub-lethally irradiated $NRGW^{41}$ female mice (fig. S9A). Following 8 weeks of engraftment, mice were treated with vehicle, imatinib, lomerizine or combination for four weeks as before and their bone marrow collected for analysis and cell quantification by flow cytometry (fig. S9B). Lomerizine and imatinib single treatments significantly reduced *(P≤0.03)* the absolute counts of human $CD45^+$, $CD34^+$, and $CD34^+CD38^-$ cells in the bone marrow when compared to vehicle control mice (Fig. 7F and G). The combination of lomerizine and imatinib was significantly *(P<0.01)* superior to imatinib alone, including in the primitive $CD34^+CD38^-$ population. Therefore, we conclude that lomerizine targets CML LSCs and enhances the effect of imatinib in a robust in vivo CML model.

DISCUSSION

We and others have shown that CML LSCs are insensitive to TKI treatment despite inhibition of BCR::ABL1 activity (*6, 7*). LSCs in both CML and AML have been shown to rewire their metabolism and rely on mitochondrial OXPHOS for survival (*11, 12, 18*). This provided a rationale for targeting mitochondrial respiration to eliminate therapy-resistant LSCs without affecting HSCs in preclinical studies (*14-16*). However, current OXPHOS inhibitors have demonstrated limitations in clinical trials due to lack of target engagement (*27*), dose limiting toxicities (*26*), or unfavorable side effects. For example, elevated blood lactate and neurotoxicity caused by the

complex I inhibitor IACS-010759 (*29*). Therefore, safer alternatives to target mitochondrial respiration are required.

By leveraging the known safety profile and pharmacology of drugs already used in the clinic, drug repurposing can reduce the time and financial expenditure needed to develop a new oncology drug and has therefore emerged as a useful approach for expanding the oncology drug pipeline. Given that most cancer cell lines are typically grown in supraphysiological glucose conditions and lack reliance on OXPHOS (while maintaining elevated rates of glycolysis), we performed a drug repurposing screen in culture conditions that force cells to use OXPHOS by using galactose as the sugar source. This approach identified lomerizine, an L-type Ca^{2+} channel blocker, as a promising candidate for blocking mitochondrial respiration in CML cells. Encouragingly, whereas Ca^{2+} overload may cause differentiation and exhaustion of HSCs (*82, 83*), previous works has demonstrated that low extracellular Ca^{2+} enhances HSC maintenance and inhibiting Ca^{2+} uptake is not detrimental to HSCs and allows for HSC division (*84, 85*), suggesting that targeting Ca^{2+} may be a promising strategy to kill leukemic cells without affecting normal blood cells. Indeed, work by Soboloff *et al*. demonstrated that inhibiting Ca^{2+} uptake in a mixture of normal and leukemic cells led to the selective elimination of leukemic cells (*86*). It is also possible that inhibiting Ca^{2+} in tumor-targeting immune cells has beneficial effect, as shown in chimeric antigen receptor (CAR) T cells, which possessed increased anti-tumor activity in vivo in an acute lymphoblastic leukemia xenograft model when mice received a store-operated calcium entry (SOCE) Ca^{2+} uptake inhibitor (*87*).

Recent preclinical studies have highlighted a role for Ca^{2+} in AML LSC survival by regulating mitochondrial metabolism (*88, 89*). In our study, transcriptome analysis revealed an upregulation of the Ca^{2+} influx channels *CACNA1D* and *TRPC6* in CML LSCs. In agreement, it has previously

been shown that the SOCE gene set (*TRPC6, STIM1, ORAI1*) is enriched in quiescent LT-HSCs compared to bulk HSCs (*90*), suggesting that *TRPC6* expression may be a feature of stem cells, that becomes dysregulated during leukemogenesis.

We also uncovered that $CD34^+$ CML cells have increased Ca^{2+} influx to the cytosol (as shown from cell response to DOG stimulation) accompanied with higher organellar Ca^{2+} buffering capacity, likely due to increased ER mass, when compared with normal counterparts. When $CD34^+$ CML cells were treated with imatinib, plasma membrane Ca^{2+} influx to the cytosol was unchanged but the amount of mitochondrial Ca^{2+} uptake was reduced, likely because of reduced mitochondrial mass. In combination with imatinib, lomerizine or genetic deletion of *CACNA1D* or *TRPC6* caused a further reduction in mitochondrial Ca^{2+} content. Lomerizine treatment also reduced integration of carbon sources (glucose and palmitate) into the TCA cycle, likely through inhibiting the activity of Ca^{2+} sensitive dehydrogenases such as IDH3. Ca^{2+} influx inhibition upon lomerizine treatment, *CACNA1D* KO or *TRPC6* KO caused a reduction in ER Ca^{2+} content, whereases imatinib treatment caused only a partial retention in ER Ca^{2+} content.

Alongside Ca^{2+} storage capacity, the quality and functionality of the ER and mitochondria is important to maintain Ca^{2+} homeostasis. We observed that imatinib causes a reduction in mitochondrial content. Although the precise mechanism for this is not clear, it is likely mediated by reduced biogenesis rather that TKI-induced mitophagy. Lomerizine treatment also caused mitogenesis inhibition, through an unknown mechanism, which may decrease mitochondrial abundance in the long-term.

One limitation in our study is that the concentration we used in our in vivo study (1-2 μM) is higher than want has been administered to humans at 40 mg dose by oral administration. Additionally, it

would be of interest how lomerizine treatment compares with pharmacological inhibition of the mitochondrial calcium uniporter, which may provide alternative option of inhibiting mitochondria Ca^{2+} influx and OXPHOS in leukemic cells (*91*). Another limitation is that we did not confirm that lomerizine treatment inhibited OXPHOS in bone marrow located leukemic cells which may have reduced mitochondrial metabolic activity due to reduced oxygen concentrations compared to classical tissue culture conditions.

Of clinical relevance, we highlight that Ca^{2+} influx inhibition with lomerizine reduces the amount of residual LSCs ex vivo and reduces CML tumor burden and LSC engraftment in vivo, an effect that is further enhanced following imatinib treatment. Therefore, sensitization of LSCs to TKI treatment upon Ca^{2+} influx inhibition with FDA-approved lomerizine represents a potential therapeutic approach to avoid some of the drawbacks and unfavorable side effects of current OXPHOS inhibitors, and to achieve DMR with the potential of TFR for patients with CML.

MATERIALS AND METHODS

Study Design

This study was designed to identify mitochondria metabolism inhibitor and to validate lomerizine, known as Ca^{2+} channel blocker, using CML models that are mainly driven by TKI-resistant CML LSCs (fig. S10). Functional approach, including unbiased transcriptional analysis of human-derived normal and CML cells, highlighted CACNA1D and TRPC6 as a potential target for Ca^{2+} influx inhibition in CML. We further validated the impact of deleting those genes using CRISPR-Cas9 technique in CML cells on mitochondrial Ca^{2+} content and subsequently mitochondrial metabolism. Using kinetic flow cytometry, we also investigated the impact of lomerizine on those Ca^{2+} channels activities in vitro. Lomerizine was tested in CML cell line xenotransplantation and CML patient derived xenograft (PDX) model, which allows measurements of human CML LSCs

after drug treatment. Mice were transplanted with CML cells by tail vain injection and randomized to the various experimental cohorts. Estimates for statistical analyses were based on the number of animals utilized per arm in each experiment based on previous investigations. To reduce the number of variables in xenograft trials, same-sex and aged mice were transplanted with the same quantity of CML cells. During assessments and experimental analyses, investigators and technicians were blinded to the experimental circumstances. All mice were cared for an unbiased fashion by animal technicians and investigators. No animals were excluded from the study. *P* values were computed using the method described in the figure legends. Except where otherwise noted, all in vitro experiments were carried out on at least three separate occasions.

Cell culture

K562 and KCL22 cell lines (DSMZ) were cultured at 5% CO_2 and 37°C in RPMI 1460 (Cat. #31870-025) supplemented with 10% FBS, 2 mM glutamine and 11 mM glucose/galactose. Primary cells were cultured at 5% CO_2 and 37 °C in a SFM comprising of Iscove's modified Dulbecco medium (Cat. #I3390) included dialyzed bovine serum albumin (BSA), insulin and transferrin (Cat. #BIT9500), 0.1 mM 2-mercaptoethanol (Cat. #21985023), 1 mM penicillin-streptomycin, and a physiological growth factor cocktail containing granulocyte-macrophage colony-stimulating factor, 0.2 ng/ml stem cell factor, and macrophage inflammatory protein (MIP)-α, interleukin (IL)-6 and 1.0 ng/ml granulocyte colony-stimulating factor (PeproTech EC) and 0.05 ng/ml leukemia inhibitory factor (StemCell Technologies) for 24 hours. For isotope assisted metabolomic experiments, primary cells were recovered overnight in SFM media, then sorted for $CD34^+CD38^-$ LSCs, and cultured in Plasmax, a more physiologically relevant media (*92*), and supplemented with 5 mM uniformly labelled ^{13}C glucose.

Coculturing stromal HS-5 and leukemic K562 cells

Stromal HS-5 (DSMZ) were grown in RPMI media till reaching 70% confluency. K562 cells were resuspended in fresh media at $0.2x10^6$/ml. Before establishing coculture, old media was aspirated from HS-5 cells followed by gentle inoculating K562 cells on top of HS-5 layer.

Reagents

Imatinib mesylate was supplied by LC Laboratories (Cat. #I-5508). Lomerizine (cat. #B1782) was dissolved in Pluronic F-127, a 10% solution in DMSO (Cat. #P3000MP) to get 20 mM stock solution, which was stored at -20 °C. For in vivo studies, 100 mg/ml lomerizine (Cat. #ab142528) was prepared by dissolving in DMSO, Tween 80, and saline in ratios of 1:2:17 and the pH was adjusted to 7 using 1M NaOH. [$^{13}C_6$] glucose (Cat. #CLM-1396) and [$^{13}C_{16}$] palmitate (Cat. #CLM-6059) were ordered from Cambridge Isotope Laboratories. BI-749327 (Cat. #3036) was purchased from Axon Medchem, EGTA was ordered from Tocris Bioscience (Cat. #67-425). Nicardipine hydrochloride was ordered from Medchem Express (Cat. #HY-12515A).

Antibodies used for Western Blotting: Phospho-CREB (Ser133) (87G3) (Cat. # 9198S), CREB (D76D11) (Cat. #4820S), Phospho-Akt (Ser473) (D9E) (Cat. #4060S), Akt (Cat. #9272S), MCU/CCDC109A (Cat. # 26312-1-AP), GAPDH (D16H11) (Cat. #5174S), Total H3 (Cat. #39763), P-ATF1 (Ser63) (Cat. #PA5-77869).

Drug repurposing screening

The screen was performed using four drug libraries. The Selleckchem library had 418 FDA-approved drugs. NIH Clinical Collections 1 and 2 (Evotec) had 281 and 446 compounds that had undergone phase I-III clinical trials and were not available in FDA-approved drug libraries. NIH's DTP oncology drug collection had 129 FDA-approved drugs. Compound libraries were kept at -80°C in 96-well plates in suitable solvents.

Cell expansion assays

Catalytic reduction of resazurin (Cat. #199303) into resorufin is accompanied with color shift from blue to pink and reflects the metabolic activity of a viable cell. This fluorometric shift (570/600 nm) was measured using Tecan Infinite 200 plate reader after 3 hours of incubation with 50 µM resazurin.

Primary samples

Primary $CD34^+$ CML cells were collected by leukapheresis from individuals initially diagnosed with CML (Ph^+) in chronic phase before initiating TKI treatment. Primary $CD34^+$ normal cells were isolated from femoral head bone marrow, derived from individuals undergoing hip replacement or leukapheresis products from patients with Ph^- hematological disorders such as myeloma or lymphoma. Primary normal $CD34^+$ cells obtained from hip replacement were enriched using the CD34 Microbead Kit (Miltenyi Biotec). Written informed consent was provided in accordance with the Declaration of Helsinki alongside Institutional Review Board approval from National Health Service Greater Glasgow and Clyde Trust (20/WS/0066). Please refer to the table S1 for more information.

Separation of $CD34^+$ cells from femoral head samples using Histopaque density gradient centrifugation

Bone marrow was homogenized without grinding in 10 mL PBS, then filtered through a 40 µm easy strainer filter (Cat. #542-040). The collected solution was spun down for 5 minutes at 400 RCF. The aspirated supernatant was discarded, and the pellet was resuspended in 6 mL PBS. The 6 mL of resuspended pellet was carefully layered on top of 8 mL of Histopaque (Cat. #10771) and centrifuged at 400 g without brakes for 30 minutes. Subsequently the middle buffy coat layer was

collected at the interface, and this was resuspended in 10 mL PBS, then washed through further centrifugation. Cells were resuspended in 100 µL of CD34 antibody and 100 µL blocking solution ultrapure kit (Cat. #130-100-453) and left at 4ºC for 30 minutes, then $CD34^+$ cells were collected following manufacturer protocol. Cells then were resuspended in serum-free media (SFM) supplemented with growth factors cocktail overnight for recovery, as previously described (*7*).

ER flow cytometry assay

ER mass was measured by staining cells with 3 µM of BODIPY ER tracker Red (Cat. #E34250) for 30 minutes before analyzing with flow cytometry.

Apoptosis assay with flow cytometry

Cells were stained for 15 minutes with 3 µg/mL Annexin V (fluorescein isothiocyanate (FITC); Cat. # 640906) and 3 µL 7-AAD (7-aminoactinomycin D; Cat. #559925), or 3 µL Annexin V with 10 µM DAPI (4′,6-diamidino-2-phenylindole; Cat. #422801), then the amount of apoptosis and cell death was measured using flow cytometry.

Cellular oxidative stress

Cells were stained with 10 µM MitoSOX Red (Cat. #M36008) or 5 µM CellROX deep Red (Cat. #C10422) and incubated at room temperature in the dark for 30 minutes. Mitosox dye was used to measure mitochondrial ROS content using the 7-AAD channel on a BD FACSVerse flow cytometer. CellRox was used to measure cytosolic ROS content using the APC channel.

Calcium quantification assay using flow cytometry

Basal cytosolic and mitochondrial Ca^{2+} content was measured by staining cells with 5 µM of Indo-1 and rhodamine AM ester (Rhod-2) for 30 minutes and data was acquired by flow cytometry using BD LSRFortessa Cell Analyser, according to supplier's protocol (Indo-1; Cat. # I1223 and

Rhod2; Cat. #R1244). The indo-1 was combined with 5 μM of the mitochondrial Ca^{2+}dye (Rhod2 AM). The reaction is analyzed as a kinetic process of the change in the amount of Ca^{2+} versus time (seconds). During the actual analysis with the flow cytometer (BD LSRFortessa; BD Biosciences), the stained cells were acutely exposed to a concentration of Ca^{2+} stressors (indicated in figure legends), the spontaneous response was acquired, and the kinetic analysis was done by FlowJo software V 10.6.01, BD Biosciences and statistically presented by Graphpad Prism 8. Stained cells were stimulated with 3 μM thapsigargin (Cat. #67526-95-8), 5 μM ionomycin (Cat. #56092-82-1), 25 μM DOG (Cat. #317505), 25 μM hyperforin (Cat. #HB3933), or 25 μM FPL64176 (Cat. #2A/252413) known to activate CACNA1D Ca^{2+} influx.

ER Ca^{2+} content was also measured through expressing a genetically encoded Ca^{2+} indicator lentiviral construct (GCAMPer, Cat. #65227, Addgene) into K562 cells as previously reported (*58*). As a control, cells were pre-treated with 5 μM 2-Aminoethoxydiphenyl borate (2APB, Cat. #D9754), an IP3R inhibitor (*93*), to retain ER Ca^{2+} content, then measured with flow cytometry upon mobilization using 25 μM m-3M3FBS (Cat. #T5699) a Phosphoinositide-specific phospholipase C (PLC) mediated IP3R stimulator, with the cells suspended in Ca^{2+} free PBS.

Mitochondrial flow cytometry assays

To assess the mitochondrial membrane potential, cells were loaded with Tetramethyl rhodamine, Methyl Ester, Perchlorate (TMRM) (Cat. #T668) for 30 minutes followed by 2X PBS washes and the fluorescent intensity was recorded by flow cytometry (excitation: 560 nm and emission: 590 nm). Mitochondrial mass was assessed by staining cells with 100 nM Mitotracker Deep Red) (Cat. #M22426) or using cells expressing mitochondrial-localized TOM20 eGFP protein.

Bacterial transformation of viral constructs

All lentiviral and retroviral based plasmid constructs were transformed using Mix&Go *E. coli* Transformation Kit & Buffer set, according to manufacturer protocol (Cat. #T3001).

Flow cytometry/FACS

For isolation of cells expressing lentiviral blast-MTS TOM20, Puro MitoTimer, mito-mKeima, or Mito-DSRed, cells were sorted with a FACSAria Fusion Cell sorter, BD Biosciences. Additionally, $CD34^+$ CML were sorted to enrich for $CD34^+CD38^-$ LSCs using FACSAria Fusion Cell sorter, BD Biosciences. For PDX experiments/cell sorting, cells were stained with anti-mouse (APC-Cy7: Cat# 557659), anti–human CD45 (FITC: Cat# 555482), anti–human CD34 (APC: Cat# 555824) and anti–human CD38 (PerCP: Cat# 303520) antibodies for 20 minutes prior to flow cytometry analysis/sorting.

Coculture experiments

Cocultured cells were distinguished using HS-5 cell surface markers, such as APC Cy-7 CD90 (Cat. # 328132) or following overexpression of pLV-Mito-DSRed (Addgene plasmid # 44386), a gift from Pantelis Tsoulfas (http://n2t.net/addgene:44386). K562 cells were isolated as CD90 negative or expressing TOM20-GFP. Primary CML samples were detected by their CD90 and CD34 surface markers expression.

Mitochondrial turnover

Mitophagy flow cytometry analysis was performed using cells expressing retroviral construct mito-mKeima (Cat. #72342, Addgene) and measured by getting the ratio of fluorescence intensities of mitochondria outside lysosome (pH=7-8) and those inside lysosomes (pH=4) as previously described (*94*). Mitochondrial biogenesis flow cytometry analysis was performed using cells expressing lentiviral pLVX puro MitoTimer (*68*). Briefly, Mito Timer expressing cells were

pulsed for 8 hours with 2 µg/ ml doxycycline (Invitrogen, Cat. # 15140-122) followed by washing out and re-exposure to treatment, for example imatinib, for another 40 hours. During the last 8 hours, cells were pulsed again using 2 µg/ml doxycycline.

CRISPR-Cas9 mediated gene editing

To target human TRPC6 and CACNA1D within genomic DNA, guide RNA (gRNA) constructs were designed and ordered from GenScript or made using the same guides according to https://zlab.bio/guide-design-resources (*CACNA1D* guide 1: CAGCAAGCGGACCACGCGAA, CACNA1D guide 2: TACATCCTAATGCTTATGTT and *TRPC6*: TGTATAGGATGACGCTGATG,).

Polymerase chain reaction (PCR) CRISPR Cas9 verification

To validate successful *CACNA1D* or *TRPC6* gene editing with CRISPR Cas9 technology, a set of unique primers was designed using the UCSC genome browser (https://genome-euro.ucsc.edu/cgi-bin/hgGateway) and Primer3 V0.4.0 (https://bioinfo.ut.ee/primer3-0.4.0/). Primers were ordered from Integrated DNA Technologies. Genomic DNA was extracted and purified using the GeneJet Genomic DNA purification kit (Cat. #K0721). Genomic DNA region flank guide DNA was PCR amplified using a set of selected primers (table S2) and amplified with *Taq* polymerase (Cat. #M0267S). PCR amplicons were purified with Monarch PCR and DNA Cleanup Kit (Cat. #T1030S). PCR amplicons were verified and quantified by Nanodrop assay and the presence of a single tight band upon running fraction of amplicon on 2% agarose gel.

Sequencing genomic DNA

The Applied Biosystems (BigDye Terminator v3.1) DNA sequencing protocol is used for the setup of sequencing reactions, precipitation of sequenced DNA and preparation for loading onto the

sequencer. The same forward primers were used to Sanger sequence the PCR amplicon where sequencing PCR products is carried out using an Applied Biosystems PRISM 3130xl (16 capillaries) sequencer. Analyses of the sequencing data are carried out using the ABI Prism Seqscape software. Genomic editing was verified by loading sequencing raw files into online tools such as Chromas V2.6.6 (http://technelysium.com.au/wp/chromas/) and Tide platform (http://shinyapps.datacurators.nl/tide/). Cellular genomic sequencing of DKO K562 cells is shown in table S3.

IDH3 activity

The nicotinamide adenine diphosphate (NAD^+) dependent IDH3 activity was measured using the IDH activity assay kit according to the manufacturer's protocol (Cat. #MAK062). The IDH3 activity was assayed in cell extracts ($1*10^6$ cells) using the IDH3 substrate and the cofactor NAD^+ in an enzyme reaction, resulting in a colorimetric product (450 nm) proportional to NADH production. Measurements were taken every 5 minutes over 1 hour to record kinetic enzyme activity for cell extract and for NADH standard samples. The activity is calculated where each unit reflects the amount of IDH3 enzyme that will produce 1.0 μmol NADH.

Respirometry and acidification rate

OCR was measured with an XF96 Seahorse Flux analyzer (Agilent Technologies). $CD34^+$ primary CML cells were supplemented with 1 mM pyruvate, 25 mM glucose and 1mM glutamine. 0.1 million cells were seeded in a 96 well microplate, 175 μl per well, which were pre-coated with Cell-Tak (Cat. #354242). Cells were spun down at 200 RCF for 1 minute and then left in a non-CO_2 incubator at 37°C for 25 minutes. An assay cartridge was loaded into the Seahorse machine during degassing of the cell plate in a non-CO_2 incubator. The cell plate was then loaded into the machine where basal OCR was acquired, followed by sequential injections of 1 μM oligomycin,

an ATP synthase (complex V) inhibitor, 1.6 μM carbonyl cyanide-4- (trifluoromethoxy) phenylhydrazone (FCCP), a mitochondrial complex IV uncoupler, and 1 μM antimycin A (complex III) and 1 μM rotenone (complex I) (all from Sigma-Aldrich). Similar steps were performed with cell lines except excluding pyruvate from Seahorse media before seeding them into cell plates. Analysis was performed according to the manufacturer's mitostress protocol. Cell lines were suspended in Seahorse media, as previously reported, without including glucose to measure the ECAR. The cell plate was loaded into the machine after which the basal ECAR was acquired, followed by sequential injections of 11 mM glucose, 1 μM oligomycin that inhibits OCR and forces cells to use glycolysis, and 4 μM 2-deoxy glucose, phospho-glucose isomerase inhibitor (all from Sigma-Aldrich). Analyses were performed according to the manufacturer's Glycostress protocol. Membrane permeabilization mitostress assay test was performed as previously reported (*95*).

Targeted isotope labelling identification

The media used for the K562 cell line was glucose-free RPMI supplemented with glucose. Primary cells were recovered in SFM complete medium and then plated in the presence of [$^{13}C_6$] glucose or [$^{13}C_{16}$] palmitate for 24 hours at a concentration of $0.2x10^6$ cells/ml in a serum-like culture medium comprising physiological metabolite concentration found in human plasma as previously described (*96*). After 24 hours, cells were washed twice with cold PBS, and intracellular metabolites were extracted with ice-cold extraction solvent (methanol, acetonitrile, and high-performance liquid chromatography (HPLC) grade water at 5:3:2 ratios respectively). The cell extracts were centrifuged at 16,000g at 4 °C for 10 minutes and supernatants were subjected to LC-MS.

A Q-Exactive Orbitrap mass spectrometer was coupled with the UltiMate 3000 HPLC system (Thermo Scientific). HPLC was carried out on a ZIC-pHILIC column (SeQuant, 15 × 0.21 cm, 5 μm) with a ZIC-pHILIC guard column (SeQuant, 2 × 0.21 cm, Merck KGaA). The organic mobile phase was 100% acetonitrile (B), and the aqueous mobile phase was 20 mM ammonium carbonate, 0.1% ammonium hydroxide (A). The metabolites were resolved over a linear gradient from 20:80 A:B to 80:20 A:B at 45°C, with a flow rate of 200 μL/minute for 22.2 minutes of total run time. All metabolites were detected across a 75–1,000 m/z mass range and at 70,000 (at 200 m/z) resolution using the Q-Exactive mass spectrometer with electrospray ionization operating in polarity switching mode. The mass accuracy was below 5 ppm for all metabolites. LC-MS raw peak intensities and retention times were identified using commercially available standard metabolites analyzed on the same LC-MS system and through the software packages, TOXID for peak retention time and TraceFinder for peak intensity (both from Thermo Fisher Scientific). Peak intensities of solvent background were subtracted, and intracellular metabolites were normalized to sample cell number and extraction volume. Relative isotopologue abundance was visualized using online Autoplotter V2.4 (https://mpietzke.shinyapps.io/AutoPlotter/) (*97*). Bioinformatics and statistical analysis of differential targeted labelling were performed with online MetaboAnalyst V5.0 (https://www.metaboanalyst.ca/MetaboAnalyst/ModuleView.xhtml) (*98*).

Cellular division tracking

Primary $CD34^+$ CML cells were stained with 0.1 μM CTV Proliferation Kit (Cat. #C34557, ThermoFisher Scientific) for 30 minutes at 37°C. The reaction was quenched by adding up to 50 mL PBS containing 10% FBS. Cells ($1x10^3$) were further stained with APC-CD34 surface marker (Cat# 555824) followed by flow cytometry assessment acquired at day 0. The remaining cells were

then resuspended in SFM complete medium and treated as indicated. After 72 hours, CTV staining coupled with CD34 expression were assessed by flow cytometry, BD FACSVerse.

CFC and LTC-IC assays

CFC were performed by gently mixing 70000 cells in 3 ml of semi-solid MethoCult H4034 Optimum (Cat. #04034), then left for 14 days, followed by counting colonies using brightfield microscopy. Cells were also assayed for LTC-IC by counting the CFC content after 5-week co-culturing CML cells with $1x10^4$ of two pre-established genetically engineered murine fibroblasts. M2-10B4 (secretes IL-3 and G-CSF) and S1/S1 (produces IL3 and SCF) in MyeloCult H5100 (Cat. #05150) supplemented with hydrocortisone in a Collagen I coated plate (Cat. #A1142802) and followed by replacing media each week.

Quantification of lomerizine in plasma using liquid chromatography tandem mass spectrometry (LC/MS)

Samples were analyzed using TSQ Altis Plus Triple Quadrupole Mass Spectrometer (Thermo Fisher Scientific) equipped with the Heated Electrospray Ionization (HESI-II) source operating in positive ion mode. The capillary voltage was set to 3500 V. The ion transfer tube temperature and the vaporizer temperature were set to 325 and 350^{o}C respectively, the sheath gas and auxiliary gas were set to flow rates of 35 and 7 (Arb). The drug was monitored using selected reaction monitoring (SRM) applying 3 transitions and the optimized parameters and transitions are summarized in the Table below. Chromatographic separation was performed on a HSS T3 column 150 mm × 2.1 mm, 1.8 μm (Waters) maintained at 45^{o}C. Gradient elution was achieved using a program with mobile phase A (water + 0.1% formic acid) and mobile phase B (acetonitrile + 0.1% formic acid) as follows: 20% B to 95% B in 8 minutes and maintained for 1 minute, then back to 20% B in 1 minute and re-equilibration for 2 minutes. The total run time of 12 minutes and

Lomerizine eluted at 5.97 minutes. The whole system was controlled by Xcalibur version 4.3. Data processing was performed using TraceFinder version 4.1. The concentration of the drug in plasma samples was determined using external calibration.

Q1 mass	Q3 mass	Dwell Time (msec)	Collision energy	Comments
469.175	181.054	199	19.25	Quantifier ion
469.175	166.071	199	36.95	Qualifier ion
469.175	203	199	25.24	Qualifier ion

Animal studies

All animal experiments were carried out in accordance with the Animals Scientific Procedures Act of 1986 and following the University of Glasgow Animal Welfare and Ethical Review Board (AWERB) under Home Office Licence. All experiments were performed under Helgason's project licence (PPL No PP2518370) and Khalaf's personal licence (PIL No I82823224). Mice were accommodated in a pathogen-free facility with day/night cycles (12 hours each). Mice were given unlimited access to food libitum pellets, soft hydrogels (when required) and water.

Mice in vivo transplantation and treatment

For KCL22 xenotransplantation, 8-13-week-old male NRGW^{41} mice were transplanted with 4x10^{6} cells suspended in 200 µl of 2% FBS/PBS. KCL22 expressing lentiviral firefly luciferase cells were selected with 5 µM puromycin in vitro culture for 10 days. For patient-derived xenotransplantation (PDX), 8-12-week-old female NRGW^{41} mice were transplanted with 1.3x10^{6} cells suspended in 200 µl of 2% FBS/PBS. The transplanted mice were administrated with vehicle, lomerizine (80 mg/kg, QD, IP injection), imatinib (50 mg/kg, BID, oral gavage), or a combination of lomerizine and imatinib for four weeks.

Statistical analysis

Data are presented as mean ± SEM or ± SD as indicated. Significance of data comparisons was achieved when probability values were ≤0.05%. Probability values were calculated using a regular one-way analysis of variance (ANOVA) for multiple comparisons, two-way ANOVA for Seahorse Flux data analysis, and an unpaired student *t*-test for two comparisons. Normality of data was checked, and log transformation or appropriate non-parametric tests performed on data with non-normal distribution. Figures were in most cases made with Prism v8 and v9 (GraphPad Software Inc). Number of samples obtained from at least 3 CML or healthy individuals, or otherwise mentioned in figure legends. All raw numerical data are presented in Data Files S1-S15.

Supplementary Materials

Fig S1-S10

Tables S1-S3

Datafile S1-S15

MDAR Reproducibility Checklist

References and Notes

1. B. J. Druker, S. Tamura, E. Buchdunger, S. Ohno, G. M. Segal, S. Fanning, J. Zimmermann, N. B. Lydon, Effects of a selective inhibitor of the Abl tyrosine kinase on the growth of Bcr-Abl positive cells. *Nature medicine* **2**, 561-566 (1996).
2. S. G. O'Brien, F. Guilhot, R. A. Larson, I. Gathmann, M. Baccarani, F. Cervantes, J. J. Cornelissen, T. Fischer, A. Hochhaus, T. Hughes, K. Lechner, J. L. Nielsen, P. Rousselot, J. Reiffers, G. Saglio, J. Shepherd, B. Simonsson, A. Gratwohl, J. M. Goldman, H. Kantarjian, K. Taylor, G. Verhoef, A. E. Bolton, R. Capdeville, B. J. Druker, I. Investigators, Imatinib compared with interferon and low-dose cytarabine for newly diagnosed chronic-phase chronic myeloid leukemia. *The New England journal of medicine* **348**, 994-1004 (2003).
3. A. Hochhaus, R. A. Larson, F. Guilhot, J. P. Radich, S. Branford, T. P. Hughes, M. Baccarani, M. W. Deininger, F. Cervantes, S. J. N. E. J. o. M. Fujihara, Long-term outcomes of imatinib treatment for chronic myeloid leukemia. **376**, 917-927 (2017).
4. F. X. Mahon, D. Rea, J. Guilhot, F. Guilhot, F. Huguet, F. Nicolini, L. Legros, A. Charbonnier, A. Guerci, B. Varet, G. Etienne, J. Reiffers, P. Rousselot, C. Intergroupe Francais des Leucemies Myeloides, Discontinuation of imatinib in patients with chronic myeloid leukaemia who have maintained complete molecular remission for at least 2 years: the prospective, multicentre Stop Imatinib (STIM) trial. *The Lancet. Oncology* **11**, 1029-1035 (2010).
5. T. L. Holyoake, D. Vetrie, The chronic myeloid leukemia stem cell: stemming the tide of persistence. *Blood* **129**, 1595-1606 (2017).
6. A. S. Corbin, A. Agarwal, M. Loriaux, J. Cortes, M. W. Deininger, B. J. Druker, Human chronic myeloid leukemia stem cells are insensitive to imatinib despite inhibition of BCR-ABL activity. *J Clin Invest* **121**, 396-409 (2011).
7. A. Hamilton, G. V. Helgason, M. Schemionek, B. Zhang, S. Myssina, E. K. Allan, F. E. Nicolini, C. Muller-Tidow, R. Bhatia, V. G. Brunton, S. Koschmieder, T. L. Holyoake, Chronic myeloid leukemia stem cells are not dependent on Bcr-Abl kinase activity for their survival. *Blood* **119**, 1501-1510 (2012).
8. J. C. Chomel, M. L. Bonnet, N. Sorel, A. Bertrand, M. C. Meunier, S. Fichelson, M. Melkus, A. Bennaceur-Griscelli, F. Guilhot, A. G. Turhan, Leukemic stem cell persistence in chronic myeloid leukemia patients with sustained undetectable molecular residual disease. *Blood* **118**, 3657-3660 (2011).
9. D. Vetrie, G. V. Helgason, M. Copland, The leukaemia stem cell: similarities, differences and clinical prospects in CML and AML. *Nat Rev Cancer* **20**, 158-173 (2020).
10. N. Van Gils, F. Denkers, L. J. F. i. O. Smit, Escape from treatment; the different faces of leukemic stem cells and therapy resistance in acute myeloid leukemia. *Frontiers in oncology* **11**, 1454 (2021).
11. Eleni D. Lagadinou, A. Sach, K. Callahan, Randall M. Rossi, Sarah J. Neering, M. Minhajuddin, John M. Ashton, S. Pei, V. Grose, Kristen M. O'Dwyer, Jane L. Liesveld, Paul S. Brookes, Michael W. Becker, Craig T. Jordan, BCL-2 Inhibition Targets Oxidative Phosphorylation and Selectively Eradicates Quiescent Human Leukemia Stem Cells. *Cell Stem Cell* **12**, 329-341 (2013).
12. E. M. Kuntz, P. Baquero, A. M. Michie, K. Dunn, S. Tardito, T. L. Holyoake, G. V. Helgason, E. J. N. m. Gottlieb, Targeting mitochondrial oxidative phosphorylation eradicates therapy-resistant chronic myeloid leukemia stem cells. **23**, 1234-1240 (2017).

13. C. R. Bartman, D. R. Weilandt, Y. Shen, W. D. Lee, Y. Han, T. TeSlaa, C. S. R. Jankowski, L. Samarah, N. R. Park, V. da Silva-Diz, M. Aleksandrova, Y. Gultekin, A. Marishta, L. Wang, L. Yang, A. Roichman, V. Bhatt, T. Lan, Z. Hu, X. Xing, W. Lu, S. Davidson, M. Wuhr, M. G. Vander Heiden, D. Herranz, J. Y. Guo, Y. Kang, J. D. Rabinowitz, Slow TCA flux and ATP production in primary solid tumours but not metastases. *Nature*, (2023).
14. T. Farge, E. Saland, F. de Toni, N. Aroua, M. Hosseini, R. Perry, C. Bosc, M. Sugita, L. Stuani, M. J. C. d. Fraisse, Chemotherapy-resistant human acute myeloid leukemia cells are not enriched for leukemic stem cells but require oxidative metabolism. *Cancer discovery* **7**, 716-735 (2017).
15. J. R. Molina, Y. Sun, M. Protopopova, S. Gera, M. Bandi, C. Bristow, T. McAfoos, P. Morlacchi, J. Ackroyd, A.-N. A. J. N. m. Agip, An inhibitor of oxidative phosphorylation exploits cancer vulnerability. *Nature medicine* **24**, 1036-1046 (2018).
16. A. Abraham, S. Qiu, B. K. Chacko, H. Li, A. Paterson, J. He, P. Agarwal, M. Shah, R. Welner, V. M. J. T. J. o. c. i. Darley-Usmar, SIRT1 regulates metabolism and leukemogenic potential in CML stem cells. *The Journal of clinical investigation* **129**, 2685-2701 (2019).
17. L. Stuani, M. Sabatier, E. Saland, G. Cognet, N. Poupin, C. Bosc, F. A. Castelli, L. Gales, E. Turtoi, C. Montersino, T. Farge, E. Boet, N. Broin, C. Larrue, N. Baran, M. Y. Cisse, M. Conti, S. Loric, T. Kaoma, A. Hucteau, A. Zavoriti, A. Sahal, P. L. Mouchel, M. Gotanegre, C. Cassan, L. Fernando, F. Wang, M. Hosseini, E. Chu-Van, L. Le Cam, M. Carroll, M. A. Selak, N. Vey, R. Castellano, F. Fenaille, A. Turtoi, G. Cazals, P. Bories, Y. Gibon, B. Nicolay, S. Ronseaux, J. R. Marszalek, K. Takahashi, C. D. DiNardo, M. Konopleva, V. Pancaldi, Y. Collette, F. Bellvert, F. Jourdan, L. K. Linares, C. Recher, J. C. Portais, J. E. Sarry, Mitochondrial metabolism supports resistance to IDH mutant inhibitors in acute myeloid leukemia. *J Exp Med* **218**, (2021).
18. L. de Beauchamp, E. Himonas, G. V. Helgason, Mitochondrial metabolism as a potential therapeutic target in myeloid leukaemia. *Leukemia* **36**, 1-12 (2022).
19. Drugging OXPHOS Dependency in Cancer. *Cancer Discov* **9**, OF10 (2019).
20. Y. Xu, D. Xue, A. Bankhead, 3rd, N. Neamati, Why All the Fuss about Oxidative Phosphorylation (OXPHOS)? *J Med Chem* **63**, 14276-14307 (2020).
21. M. Sanchez, L. Gastaldi, M. Remedi, A. Caceres, C. Landa, Rotenone-induced toxicity is mediated by Rho-GTPases in hippocampal neurons. *Toxicol Sci* **104**, 352-361 (2008).
22. R. Betarbet, T. B. Sherer, G. MacKenzie, M. Garcia-Osuna, A. V. Panov, J. T. Greenamyre, Chronic systemic pesticide exposure reproduces features of Parkinson's disease. *Nat Neurosci* **3**, 1301-1306 (2000); published online EpubDec (10.1038/81834).
23. F. Janku, P. LoRusso, A. S. Mansfield, R. Nanda, A. Spira, T. Wang, A. Melhem-Bertrandt, J. Sugg, H. A. Ball, First-in-human evaluation of the novel mitochondrial complex I inhibitor ASP4132 for treatment of cancer. *Invest New Drugs* **39**, 1348-1356 (2021).
24. J. A. Dykens, J. Jamieson, L. Marroquin, S. Nadanaciva, P. A. Billis, Y. Will, Biguanide-induced mitochondrial dysfunction yields increased lactate production and cytotoxicity of aerobically-poised HepG2 cells and human hepatocytes in vitro. *Toxicol Appl Pharmacol* **233**, 203-210 (2008).

25. H. R. Bridges, A. J. Jones, M. N. Pollak, J. Hirst, Effects of metformin and other biguanides on oxidative phosphorylation in mitochondria. *Biochem J* **462**, 475-487 (2014).
26. F. Janku, S. H. Beom, Y. W. Moon, T. W. Kim, Y. G. Shin, D. S. Yim, G. M. Kim, H. S. Kim, S. Y. Kim, J. H. Cheong, Y. W. Lee, B. Geiger, S. Yoo, A. Thurston, D. Welsch, M. S. Rudoltz, S. Y. Rha, First-in-human study of IM156, a novel potent biguanide oxidative phosphorylation (OXPHOS) inhibitor, in patients with advanced solid tumors. *Invest New Drugs* **40**, 1001-1010 (2022).
27. G. A. Reed, G. J. Schiller, S. Kambhampati, M. S. Tallman, D. Douer, M. D. Minden, K. W. Yee, V. Gupta, J. Brandwein, Y. Jitkova, M. Gronda, R. Hurren, A. Shamas-Din, A. C. Schuh, A. D. Schimmer, A Phase 1 study of intravenous infusions of tigecycline in patients with acute myeloid leukemia. *Cancer medicine* **5**, 3031-3040 (2016).
28. J. R. Molina, Y. Sun, M. Protopopova, S. Gera, M. Bandi, C. Bristow, T. McAfoos, P. Morlacchi, J. Ackroyd, A. A. Agip, G. Al-Atrash, J. Asara, J. Bardenhagen, C. C. Carrillo, C. Carroll, E. Chang, S. Ciurea, J. B. Cross, B. Czako, A. Deem, N. Daver, J. F. de Groot, J. W. Dong, N. Feng, G. Gao, J. Gay, M. G. Do, J. Greer, V. Giuliani, J. Han, L. Han, V. K. Henry, J. Hirst, S. Huang, Y. Jiang, Z. Kang, T. Khor, S. Konoplev, Y. H. Lin, G. Liu, A. Lodi, T. Lofton, H. Ma, M. Mahendra, P. Matre, R. Mullinax, M. Peoples, A. Petrocchi, J. Rodriguez-Canale, R. Serreli, T. Shi, M. Smith, Y. Tabe, J. Theroff, S. Tiziani, Q. Xu, Q. Zhang, F. Muller, R. A. DePinho, C. Toniatti, G. F. Draetta, T. P. Heffernan, M. Konopleva, P. Jones, M. E. Di Francesco, J. R. Marszalek, An inhibitor of oxidative phosphorylation exploits cancer vulnerability. *Nature medicine* **24**, 1036-1046 (2018).
29. T. A. Yap, N. Daver, M. Mahendra, J. Zhang, C. Kamiya-Matsuoka, F. Meric-Bernstam, H. M. Kantarjian, F. Ravandi, M. E. Collins, M. E. D. Francesco, E. E. Dumbrava, S. Fu, S. Gao, J. P. Gay, S. Gera, J. Han, D. S. Hong, E. J. Jabbour, Z. Ju, D. D. Karp, A. Lodi, J. R. Molina, N. Baran, A. Naing, M. Ohanian, S. Pant, N. Pemmaraju, P. Bose, S. A. Piha-Paul, J. Rodon, C. Salguero, K. Sasaki, A. K. Singh, V. Subbiah, A. M. Tsimberidou, Q. A. Xu, M. Yilmaz, Q. Zhang, Y. Li, C. A. Bristow, M. B. Bhattacharjee, S. Tiziani, T. P. Heffernan, C. P. Vellano, P. Jones, C. J. Heijnen, A. Kavelaars, J. R. Marszalek, M. Konopleva, Complex I inhibitor of oxidative phosphorylation in advanced solid tumors and acute myeloid leukemia: phase I trials. *Nature medicine* **29**, 115-126 (2023).
30. R. M. Denton, Regulation of mitochondrial dehydrogenases by calcium ions. *Biochim Biophys Acta* **1787**, 1309-1316 (2009).
31. A.-C. Martinez-Torres, C. Quiney, T. Attout, H. Boullet, L. Herbi, L. Vela, S. Barbier, D. Chateau, E. Chapiro, F. J. P. m. Nguyen-Khac, CD47 agonist peptides induce programmed cell death in refractory chronic lymphocytic leukemia B cells via PLCγ1 activation: evidence from mice and humans. *PLoS medicine* **12**, e1001796 (2015).
32. C. Ge, H. Huang, F. Huang, T. Yang, T. Zhang, H. Wu, H. Zhou, Q. Chen, Y. Shi, Y. J. P. o. t. N. A. o. S. Sun, Neurokinin-1 receptor is an effective target for treating leukemia by inducing oxidative stress through mitochondrial calcium overload. *Proceedings of the National Academy of Sciences* **116**, 19635-19645 (2019).
33. M. Prakriya, R. S. Lewis, Store-Operated Calcium Channels. *Physiological reviews* **95**, 1383-1436 (2015).

34. G. Szabadkai, A. M. Simoni, R. Rizzuto, Mitochondrial Ca2+ uptake requires sustained Ca2+ release from the endoplasmic reticulum. *Journal of Biological Chemistry* **278**, 15153-15161 (2003).
35. G. Bustos, P. Cruz, A. Lovy, C. Cárdenas, Endoplasmic reticulum–mitochondria calcium communication and the regulation of mitochondrial metabolism in cancer: a novel potential target. *Frontiers in oncology* **7**, 199 (2017).
36. A. C. Dolphin, A short history of voltage-gated calcium channels. *Br J Pharmacol* **147 Suppl 1**, S56-S62 (2006)10.1038/sj.bjp.0706442).
37. D. E. Clapham, TRP channels as cellular sensors. *Nature* **426**, 517-524 (2003).
38. B. Robinson, R. Petrova-Benedict, J. Buncic, D. J. B. m. Wallace, m. biology, Nonviability of cells with oxidative defects in galactose medium: a screening test for affected patient fibroblasts. *Biochemical medicine and metabolic biology* **48**, 122-126 (1992).
39. L. D. Marroquin, J. Hynes, J. A. Dykens, J. D. Jamieson, Y. J. T. s. Will, Circumventing the Crabtree effect: replacing media glucose with galactose increases susceptibility of HepG2 cells to mitochondrial toxicants. *Toxicological sciences* **97**, 539-547 (2007).
40. V. M. Gohil, S. A. Sheth, R. Nilsson, A. P. Wojtovich, J. H. Lee, F. Perocchi, W. Chen, C. B. Clish, C. Ayata, P. S. Brookes, V. K. Mootha, Nutrient-sensitized screening for drugs that shift energy metabolism from mitochondrial respiration to glycolysis. *Nature Biotechnology* **28**, 249-255 (2010).
41. M. Selt, C. A. Bartlett, A. R. Harvey, S. A. Dunlop, M. Fitzgerald, Limited restoration of visual function after partial optic nerve injury; a time course study using the calcium channel blocker lomerizine. *Brain research bulletin* **81**, 467-471 (2010).
42. T. Iwamoto, T. Morita, T. Kanazawa, H. Ohtaka, K. Ito, Effects of KB-2796, a new calcium antagonist, and other diphenylpiperazines on [3H]nitrendipine binding. *Jpn J Pharmacol* **48**, 241-247 (1988).
43. S. Iwasaki, M. Ushio, Y. Chihara, K. Ito, K. Sugasawa, T. J. A. O.-L. Murofushi, Migraine-associated vertigo: clinical characteristics of Japanese patients and effect of lomerizine, a calcium channel antagonist. *Acta Oto-Laryngologica* **127**, 45-49 (2007).
44. M. T. Scott, K. Korfi, P. Saffrey, L. E. Hopcroft, R. Kinstrie, F. Pellicano, C. Guenther, P. Gallipoli, M. Cruz, K. Dunn, Epigenetic Reprogramming Sensitizes CML Stem Cells to Combined EZH2 and Tyrosine Kinase InhibitionEZH2 and Tyrosine Kinase Inhibition in CML Stem Cells. *Cancer discovery* **6**, 1248-1257 (2016).
45. O. L. E. Thastrup, P. J. Cullen, B. K. Drøbak, M. R. Hanley, A. P. Dawson, Thapsigargin, a tumor promoter, discharges intracellular Ca2+ stores by specific inhibition of the endoplasmic reticulum Ca2 (+)-ATPase. *Proceedings of the National Academy of Sciences* **87**, 2466-2470 (1990).
46. R. DeFronzo, G. A. Fleming, K. Chen, T. A. Bicsak, Metformin-associated lactic acidosis: Current perspectives on causes and risk. *Metabolism* **65**, 20-29 (2016).
47. M. Fulop, H. D. Hoberman, Phenformin-associated metabolic acidosis. *Diabetes* **25**, 292-296 (1976).
48. K. Birsoy, T. Wang, W. W. Chen, E. Freinkman, M. Abu-Remaileh, D. M. Sabatini, An Essential Role of the Mitochondrial Electron Transport Chain in Cell Proliferation Is to Enable Aspartate Synthesis. *Cell* **162**, 540-551 (2015).
49. R. M. Denton, Regulation of mitochondrial dehydrogenases by calcium ions. *Biochimica et Biophysica Acta (BBA)-Bioenergetics* **1787**, 1309-1316 (2009).

50. F. Pellicano, L. Park, L. E. M. Hopcroft, M. M. Shah, L. Jackson, M. T. Scott, C. J. Clarke, A. Sinclair, S. A. Abraham, A. Hair, G. V. Helgason, M. Aspinall-O'Dea, R. Bhatia, G. Leone, K. R. Kranc, A. D. Whetton, T. L. Holyoake, hsa-mir183/EGR1-mediated regulation of E2F1 is required for CML stem/progenitor cell survival. *Blood* **131**, 1532-1544 (2018).
51. K. M. Rattigan, Z. Brabcova, D. Sarnello, M. M. Zarou, K. Roy, R. Kwan, L. de Beauchamp, A. Dawson, A. Ianniciello, A. Khalaf, E. R. Kalkman, M. T. Scott, K. Dunn, D. Sumpton, A. M. Michie, M. Copland, S. Tardito, E. Gottlieb, G. Vignir Helgason, Pyruvate anaplerosis is a targetable vulnerability in persistent leukaemic stem cells. *Nature Communications* **14**, 4634 (2023).
52. V. Aires, A. Hichami, G. Boulay, N. A. Khan, Activation of TRPC6 calcium channels by diacylglycerol (DAG)-containing arachidonic acid: a comparative study with DAG-containing docosahexaenoic acid. *Biochimie* **89**, 926-937 (2007).
53. H. Lee, J. W. Kim, D. K. Kim, D. K. Choi, S. Lee, J. H. Yu, O.-B. Kwon, J. Lee, D.-S. Lee, J. H. J. I. j. o. m. s. Kim, Calcium channels as novel therapeutic targets for ovarian cancer stem cells. *International Journal of Molecular Sciences* **21**, 2327 (2020).
54. A. J. G. Baxter, J. Dixon, F. Ince, C. N. Manners, S. J. Teague, Discovery and synthesis of methyl 2, 5-dimethyl-4-[2-(phenylmethyl) benzoyl]-1H-pyrrole-3-carboxylate (FPL 64176) and analogs: the first examples of a new class of calcium channel activator. *Journal of medicinal chemistry* **36**, 2739-2744 (1993).
55. K. Leuner, V. Kazanski, M. Muller, K. Essin, B. Henke, M. Gollasch, C. Harteneck, W. E. Müller, Hyperforin—a key constituent of St. John's wort specifically activates TRPC6 channels. *The FASEB Journal* **21**, 4101-4111 (2007).
56. S. Thellung, T. Florio, V. Villa, A. Corsaro, S. Arena, C. Amico, M. Robello, M. Salmona, G. Forloni, O. Bugiani, F. Tagliavini, G. Schettini, Apoptotic cell death and impairment of L-type voltage-sensitive calcium channel activity in rat cerebellar granule cells treated with the prion protein fragment 106-126. *Neurobiology of disease* **7**, 299-309 (2000).
57. B. L. Lin, D. Matera, J. F. Doerner, N. Zheng, D. Del Camino, S. Mishra, H. Bian, S. Zeveleva, X. Zhen, N. T. Blair, J. A. Chong, D. P. Hessler, D. Bedja, G. Zhu, G. K. Muller, M. J. Ranek, L. Pantages, M. McFarland, M. R. Netherton, A. Berry, D. Wong, G. Rast, H. S. Qian, S. M. Weldon, J. J. Kuo, A. Sauer, C. Sarko, M. M. Moran, D. A. Kass, S. S. Pullen, In vivo selective inhibition of TRPC6 by antagonist BI 749327 ameliorates fibrosis and dysfunction in cardiac and renal disease. *Proc Natl Acad Sci U S A* **116**, 10156-10161 (2019).
58. M. J. Henderson, H. A. Baldwin, C. A. Werley, S. Boccardo, L. R. Whitaker, X. Yan, G. T. Holt, E. R. Schreiter, L. L. Looger, A. E. Cohen, D. S. Kim, B. K. Harvey, A Low Affinity GCaMP3 Variant (GCaMPer) for Imaging the Endoplasmic Reticulum Calcium Store. *PloS one* **10**, e0139273 (2015).
59. Y.-S. Bae, T. G. Lee, J. C. Park, J. H. Hur, Y. Kim, K. Heo, J.-Y. Kwak, P.-G. Suh, S. H. Ryu, Identification of a compound that directly stimulates phospholipase C activity. *Molecular pharmacology* **63**, 1043-1050 (2003).
60. T. Maruyama, T. Kanaji, S. Nakade, T. Kanno, K. J. T. J. o. B. Mikoshiba, 2APB, 2-aminoethoxydiphenyl borate, a membrane-penetrable modulator of Ins (1, 4, 5) P3-induced Ca2+ release. **122**, 498-505 (1997).

61. L. Missiaen, G. Callewaert, H. De Smedt, J. B. Parys, 2-Aminoethoxydiphenyl borate affects the inositol 1,4,5-trisphosphate receptor, the intracellular Ca2+pump and the non-specific Ca2+leak from the non-mitochondrial Ca2+stores in permeabilized A7r5 cells. *Cell Calcium* **29**, 111-116 (2001).
62. C. Bellodi, M. R. Lidonnici, A. Hamilton, G. V. Helgason, A. R. Soliera, M. Ronchetti, S. Galavotti, K. W. Young, T. Selmi, R. Yacobi, R. A. Van Etten, N. Donato, A. Hunter, D. Dinsdale, E. Tirro, P. Vigneri, P. Nicotera, M. J. Dyer, T. Holyoake, P. Salomoni, B. Calabretta, Targeting autophagy potentiates tyrosine kinase inhibitor-induced cell death in Philadelphia chromosome-positive cells, including primary CML stem cells. *J Clin Invest* **119**, 1109-1123 (2009).
63. A. Ianniciello, M. M. Zarou, K. M. Rattigan, M. Scott, A. Dawson, K. Dunn, Z. Brabcova, E. R. Kalkman, C. Nixon, A. M. Michie, M. Copland, D. Vetrie, M. Ambler, B. Saxty, G. V. Helgason, ULK1 inhibition promotes oxidative stress-induced differentiation and sensitizes leukemic stem cells to targeted therapy. *Science translational medicine* **13**, eabd5016 (2021).
64. M. Lazarou, D. A. Sliter, L. A. Kane, S. A. Sarraf, C. Wang, J. L. Burman, D. P. Sideris, A. I. Fogel, R. J. J. N. Youle, The ubiquitin kinase PINK1 recruits autophagy receptors to induce mitophagy. *Nature* **524**, 309-314 (2015).
65. C. Wang, A Sensitive and Quantitative mKeima Assay for Mitophagy via FACS. *Current protocols in cell biology* **86**, e99 (2020).
66. C. Liu, T. E. Hermann, Characterization of ionomycin as a calcium ionophore. *The Journal of biological chemistry* **253**, 5892-5894 (1978).
67. G. Hernandez, C. Thornton, A. Stotland, D. Lui, J. Sin, J. Ramil, N. Magee, A. Andres, G. Quarato, R. S. Carreira, M. R. Sayen, R. Wolkowicz, R. A. Gottlieb, MitoTimer. *Autophagy* **9**, 1852-1861 (2013).
68. P. Martín-Maestro, R. Gargini, E. García, G. Perry, J. Avila, V. J. O. M. García-Escudero, C. Longevity, Slower dynamics and aged mitochondria in sporadic Alzheimer's disease. *Oxidative Medicine and Cellular Longevity* **2017**, (2017).
69. C. Mauvezin, T. P. Neufeld, Bafilomycin A1 disrupts autophagic flux by inhibiting both V-ATPase-dependent acidification and Ca-P60A/SERCA-dependent autophagosome-lysosome fusion. *Autophagy* **11**, 1437-1438 (2015).
70. A. W. Ferree, K. Trudeau, E. Zik, I. Y. Benador, G. Twig, R. A. Gottlieb, O. S. J. A. Shirihai, MitoTimer probe reveals the impact of autophagy, fusion, and motility on subcellular distribution of young and old mitochondrial protein and on relative mitochondrial protein age. *Autophagy* **9**, 1887-1896 (2013).
71. P. J. Fernandez-Marcos, J. J. T. A. j. o. c. n. Auwerx, Regulation of PGC-1α, a nodal regulator of mitochondrial biogenesis. *The American journal of clinical nutrition* **93**, 884S-890S (2011).
72. H. Herrmann, I. Sadovnik, G. Eisenwort, T. Rülicke, K. Blatt, S. Herndlhofer, M. Willmann, G. Stefanzl, S. Baumgartner, G. J. B. a. Greiner, Delineation of target expression profiles in CD34+/CD38− and CD34+/CD38+ stem and progenitor cells in AML and CML. *Blood Advances* **4**, 5118-5132 (2020).
73. T. O'Hare, W. C. Shakespeare, X. Zhu, C. A. Eide, V. M. Rivera, F. Wang, L. T. Adrian, T. Zhou, W. S. Huang, Q. Xu, C. A. Metcalf, 3rd, J. W. Tyner, M. M. Loriaux, A. S. Corbin, S. Wardwell, Y. Ning, J. A. Keats, Y. Wang, R. Sundaramoorthi, M. Thomas, D. Zhou, J. Snodgrass, L. Commodore, T. K. Sawyer, D. C. Dalgarno, M. W. Deininger, B.

J. Druker, T. Clackson, AP24534, a pan-BCR-ABL inhibitor for chronic myeloid leukemia, potently inhibits the T315I mutant and overcomes mutation-based resistance. *Cancer Cell* **16**, 401-412 (2009).
74. A. A. Wylie, J. Schoepfer, W. Jahnke, S. W. Cowan-Jacob, A. Loo, P. Furet, A. L. Marzinzik, X. Pelle, J. Donovan, W. Zhu, S. Buonamici, A. Q. Hassan, F. Lombardo, V. Iyer, M. Palmer, G. Berellini, S. Dodd, S. Thohan, H. Bitter, S. Branford, D. M. Ross, T. P. Hughes, L. Petruzzelli, K. G. Vanasse, M. Warmuth, F. Hofmann, N. J. Keen, W. R. Sellers, The allosteric inhibitor ABL001 enables dual targeting of BCR-ABL1. *Nature* **543**, 733-737 (2017).
75. N. J. Donato, J. Y. Wu, J. Stapley, G. Gallick, H. Lin, R. Arlinghaus, M. Talpaz, BCR-ABL independence and LYN kinase overexpression in chronic myelogenous leukemia cells selected for resistance to STI571. *Blood* **101**, 690-698 (2003).
76. R. Moschoi, V. Imbert, M. Nebout, J. Chiche, D. Mary, T. Prebet, E. Saland, R. Castellano, L. Pouyet, Y. Collette, N. Vey, C. Chabannon, C. Recher, J. E. Sarry, D. Alcor, J. F. Peyron, E. Griessinger, Protective mitochondrial transfer from bone marrow stromal cells to acute myeloid leukemic cells during chemotherapy. *Blood* **128**, 253-264 (2016).
77. M. D. Kolba, W. Dudka, M. Zaręba-Kozioł, A. Kominek, P. Ronchi, L. Turos, P. Chroscicki, J. Wlodarczyk, Y. Schwab, A. J. C. d. Klejman, disease, Tunneling nanotube-mediated intercellular vesicle and protein transfer in the stroma-provided imatinib resistance in chronic myeloid leukemia cells. **10**, 817 (2019).
78. A. Adamo, P. Delfino, A. Gatti, A. Bonato, P. Takam Kamga, R. Bazzoni, S. Ugel, A. Mercuri, S. Caligola, M. J. F. i. C. Krampera, D. Biology, HS-5 and HS-27A stromal cell lines to study bone marrow mesenchymal stromal cell-mediated support to cancer development. **8**, 584232 (2020).
79. B. M. Kitay, R. McCormack, Y. Wang, P. Tsoulfas, R. G. Zhai, Mislocalization of neuronal mitochondria reveals regulation of Wallerian degeneration and NMNAT/WLD(S)-mediated axon protection independent of axonal mitochondria. *Hum Mol Genet* **22**, 1601-1614 (2013).
80. P. H. Miller, G. Rabu, M. MacAldaz, D. J. Knapp, A. M. Cheung, K. Dhillon, N. Nakamichi, P. A. Beer, L. D. Shultz, R. K. Humphries, C. J. Eaves, Analysis of parameters that affect human hematopoietic cell outputs in mutant c-kit-immunodeficient mice. *Exp Hematol* **48**, 41-49 (2017).
81. Y. Ren, T. Liu, G. Song, Y. Hu, J. Liang, Determination of lomerizine in human plasma by liquid chromatography/tandem mass spectrometry and its application to a pharmacokinetic study. *J Chromatogr B Analyt Technol Biomed Life Sci* **947-948**, 96-102 (2014).
82. N. Wang, J. Yin, N. You, S. Yang, D. Guo, Y. Zhao, Y. Ru, X. Liu, H. Cheng, Q. Ren, T. Cheng, X. Ma, TWIST1 preserves hematopoietic stem cell function via the CACNA1B/Ca2+/mitochondria axis. *Blood* **137**, 2907-2919 (2021).
83. C. M. V. Barbosa, R. A. Fock, A. A. Hastreiter, C. Reutelingsperger, M. Perretti, E. J. Paredes-Gamero, S. H. P. Farsky, Extracellular annexin-A1 promotes myeloid/granulocytic differentiation of hematopoietic stem/progenitor cells via the Ca2+/MAPK signalling transduction pathway. *Cell Death Discovery* **5**, 135 (2019).
84. L. L. Luchsinger, A. Strikoudis, N. M. Danzl, E. C. Bush, M. O. Finlayson, P. Satwani, M. Sykes, M. Yazawa, H.-W. J. C. S. C. Snoeck, Harnessing hematopoietic stem cell low

intracellular calcium improves their maintenance in vitro. *Cell Stem Cell* **25**, 225-240. e227 (2019).
85. T. Umemoto, M. Hashimoto, T. Matsumura, A. Nakamura-Ishizu, T. J. J. o. E. M. Suda, Ca2+–mitochondria axis drives cell division in hematopoietic stem cells. *Journal of Experimental Medicine* **215**, 2097-2113 (2018).
86. J. Soboloff, Y. Zhang, M. Minden, S. A. J. E. H. Berger, Sensitivity of myeloid leukemia cells to calcium influx blockade: application to bone marrow purging. *Experimental Hematology* **30**, 1219-1226 (2002).
87. M. Shao, X. Teng, X. Guo, H. Zhang, Y. Huang, J. Cui, X. Si, L. Ding, X. Wang, X. J. A. S. Li, Inhibition of Calcium Signaling Prevents Exhaustion and Enhances Anti-Leukemia Efficacy of CAR-T Cells via SOCE-Calcineurin-NFAT and Glycolysis Pathways. *Advanced Science* **9**, 2103508 (2022).
88. A. Inguva, K. L. Engel, H. Tolison, M. J. Althoff, S. Pei, M. L. Amaya, A. Krug, M. Minhajuddin, C. L. Jones, A. E. J. B. Gillen, Intracellular Calcium Localization Mediates the Activity of Venetoclax in Targeting Acute Myeloid Leukemia Stem Cells. **140**, 5922-5923 (2022).
89. X. He, C. Hawkins, L. Lawley, M. Wunderlich, B. Mizukawa, X.-m. Zha, S. Halene, J. J. B. Fang, The GPR68/BCL2 Axis Remodels Metabolism in AML By Relocating Calcium. *Blood* **134**, 2661 (2019).
90. T. Fukushima, Y. Tanaka, F. K. Hamey, C.-H. Chang, T. Oki, S. Asada, Y. Hayashi, T. Fujino, T. Yonezawa, R. Takeda, Discrimination of dormant and active hematopoietic stem cells by G0 marker reveals dormancy regulation by cytoplasmic calcium. *Cell Reports* **29**, 4144-4158 (2019).
91. A. I. Sheth, K. Engel, H. Tolison, M. J. Althoff, M. L. Amaya, A. Krug, T. Young, S. Pei, S. B. Patel, M. Minhajuddin, A. Winters, R. Miller, I. Shelton, J. St-Germain, T. Ling, C. Jones, B. Raught, A. Gillen, M. Ransom, S. Staggs, C. A. Smith, D. A. Pollyea, B. M. Stevens, C. T. Jordan, Targeting Acute Myeloid Leukemia Stem Cells Through Perturbation of Mitochondrial Calcium. *bioRxiv*, (2023).
92. J. Vande Voorde, T. Ackermann, N. Pfetzer, D. Sumpton, G. Mackay, G. Kalna, C. Nixon, K. Blyth, E. Gottlieb, S. J. S. a. Tardito, Improving the metabolic fidelity of cancer models with a physiological cell culture medium. **5**, eaau7314 (2019).
93. J. Xiao, D. Liang, H. Zhao, Y. Liu, H. Zhang, X. Lu, Y. Liu, J. Li, L. Peng, Y. H. Chen, 2-Aminoethoxydiphenyl borate, a inositol 1,4,5-triphosphate receptor inhibitor, prevents atrial fibrillation. *Experimental biology and medicine (Maywood, N.J.)* **235**, 862-868 (2010).
94. C. Wang, A sensitive and quantitative mKeima assay for mitophagy via FACS. *Current protocols in cell biology* **86**, e99 (2020).
95. J. K. Salabei, A. A. Gibb, B. G. J. N. p. Hill, Comprehensive measurement of respiratory activity in permeabilized cells using extracellular flux analysis. *Nature Protocols* **9**, 421-438 (2014).
96. J. Vande Voorde, T. Ackermann, N. Pfetzer, D. Sumpton, G. Mackay, G. Kalna, C. Nixon, K. Blyth, E. Gottlieb, S. Tardito, Improving the metabolic fidelity of cancer models with a physiological cell culture medium. *Science advances* **5**, eaau7314 (2019).
97. M. Pietzke, A. Vazquez, Metabolite AutoPlotter - an application to process and visualise metabolite data in the web browser. *Cancer & metabolism* **8**, 15 (2020).

98. Z. Pang, J. Chong, G. Zhou, D. A. de Lima Morais, L. Chang, M. Barrette, C. Gauthier, P.-É. Jacques, S. Li, J. Xia, MetaboAnalyst 5.0: narrowing the gap between raw spectra and functional insights. *Nucleic Acids Research* **49**, W388-W396 (2021).
99. J. R. Liang, E. Lingeman, T. Luong, S. Ahmed, M. Muhar, T. Nguyen, J. A. Olzmann, J. E. Corn, A Genome-wide ER-phagy Screen Highlights Key Roles of Mitochondrial Metabolism and ER-Resident UFMylation. *Cell* **180**, 1160-1177 e1120 (2020).

Acknowledgments: We thank all patients and healthy donors who donated samples and the National Health Service (NHS) Greater Glasgow and Clyde Biorepository, A. Hair for sample processing and T. Gilbey for cell sorting. We thank C. J. Eaves for providing NRGW^{41} mice (*80*), A. Faisal Taqi and A. G. West for help with gene editing confirmation, V. Garcia for providing MitoTimer construct (*68*) and J. R. Liang and J. Corn for providing TOM20 eGFP construct (*99*). We thank the Core Services and Advanced Technologies at the Cancer Research UK Beatson Institute (C596/A17196; A31287) and the Cancer Research UK Beatson Institute mouse facility staff for housing of mice and help with xenograft experiments. S.T. is the inventor of Plasmax cell culture medium. Schematic graphs in Figures 1D, 2C, 7C and supplementary figures S9A and S10 were generated in BioRender - biorender.com.

Funding: This work was supported by Newton-Mosharafa Fund Scholarship (awarded to A.K.). Cancer Research UK (A29754, to G.V.H.), University of Glasgow PhD Studentship (to L.B), Chief Scientist Office (CGA/18/02, to L.B and G.V.H), Blood Cancer UK (formerly Bloodwise; Ref 18006, to G.V.H), The Howat Foundation (to G.V.H.) and Friends of Paul O'Gorman Leukaemia Research Centre (o G.V.H.). Cancer Research UK (A23982) to S.T. and D.S.

Author contributions: A.K. and G.V.H. developed the concept and designed the experiments. A.K. performed most of the experiments. L.B., E.K., D.J. and E.S. performed the drug repurposing screen. L.B., E.K., K.R., E.H., E.S.A.S, M.T.S. and K.D. assisted with in vitro and/or in vivo studies, including data analysis. S.T., D.S. and M.C. provided technical or material support. A.K., J.J. and G.V.H. wrote the manuscript, and all the other authors reviewed it. G.V.H. supervised the work.

Competing interests: M.C. has received research funding from Cyclacel and Incyte, is/has been an advisory board member for Novartis, Incyte, Jazz Pharmaceuticals, Pfizer and Servier, and has received honoraria from Astellas, Novartis, Incyte, Pfizer and Jazz Pharmaceuticals. All other authors declare that they have no competing interests.

Data and materials availability: The publicly available datasets used in this study are available in the EMBL-EBI database under accession code E-MTAB-2581 and E-MTAB-2594 and Gene Expression Omnibus (GEO) database under accession code GSE216837. Relevant codes have been archived in Zenodo repository. LCMS data for analysis of patient samples is in source files. To protect patient privacy, raw LCMS files generated in this study are available upon request to the corresponding author immediately once approval of biobanks ethical approval panel is granted and access will not be time limited. The LCMS samples will be maintained long-term (>10 years) and raw LCMS files will be maintained indefinitely (>10 years on institutes network drive, Redundant Array of Independent Disks (RAID)). Additional information concerning relevant codes and human samples can be obtained from the corresponding author. (Vignir.Helgason@Glasgow.ac.uk). Other source data are provided with this paper.

Figure legends

Fig. 1. **Drug screening reveals lomerizine as a potent mitochondrial respiration inhibitor in CML cell lines.**

(A) OCR and ECAR in K562 and KCL22 cells grown in presence of either 11 mM glucose or 11 mM galactose for 48 hours (*n*=5 wells per condition, representative of *n*=2 independent experiments). Mean ± SD. **(B-C)** Viability measurement using resazurin in K562 cells grown in culture media supplemented with either 11 mM glucose or 11 mM galactose and subjected at same time to increasing concentration of rotenone (**B**) or omacetaxine (**C**) for 24 hours (*n*=3 wells per condition from individual experiment). Mean ± SD. **(D)** Screening approach to identify potential mitochondria respiration inhibitors in CML cells. Cells were treated with 1,274 FDA approved compounds in glucose or galactose media for 3 days followed by resazurin viability assay. Compounds that showed preferential viability inhibition in galactose were selected as potential mitochondria respiration inhibitors. **(E)** Representative OCR profile and quantification of associated basal, maximal, and ATP-linked OCR following treatment with 200 nM EGTA, or 2 mM $CaCl_2$ for 24 hours (n=3 independent experiments). **(F)** Cell count and (**G**) apoptosis following treatment with 200 nM EGTA, or 2 mM $CaCl_2$ for 3 days (*n*=3 independent experiments). For E-G means ± *P*. values were calculated using ANOVA and Tukey or Dunnet's tests was performed to correct for multiple comparisons. NDC, no drug control.

Fig. 2. **Ca^{2+} signaling is upregulated in CML LSCs.**

(A) Normalized enrichment scores extracted from the E-MTAB-2581 transcriptome dataset ($CD34^+CD38^-$ CML and normal cells). **(B)** Representative flow cytometry histogram illustrating

ER mass and relative MFI in $CD34^+$ CML cells and $CD34^+$ normal cells (*n*=3 individual samples each). Means ± *P.* values were calculated using unpaired Student's t-test. **(C)** Experimental approach to measure cytosolic and mitochondrial Ca^{2+} content in response to acute stimulation following culture in presence or absence of treatment for 24 hours and simultaneous staining with 5 µM indo-1 and rhod-2 Ca^{2+} dyes. **(D-E)** Representative flow cytometry profile and relative statistical analyses of (**D**) basal cytosolic and (**E**) mitochondrial Ca^{2+} amounts in $CD34^+$ CML cells and $CD34^+$ normal cells. **(F-G)** Representative kinetic flow cytometry and relative (**F**) cytosolic and (**G**) mitochondrial Ca^{2+} amounts in $CD34^+$ CML and normal cells after acute exposure to 2.5 µM thapsigargin. For D-G, cells were isolated from individuals with CML (*n*=3) or healthy donors (*n*=4), means ± SEM and *P.* values were calculated using unpaired Student's t-test.

Fig. 3. Lomerizine targets mitochondrial metabolism in CML cells.

(A) Peak intensities showing LC-MS quantification of isotopologue metabolites in untreated K562 cells or following treatment with 5 µM lomerizine or 20 nM IACS-010759, cultured in $^{13}C_6$ glucose for 24 hours (*n*=3 wells per group from individual experiment). Data is representative of one of two biological replicates. Means ± SD. *P.* values were calculated using one-way ANOVA and Fisher's LSD test for multiple comparisons. **(B)** Quantification of isotopologue metabolites in sorted $CD34^+38^-$ CML LSCs following treatment with 10 µM lomerizine, 1 µM imatinib, or the combination, cultured in $^{13}C_6$ glucose for 24 (*n*=3). Means ± SEM. P. values were calculated using multiple Student t-tests. **(C)** Amount of IDH3 activity in K562 cells exposed to 5 µM lomerizine, 1 µM imatinib, or the combination for 4 hours (*n*=4 independent experiments). Means ± *P.* values were calculated using one-way ANOVA and Tukey test was performed to correct for multiple comparisons. **(D)** Representative OCR profile and associated quantification of basal, maximal and

ATP-linked OCR following 12 hours treatment with 5 µM lomerizine, 0.5 µM imatinib, or the combination in K562 cells (*n*=3 independent experiments). Means ± *P*. values were calculated using two-way ANOVA test and Tukey test was performed to correct for multiple comparisons. Med, medium; NDC, no drug control; Lom, lomerizine.

Fig. 4. Lomerizine depletes mitochondrial Ca^{2+} through CACNA1D and TRPC6 inhibition.

(**A-B**) Microarray datasets E-MTAB-2581 (LSC versus HSC and LSC versus LPC), E-MTAB-2594 (± imatinib 8 hours and 7 days), and the RNA sequencing dataset GSE216837 (± imatinib 48 hours) were interrogated. (**A**) *CACNA1D* and (**B**) *TRPC6* expression is presented. **(C-D)** Representative kinetic flow cytometry profile as well as the relative (**C**) cytosolic and (**D**) mitochondrial Ca^{2+} contents in $CD34^+$ CML (*n*=3) and normal cells (*n*=4) after acute exposure to 25 µM DOG. **(E)** Relative cytosolic and mitochondrial Ca^{2+} content in response to 25 µM DOG stimulation in untreated, 10 µM lomerizine or 1 µM imatinib treated K562 cells for 24 hours (*n*=4 independent experiments). **(F)** Relative cytosolic and mitochondrial Ca^{2+} content in response to 25 µM FPL stimulation in untreated, 10 µM lomerizine, 10 µM nicardipine, 1 µM imatinib or combination with imatinib treated K562 cells for 24 hours (*n*=3 independent experiments). **(G)** Relative cytosolic and mitochondrial Ca^{2+} content in response to 25 µM hyperforin stimulation in untreated, 10 µM lomerizine, 2.5 µM BI, 1 µM imatinib, or combination with imatinib treated K562 cells for 24 hours (*n*=3 independent experiments). **(H)** Relative cytosolic and mitochondrial Ca^{2+} content in response to 3 µM thapsigargin stimulation in untreated, 10 µM lomerizine or 1 µM imatinib treated K562 cells for 24 hours (*n*=3 independent experiments). (D-H) show means ± SEM where *P*. values were calculated using one-way ANOVA test. Dunnett test was performed to correct for (C and F) multiple comparisons. Tukey test was performed to correct for (F and G)

multiple comparisons. **(I-J)** Representative kinetic flow cytometry illustrating relative ER Ca^{2+} content in response to (**I**) IP3R stimulation using 25 µM m-3M3FBS in untreated, 10 µM lomerizine, 1 µM imatinib, and the combination or in (**J**) untreated, 5 µM 2APB, and the combination of 2APB + lomerizine, or 2APB + imatinib treated GCAPMer-expressing K562 cells for 24 hours (*n*=3 independent experiments). **(K)** Combined analysis of (H) and (G). Means ± *P*. values were calculated using one-way ANOVA test and Tukey test was performed to correct for multiple comparisons. BI, BI-749327; HSC, hematopoietic stem cell; Ima, imatinib; Lom, lomerizine: LSC, leukemic stem cell; LPC, leukemia progenitor cell; NDC, no drug control; Norm, normal; Nic, nicardipine.

Fig. 5. CACNA1D and TRPC6 deletion depletes Ca^{2+} and targets mitochondrial metabolism.

(A-B) Relative cytosolic (**A**) and mitochondrial Ca^{2+} (**B**) content in response to 25 µM FPL64176 (left) or 25 µM hyperforin (right) stimulation in control and KO K562 cells ± 1 µM imatinib for 24 hours (*n*= 3 independent experiments). **(C-D)** ER Ca^{2+} mobilization to (**C**) cytosol and (**D**) mitochondria in response to 3 µM thapsigargin stimulation in control and CACNA1D KO K562 cells (left) or in control and TRPC6 KO K562 cells (right), ± 1 µM imatinib for 24 hours. CACNA1D KO K562 cells were generated using two different gRNAs. **(E-F)** Relative basal, maximal and ATP-linked OCR in (**E**) control and CACNA1D KO K562 cells or (**F**) control and TRPC6 KO cells, ± 1 µM imatinib for 12 hours (*n*= 3 independent experiments). **(G)** Relative IDH3 activity in control and CACNA1D KO (left), or control and TRPC6 KO K562 cells (right), ± 1 µM imatinib for 12 hours (*n*=4 independent experiments). **(H)** Amount of apoptosis in control and CACNA1D KO K562 cells (left) or in control and TRPC6 KO K562 cells (right), ± 0.5 µM imatinib for 72 hours. Cells were stained with APC Annexin V and DAPI. **(I-J)** Cell density as

measured daily for consecutive 3 days in (**I**) control and CACNA1D KO K562 cells or in (**J**) control and TRPC6 KO K562 cells, ± 0.5 µM imatinib for 72 hours (*n*=4 independent experiments). All mean ± *P*. values were calculated using ANOVA test and Tukey test was performed to correct for multiple comparisons. KO, knockout; TRP, TRPC6; VC, vector control.

Fig. 6. Lomerizine selectively targets primitive CML cells *ex vivo*.

(A-B) $CD34^+$ CML (*n*=3) or non-CML (*n*=3) cells were left untreated or treated with 10 µM lomerizine, 1 µM imatinib or combination for 24 hours. Relative cytosolic (left) and mitochondrial (right) Ca^{2+} content in response to 2.5 µM ionomycin stimulation in $CD34^+$ CML (**A**) and $CD34^+$ normal (**B**) samples. (**C**) Basal, maximal and ATP-linked OCR in CML cells treated with the prior described treatment. Means ± SEM and *P*. values were calculated using ANOVA and multiple values were corrected using Tukey test. **(D-K)** $CD34^+$ CML cells and $CD34^+$ normal cells were left untreated or treated with 10 µM lomerizine, 1 µM imatinib, or combination for 3 days (n≥3 $CD34^+$ CML or normal samples). (D, F) Cell density and (E, G) cell viability were measured by manual counting and flow cytometry, respectively. (H, I) Colony-forming cell (CFC) was performed by leaving cells in MethoCult for another 12 days**.** (J, K) $CD34^+CD133^+$ expression was measured by flow cytometry. **(L-M)** $CD34^+$ CML cells were left untreated or treated with 10 µM lomerizine, 1 µM imatinib, or combination for 3 days (*n*=4 individual CML samples). (**L**) CTV count and (**M**) LTC-IC were measured. Values of CTV counts were obtained through counting events in each division. LTC-IC was performed by further culturing cells in MyeloCult for another 5 weeks. (A-M) Means ± SEM and *P*. values were calculated using one-way ANOVA and Tukey test was used for multiple comparisons corrections. Ima, imatinib; NDC, no drug control; Lom, lomerizine.

Fig. 7. Lomerizine inhibits CML tumor burden and targets LSCs in vivo.

(A) NRGW^{41} mice weights (left Y axis) receiving vehicle or weekly escalating I.P. dose of lomerizine (pink squares), starting from 10 mg/kg at week one to 80 mg/kg at week 4 (see right Y axis). On the last day of every week, blood was collected after 1 hour of drug administration. Following the last dose by 24 hours, mice were culled for blood collection. **(B)** Serum was extracted from blood samples and lomerizine concentration was quantified using LC-MS. **(C)** Experimental approach of KCL22 xenotransplantation into NRGW^{41} mice. Mice were transplanted with 4X10^{6} KCL22 cells and left for 2 weeks followed by another 4 weeks of treatments (vehicle, 80 mg/kg lomerizine I.P. once daily, 50 mg twice daily oral gavage of imatinib, or combination of lomerizine with imatinib). Mice were left to measure tumor burden and survival analysis. **(D)** Combined images of extramedullary tumors (left) and their number (right) harvested per sacrificed mouse (*n*= 5-6 per group). Mean ± *P*. values were calculated using one-way ANOVA test and Tukey was performed to correct for multiple comparisons. **(E)** Kaplan-Meier survival analysis of mice from C. *P.* value was calculated using the log-rank (Mantel-Cox) test between every two group as well as overall *P*. value without group specification. (**F-G**) Patient-derived xenograft (PDX) into NRGW^{41} mice (experimental plan is shown in fig S9A). **(F)** Flow cytometry gating strategy and **(G)** the logarithmic transformed absolute counts of human CD45^{+} cells, CD34^{+} cells, and CD34^{+}CD38^{-} cells of sacrificed NRGW^{41} mice from PDX experiment after receiving vehicle, 80 mg/kg lomerizine once daily I.P., 100 mg/kg imatinib twice daily by oral gavage, or combination of lomerizine and imatinib for 4 weeks. Means ± *P*. values were calculated using one-way ANOVA test and Bonferroni was performed to correct for multiple

comparisons. Data passed normality test only on logarithmic transformed values. Ima, imatinib; Lom, lomerizine.

Fig. 1

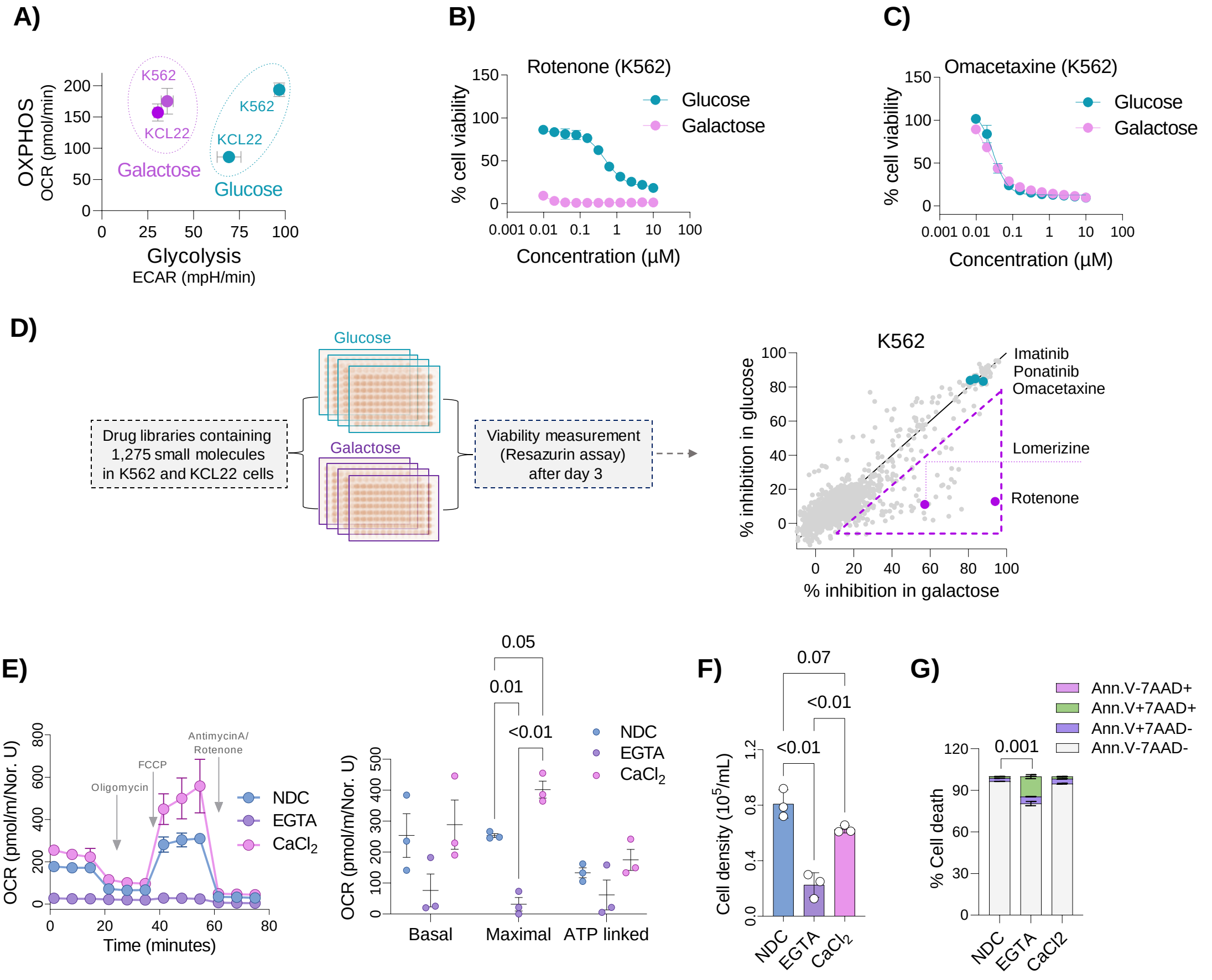
A)
OXPHOS
OCR (pmol/min)
200
150
100
50
0
K562
KCL22
Galactose
K562
KCL22
Glucose
0
25
50
75
100
Glycolysis
ECAR (mpH/min)
B)
Rotenone (K562)
% cell viability
150
100
50
0
Glucose
Galactose
0.001 0.01 0.1 1 10 100
Concentration (µM)
C)
Omacetaxine (K562)
% cell viability
150
100
50
0
Glucose
Galactose
0.001 0.01 0.1 1 10 100
Concentration (µM)
D)
Glucose
Galactose
Drug libraries containing
1,275 small molecules
in K562 and KCL22 cells
Viability measurement
(Resazurin assay)
after day 3
K562
% inhibition in glucose
100
80
60
40
20
0
Imatinib
Ponatinib
Omacetaxine
Lomerizine
Rotenone
0 20 40 60 80 100
% inhibition in galactose
E)
OCR (pmol/m/Nor. U)
800
600
400
200
0
Oligomycin
FCCP
AntimycinA/
Rotenone
NDC
EGTA
CaCl2
0 20 40 60 80
Time (minutes)
OCR (pmol/m/Nor. U)
0 100 200 300 400 500
0.05
0.01
<0.01
NDC
EGTA
CaCl2
Basal
Maximal
ATP linked
F)
Cell density (10^5/mL)
1.2
0.8
0.4
0.0
0.07
<0.01
<0.01
NDC
EGTA
CaCl2
G)
Ann.V-7AAD+
Ann.V+7AAD+
Ann.V+7AAD-
Ann.V-7AAD-
% Cell death
120
90
60
30
0
0.001
NDC
EGTA
CaCl2

Fig. 2

A)

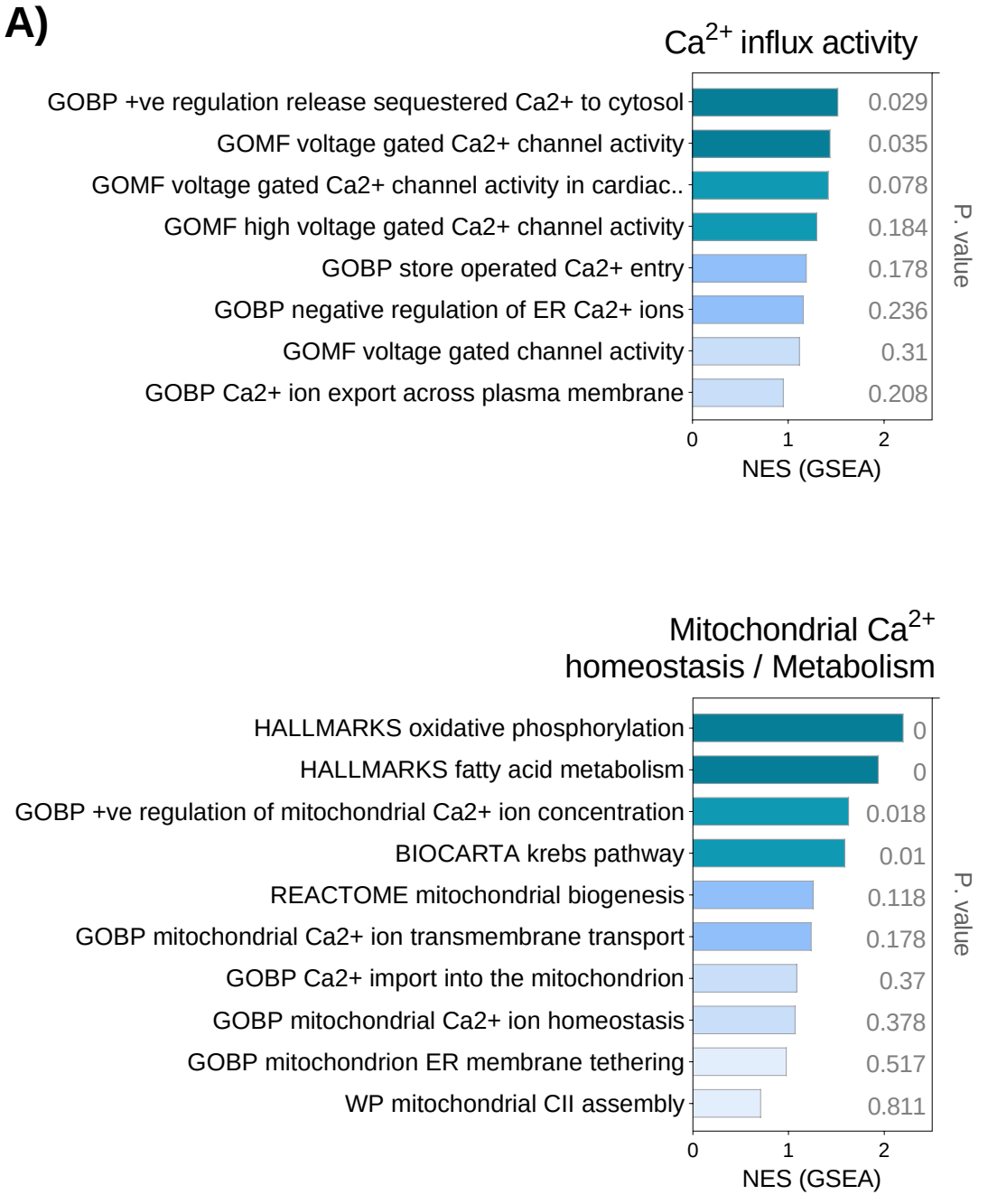

B)

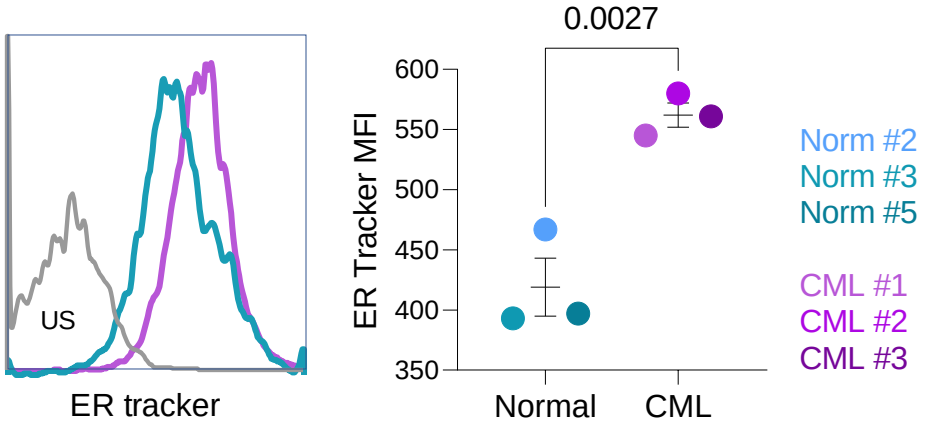

C)

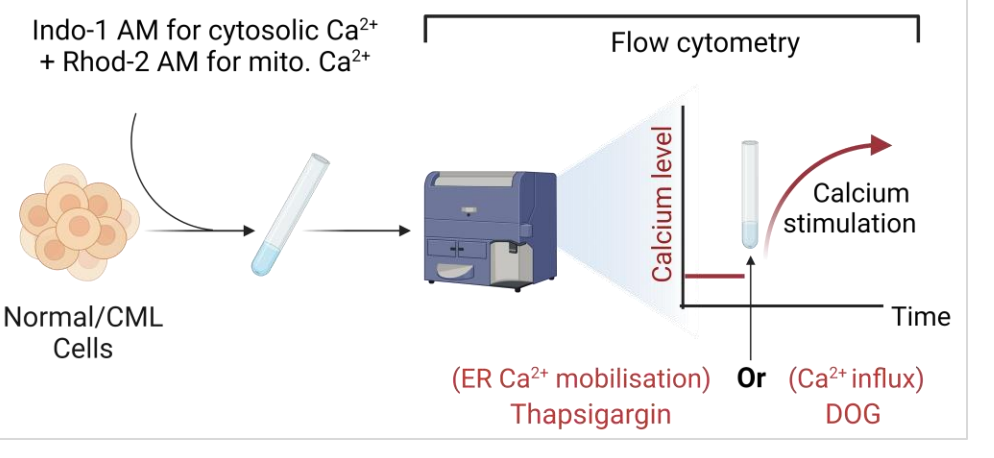

D)

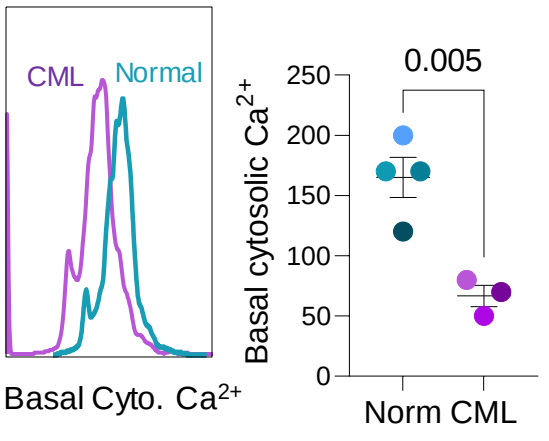

E)

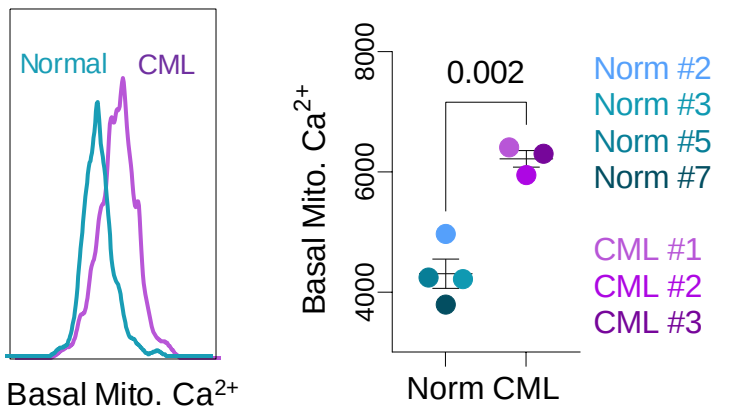

F)

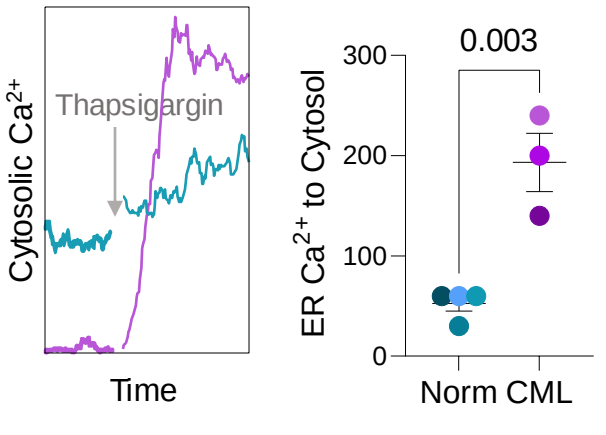

G)

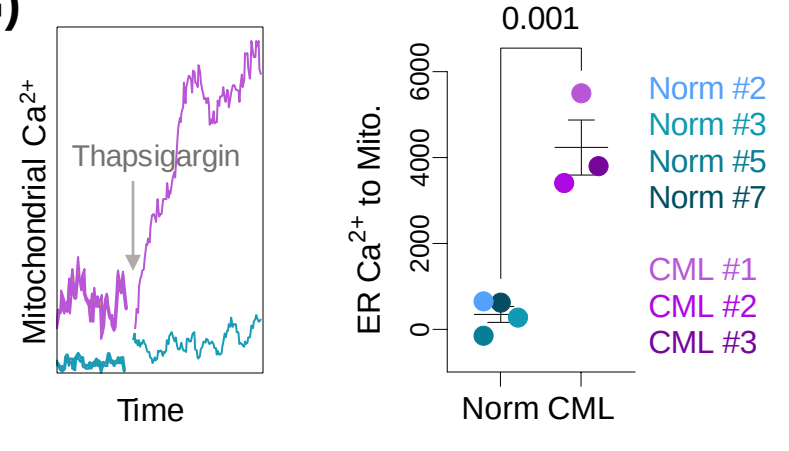

Fig. 3

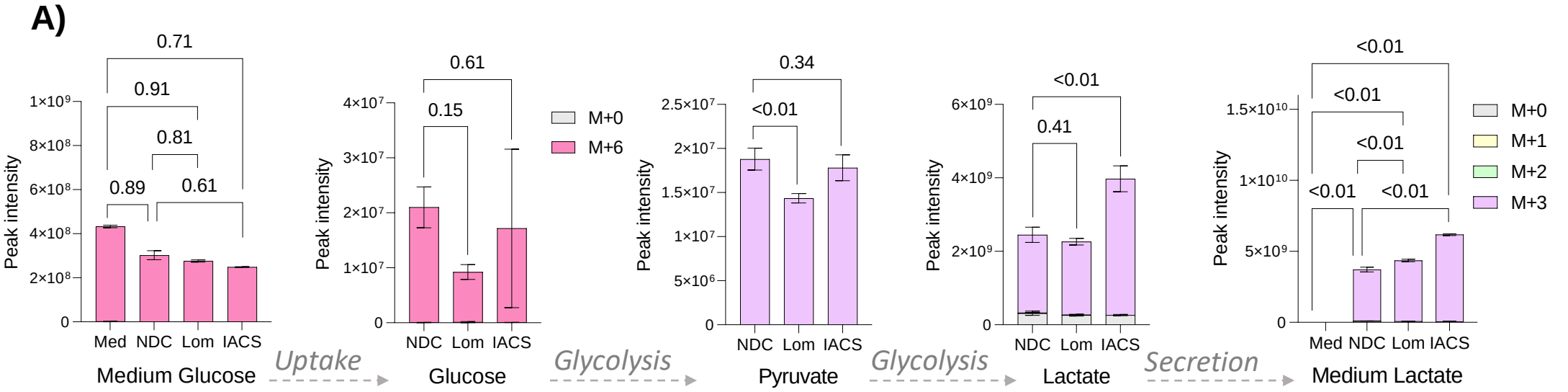
A)
Peak intensity
Med NDC Lom IACS
Medium Glucose
Uptake
Glucose
Glycolysis
Pyruvate
Glycolysis
Lactate
Secretion
Medium Lactate
M+0
M+1
M+2
M+3
M+4
M+5
M+6
M+7
M+8
Citrate
TCA cycle
AKG
TCA cycle
Succinate
TCA cycle
Malate
Aspartate
ATP
CTP
UTP

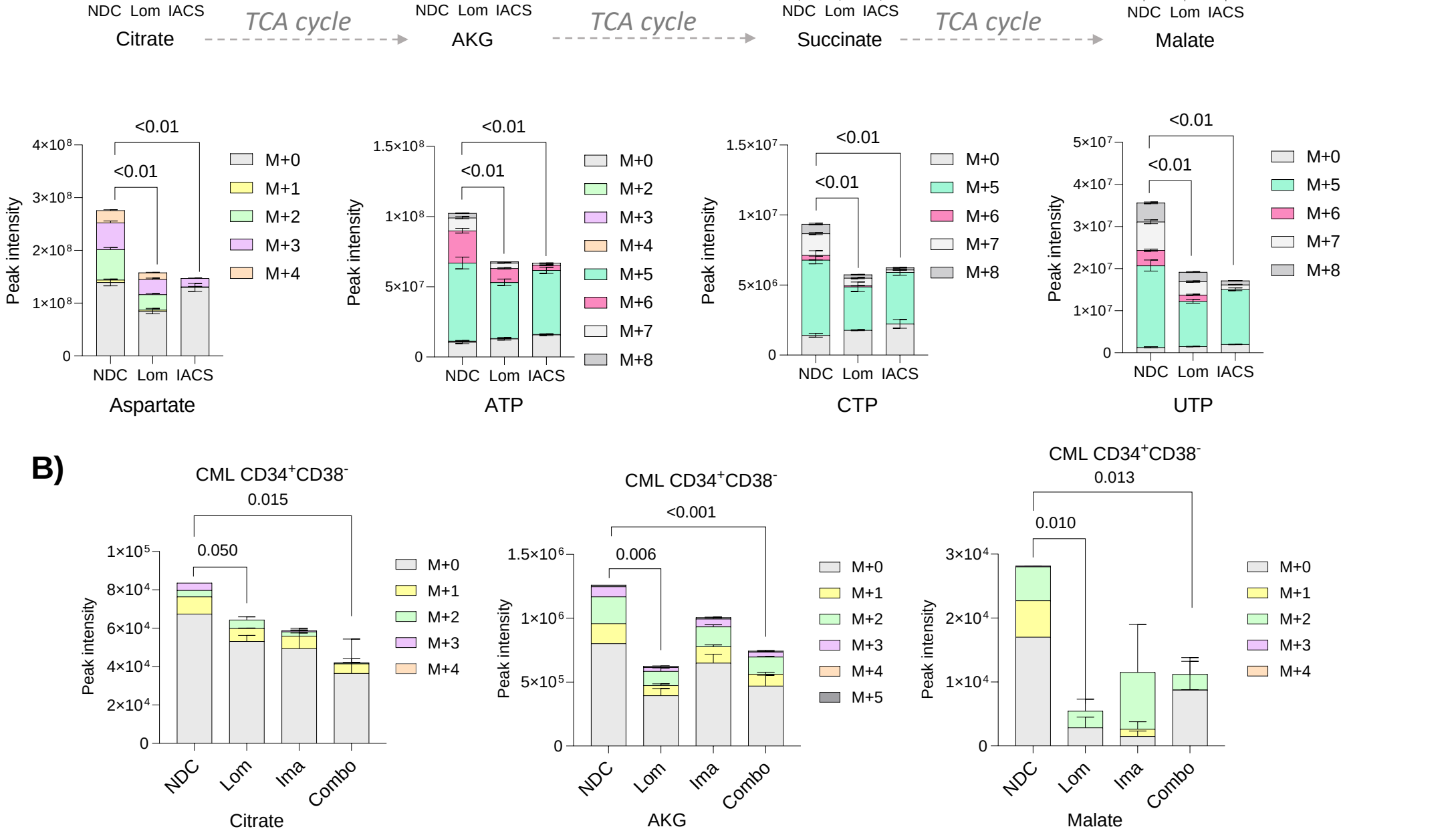
B)
CML CD34+CD38-
Peak intensity
NDC Lom Ima Combo
Citrate
AKG
Malate
M+0
M+1
M+2
M+3
M+4
M+5

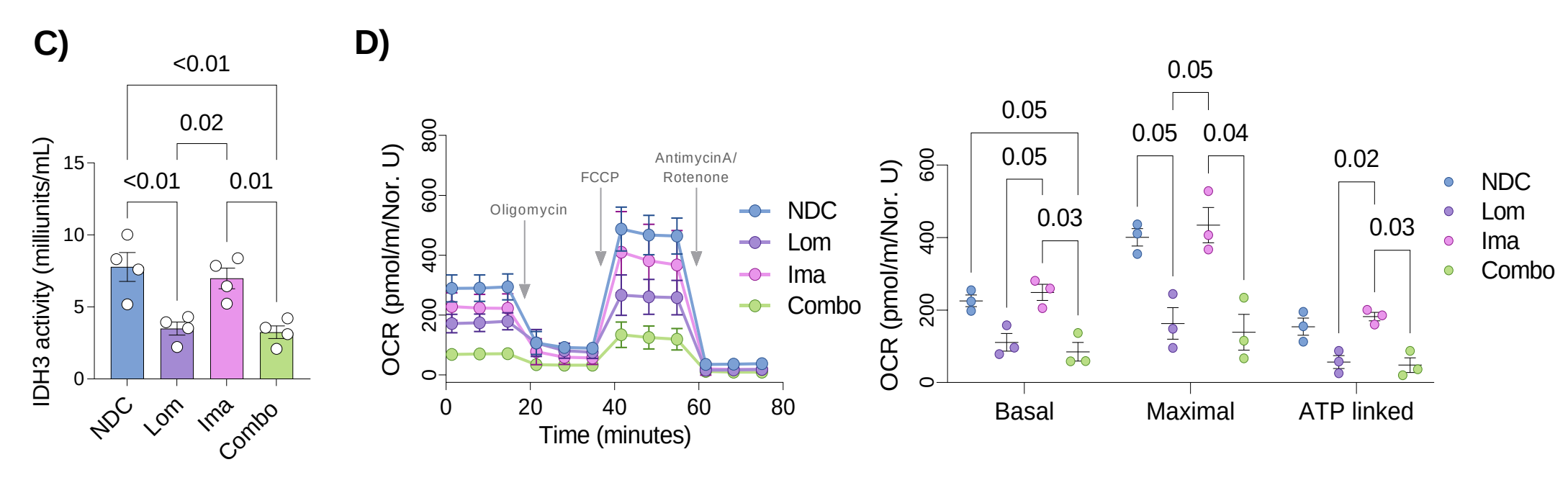
C)
IDH3 activity (milliunits/mL)
NDC Lom Ima Combo
D)
OCR (pmol/m/Nor. U)
Time (minutes)
Oligomycin
FCCP
AntimycinA/
Rotenone
NDC
Lom
Ima
Combo
Basal
Maximal
ATP linked

Fig. 4

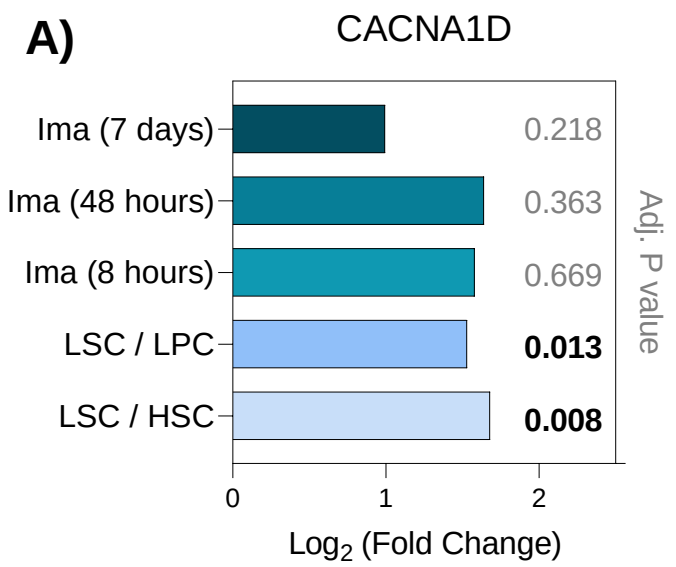
A)
CACNA1D
Ima (7 days)
Ima (48 hours)
Ima (8 hours)
LSC / LPC
LSC / HSC
0.218
0.363
0.669
0.013
0.008
Adj. P value
0
1
2
Log2 (Fold Change)

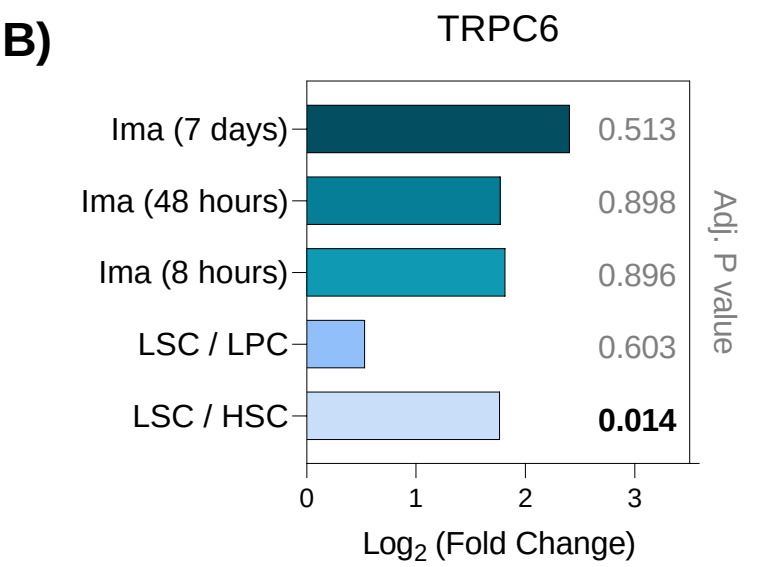
B)
TRPC6
Ima (7 days)
Ima (48 hours)
Ima (8 hours)
LSC / LPC
LSC / HSC
0.513
0.898
0.896
0.603
0.014
Adj. P value
0
1
2
3
Log2 (Fold Change)

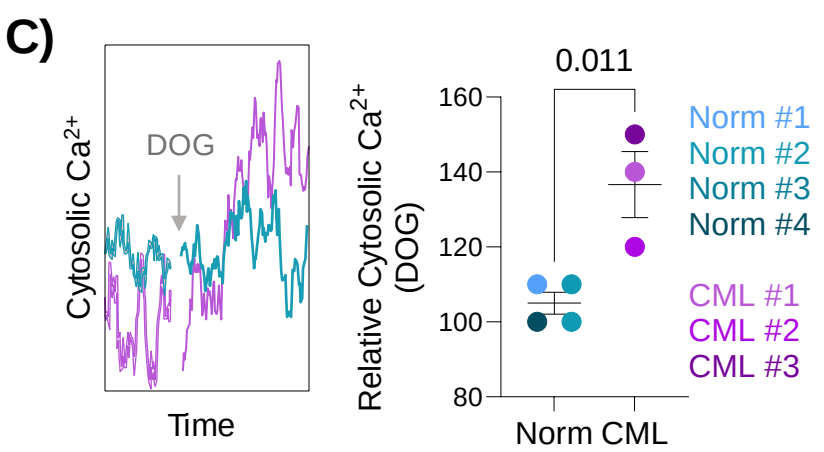
C)
Cytosolic Ca2+
DOG
Time
Relative Cytosolic Ca2+ (DOG)
0.011
Norm CML
Norm #1
Norm #2
Norm #3
Norm #4
CML #1
CML #2
CML #3

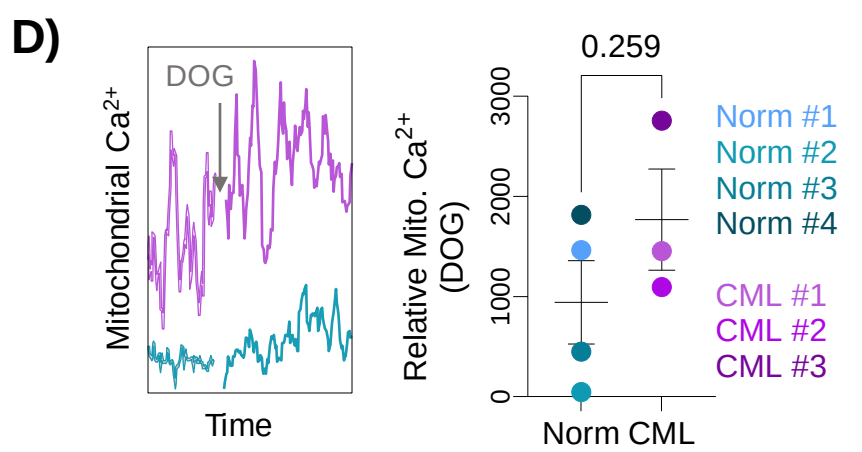
D)
Mitochondrial Ca2+
DOG
Time
Relative Mito. Ca2+ (DOG)
0.259
Norm CML
Norm #1
Norm #2
Norm #3
Norm #4
CML #1
CML #2
CML #3

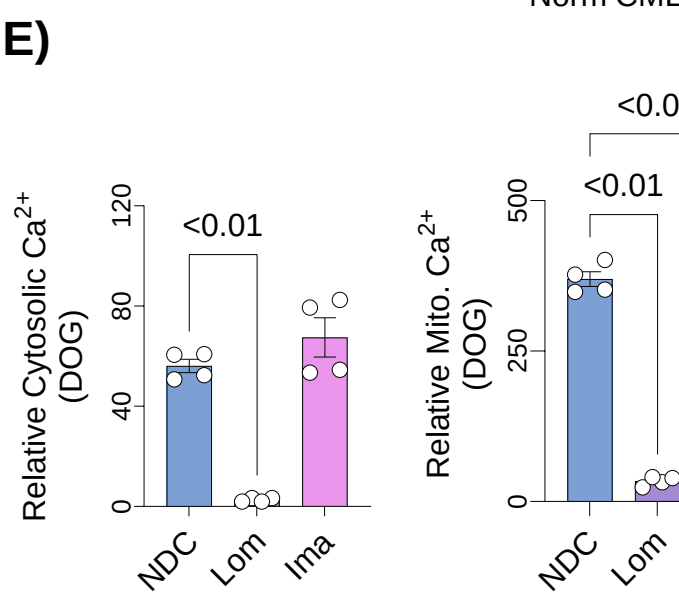
E)
Relative Cytosolic Ca2+ (DOG)
<0.01
NDC
Lom
Ima
Relative Mito. Ca2+ (DOG)
<0.01
<0.01

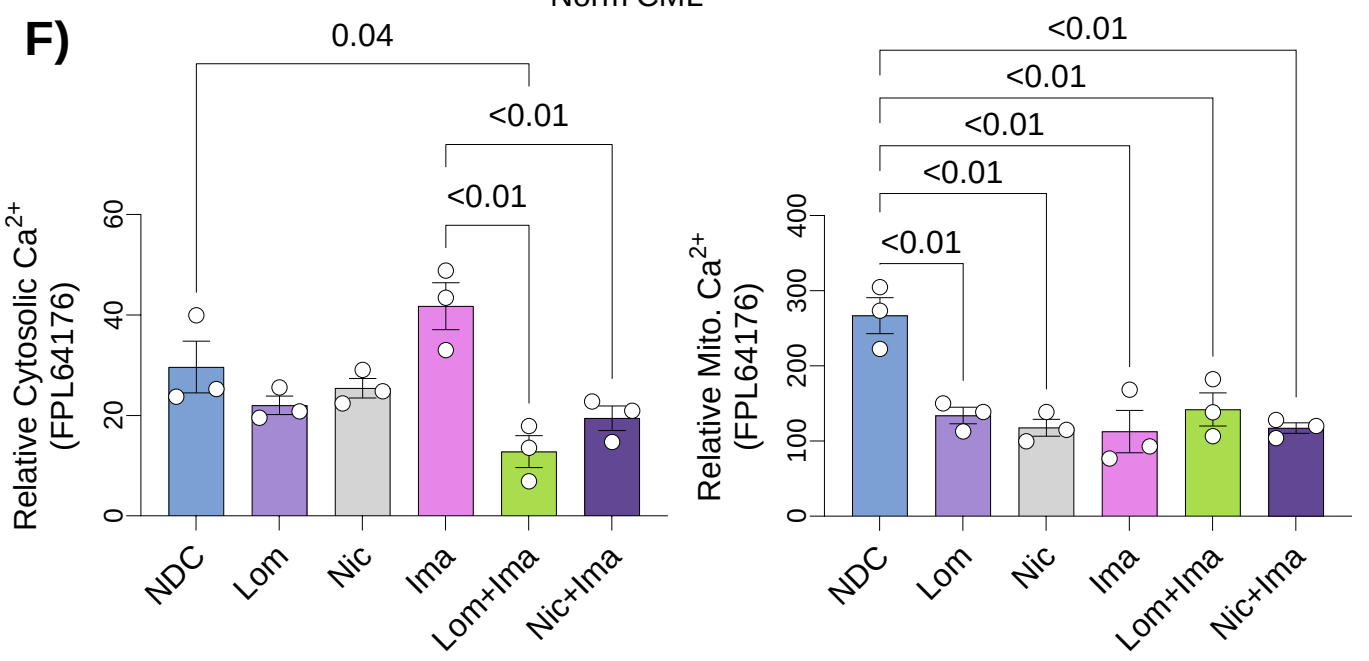
F)
Relative Cytosolic Ca2+ (FPL64176)
0.04
<0.01
<0.01
NDC
Lom
Nic
Ima
Lom+Ima
Nic+Ima
Relative Mito. Ca2+ (FPL64176)
<0.01
<0.01
<0.01
<0.01
<0.01

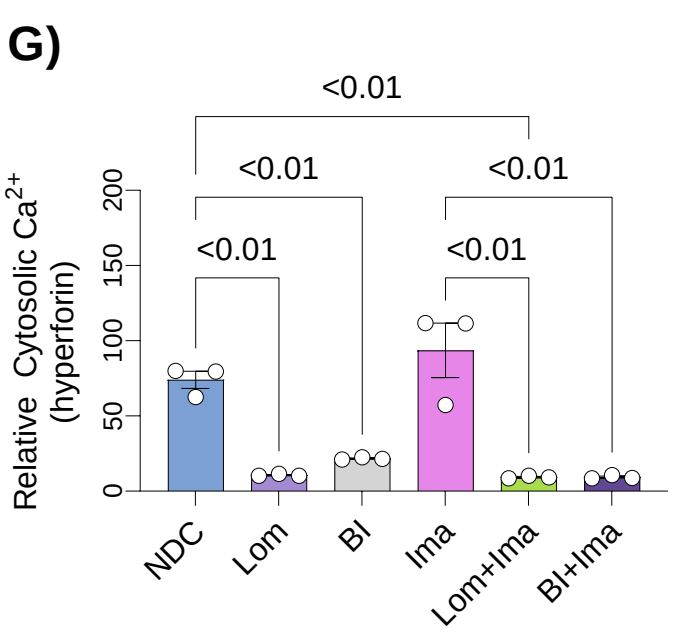
G)
Relative Cytosolic Ca2+ (hyperforin)
<0.01
<0.01
<0.01
<0.01
<0.01
NDC
Lom
Bl
Ima
Lom+Ima
Bl+Ima
Relative Mito. Ca2+ (hyperforin)
<0.01
0.01
<0.01
<0.01
<0.01
<0.01

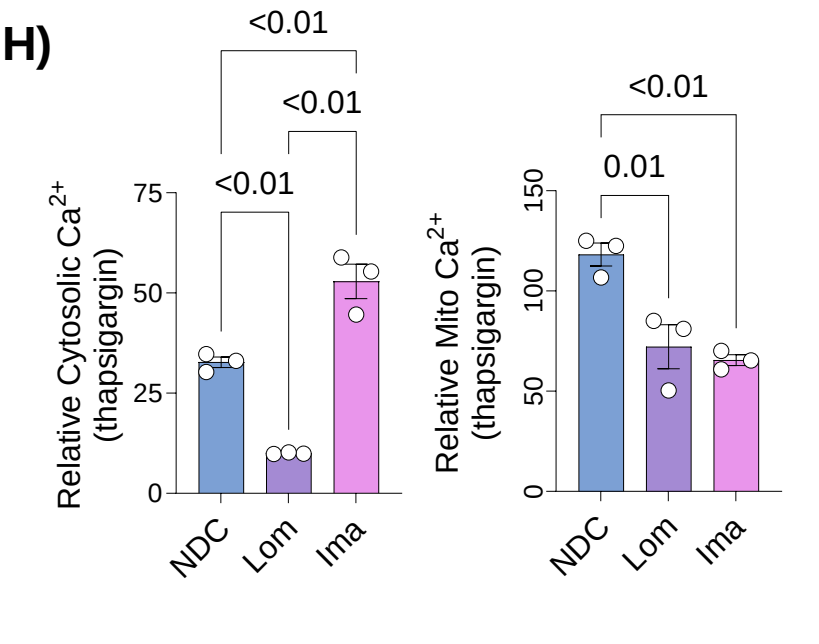
H)
Relative Cytosolic Ca2+ (thapsigargin)
<0.01
<0.01
<0.01
NDC
Lom
Ima
Relative Mito Ca2+ (thapsigargin)
<0.01
0.01
NDC
Lom
Ima

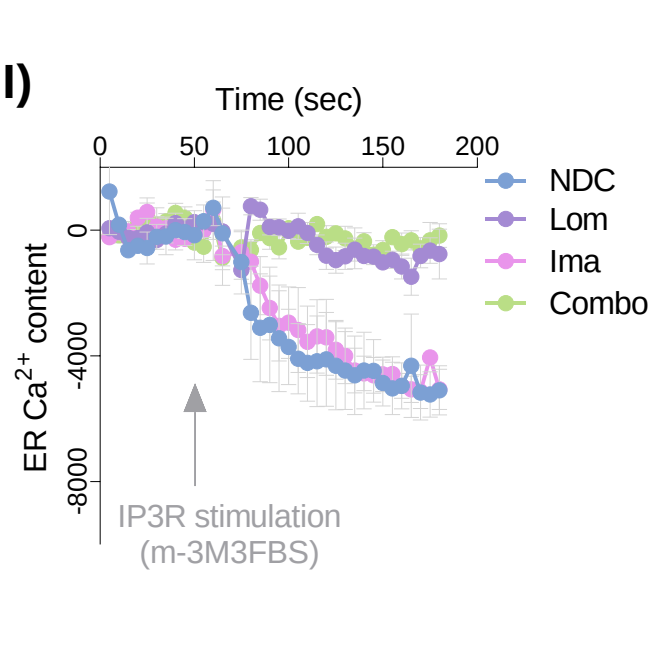
I)
Time (sec)
ER Ca2+ content
NDC
Lom
Ima
Combo
IP3R stimulation
(m-3M3FBS)

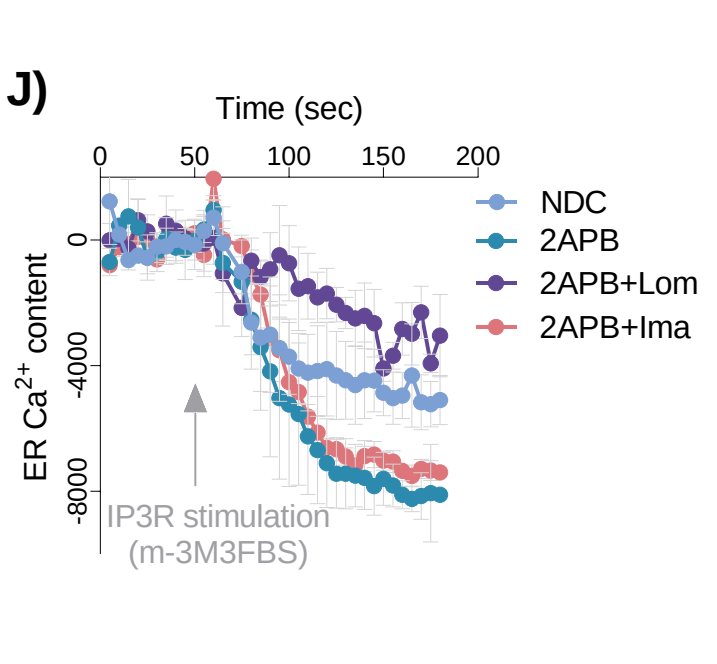
J)
Time (sec)
ER Ca2+ content
NDC
2APB
2APB+Lom
2APB+Ima
IP3R stimulation
(m-3M3FBS)

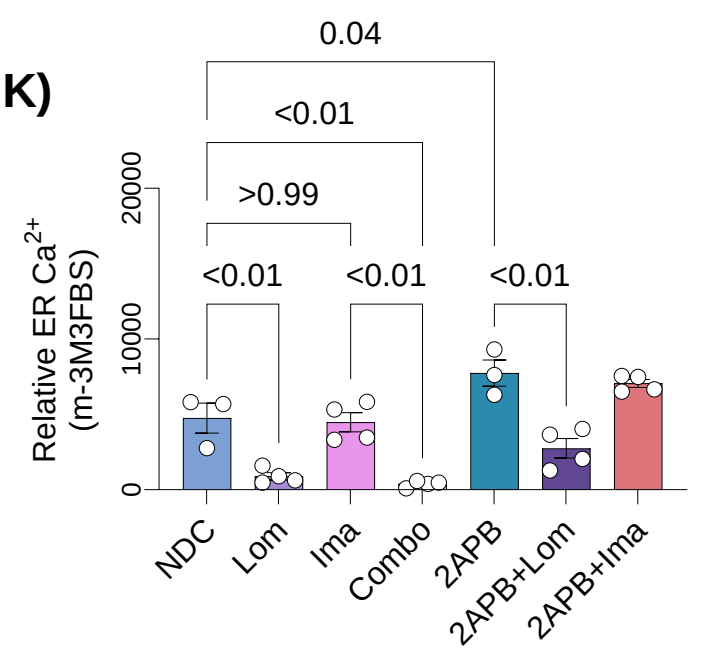
K)
Relative ER Ca2+ (m-3M3FBS)
0.04
<0.01
>0.99
<0.01
<0.01
<0.01
NDC
Lom
Ima
Combo
2APB
2APB+Lom
2APB+Ima

Fig. 5

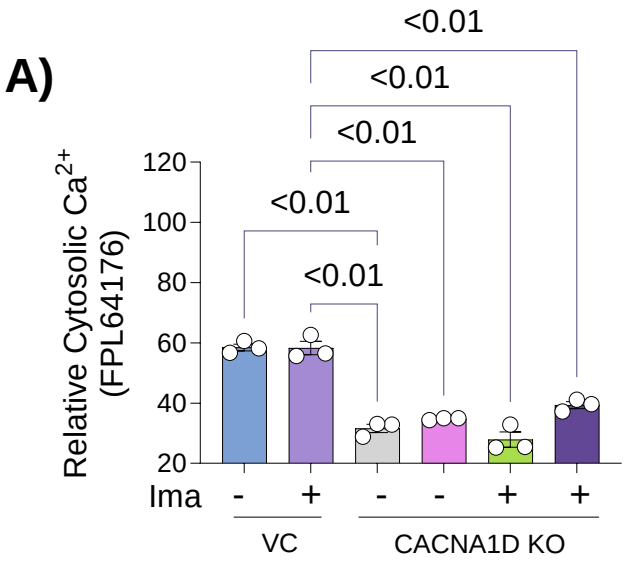
A)
Relative Cytosolic Ca2+ (FPL64176)
<0.01
<0.01
<0.01
<0.01
<0.01
120
100
80
60
40
20
Ima - + - - + +
VC
CACNA1D KO

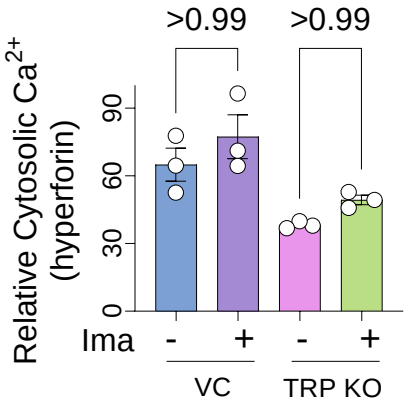
Relative Cytosolic Ca2+ (hyperforin)
>0.99
>0.99
90
60
30
0
Ima - + - +
VC
TRP KO

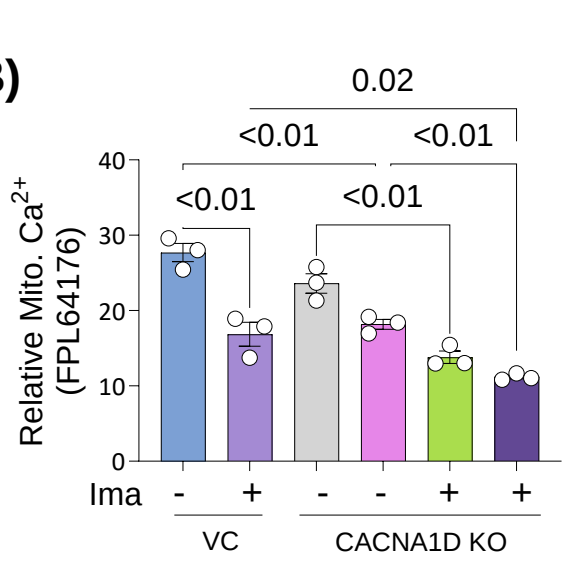
B)
Relative Mito. Ca2+ (FPL64176)
0.02
<0.01
<0.01
<0.01
<0.01
40
30
20
10
0
Ima - + - - + +
VC
CACNA1D KO

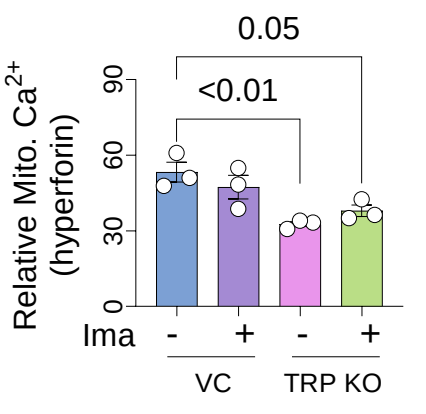
Relative Mito. Ca2+ (hyperforin)
0.05
<0.01
90
60
30
0
Ima - + - +
VC
TRP KO

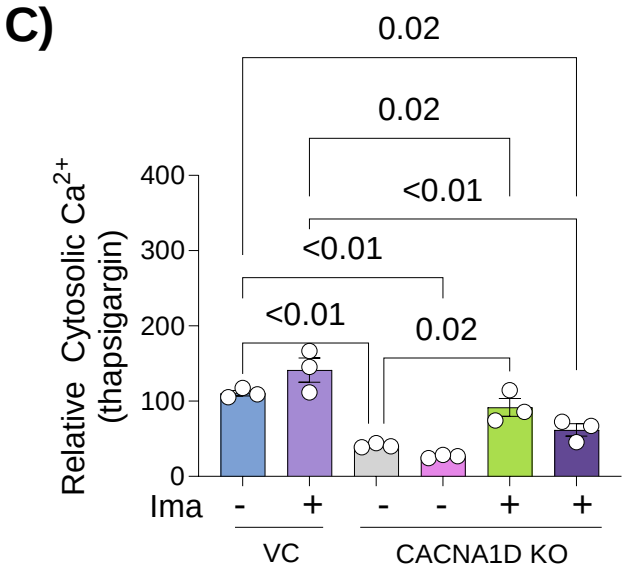
C)
Relative Cytosolic Ca2+ (thapsigargin)
0.02
0.02
<0.01
<0.01
<0.01
0.02
400
300
200
100
0
Ima - + - - + +
VC
CACNA1D KO

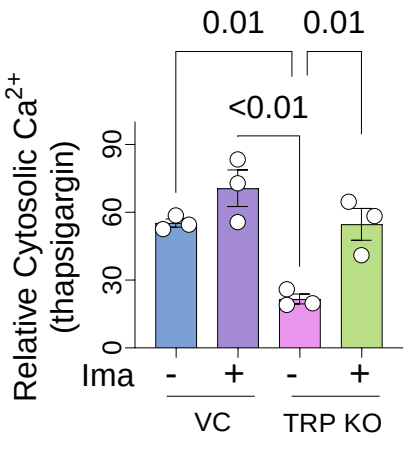
Relative Cytosolic Ca2+ (thapsigargin)
0.01
0.01
<0.01
90
60
30
0
Ima - + - +
VC
TRP KO

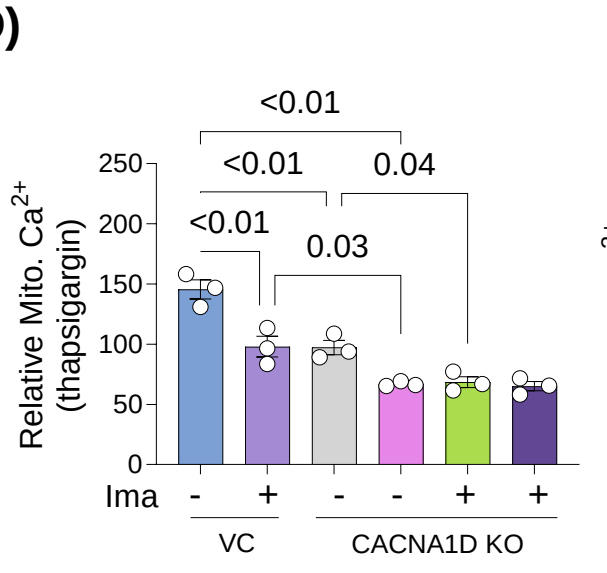
D)
Relative Mito. Ca2+ (thapsigargin)
<0.01
<0.01
0.04
<0.01
0.03
250
200
150
100
50
0
Ima - + - - + +
VC
CACNA1D KO

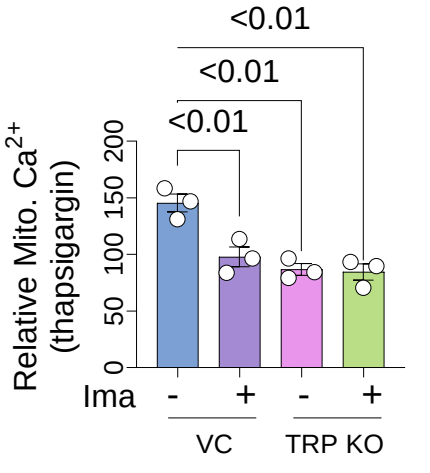
Relative Mito. Ca2+ (thapsigargin)
<0.01
<0.01
<0.01
<0.01
<0.01
200
150
100
50
0
Ima - + - +
VC
TRP KO

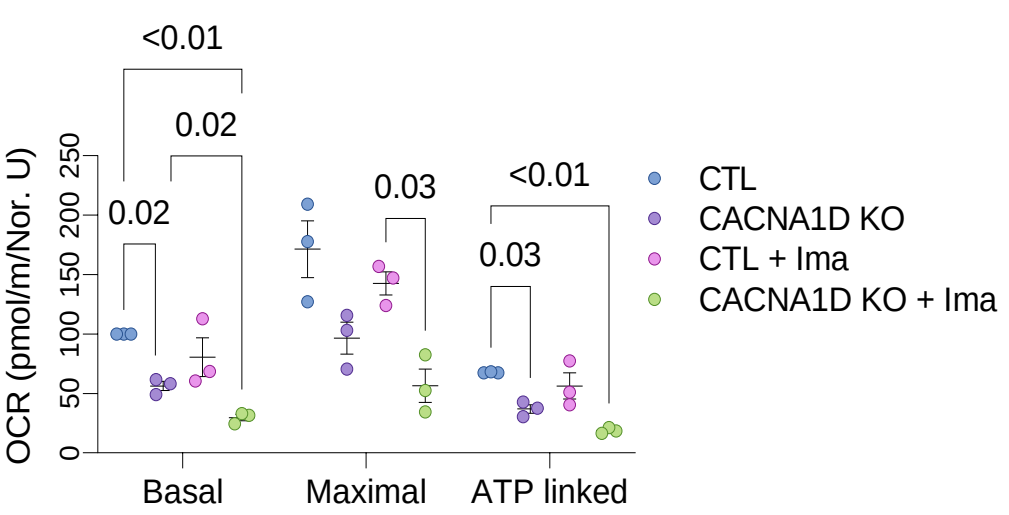
E)
OCR (pmol/m/Nor. U)
<0.01
0.02
0.02
0.03
0.03
<0.01
250
200
150
100
50
0
Basal
Maximal
ATP linked
CTL
CACNA1D KO
CTL + Ima
CACNA1D KO + Ima

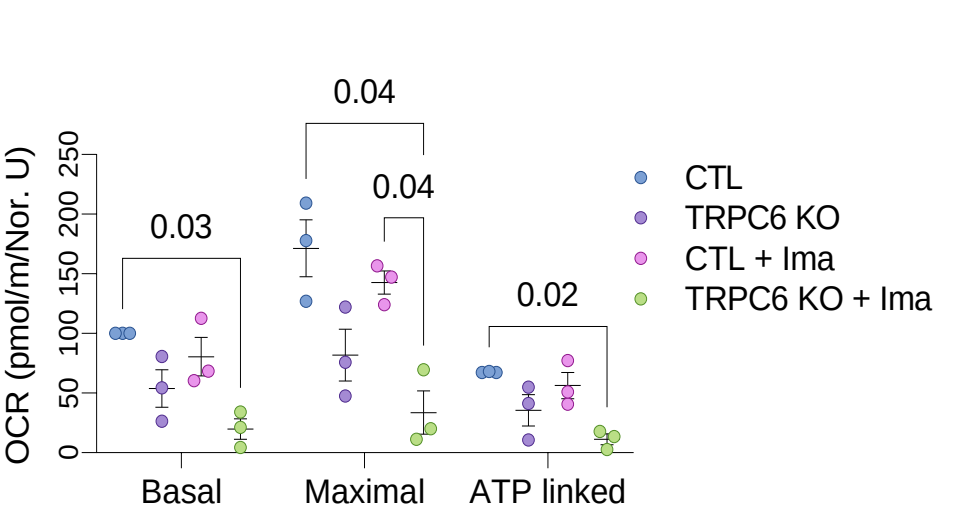
F)
OCR (pmol/m/Nor. U)
0.04
0.03
0.04
0.02
250
200
150
100
50
0
Basal
Maximal
ATP linked
CTL
TRPC6 KO
CTL + Ima
TRPC6 KO + Ima

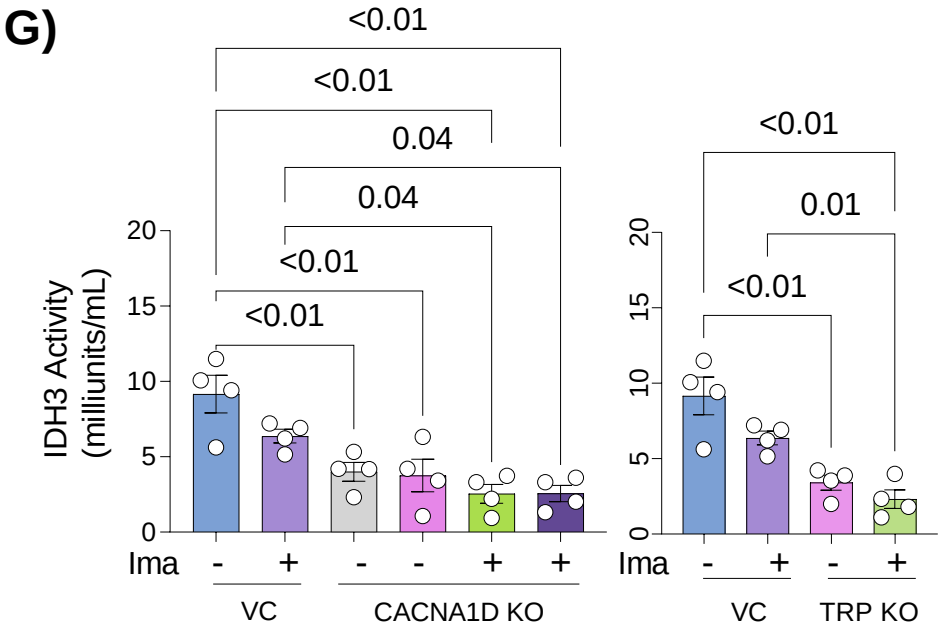
G)
IDH3 Activity (milliunits/mL)
<0.01
<0.01
0.04
0.04
<0.01
<0.01
20
15
10
5
0
Ima - + - - + +
VC
CACNA1D KO

<0.01
0.01
<0.01
20
15
10
5
0
Ima - + - +
VC
TRP KO

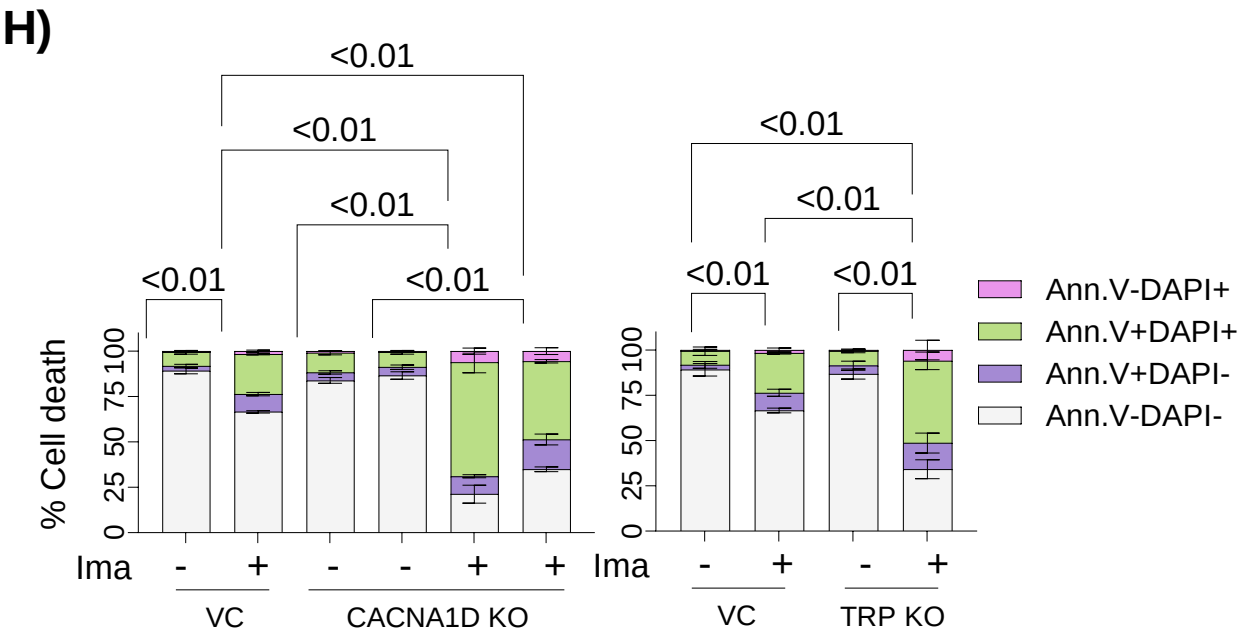
H)
<0.01
<0.01
<0.01
<0.01
<0.01
<0.01
<0.01
<0.01
% Cell death
100
75
50
25
0
Ima - + - - + +
VC
CACNA1D KO
Ima - + - +
VC
TRP KO
Ann.V-DAPI+
Ann.V+DAPI+
Ann.V+DAPI-
Ann.V-DAPI-

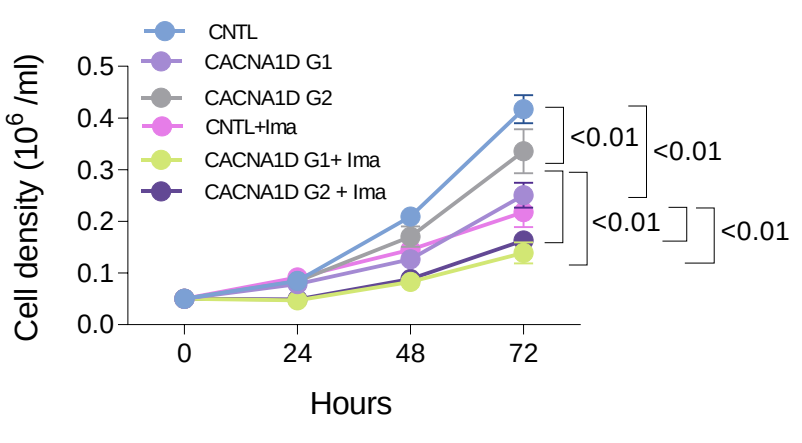
I)
CNTL
CACNA1D G1
CACNA1D G2
CNTL+Ima
CACNA1D G1+ Ima
CACNA1D G2 + Ima
Cell density (10^6 /ml)
0.5
0.4
0.3
0.2
0.1
0.0
0
24
48
72
Hours
<0.01
<0.01
<0.01
<0.01

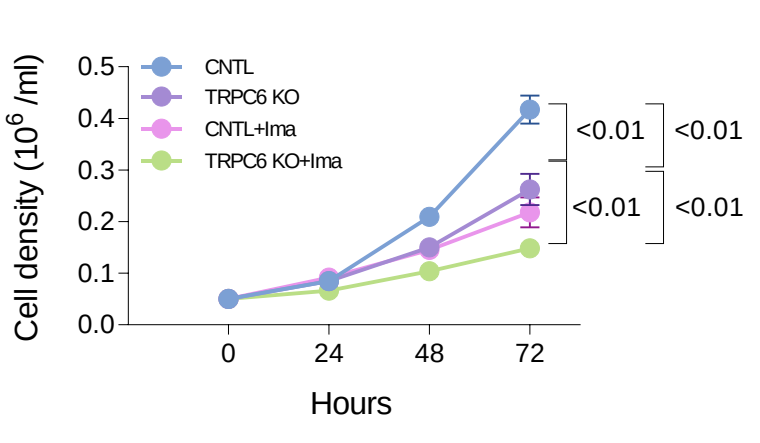
J)
CNTL
TRPC6 KO
CNTL+Ima
TRPC6 KO+Ima
Cell density (10^6 /ml)
0.5
0.4
0.3
0.2
0.1
0.0
0
24
48
72
Hours
<0.01
<0.01
<0.01
<0.01

Fig. 6

A)
Relative Cytosolic Ca2+ (ionomycin)
.003
.010
.002
Relative Mito. Ca2+ (ionomycin)
.004
.003
NDC
Lom
Ima
Combo
CML #1
CML #2
CML #3
B)
.008
.046
.047
N#1
N#2
N#6
C)
OCR (pmol/min/Norm. U)
0.01
0.04
<0.01
0.02
0.03
<0.01
0.03
Basal
Maximal
ATP linked
CML #1
CML #3
CML #8
D)
<.001
.016
Cell density (10^5/mL)
CML #1
CML #3
CML #4
CML #7
CML #10
E)
<.001
.003
.041
.047
% of live cells
F)
Cell density (10^5/mL)
N#8
N#9
N#10
N#11
N#12
G)
.043
.032
H)
<.001
<.001
<.001
<.001
.028
.004
.050
Relative CFC (Count/NDC)
I)
<.001
<.001
<.001
Relative CFC (Count/NDC)
Oma
J)
.014
.003
.003
% CD34+CD133+ (Count/NDC)
K)
<.001
.010
<.001
.005
Comb
L)
<0.01
0.01
0.11
<0.01
0.05
0.32
0.06
0.21
<0.01
0.02
0.34
0.13
0.10
0.07
<0.01
0.07
CTV Count
D3
D2
D1
D0
CML #1
CML #3
CML #6
CML #9
M)
<.001
<.001
<.001
.040
Relative LTC-IC (Count/NDC)

Fig. 7

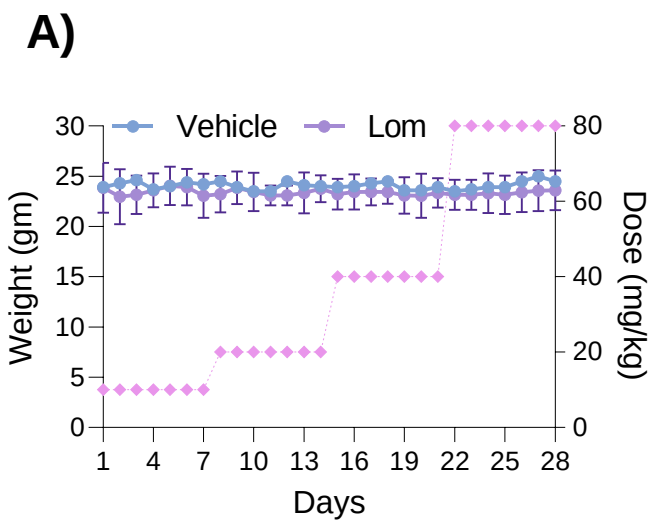
A)
Vehicle
Lom
Weight (gm)
Dose (mg/kg)
Days

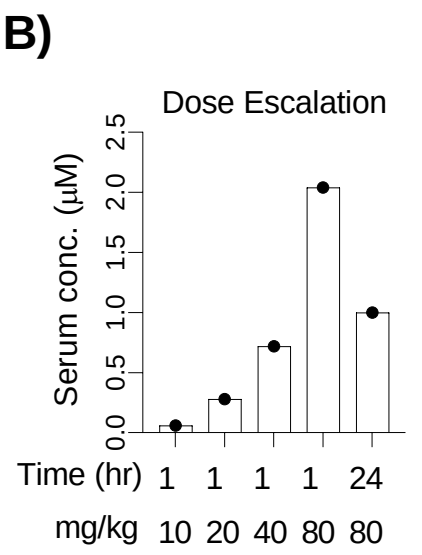
B)
Dose Escalation
Serum conc. (µM)
Time (hr) 1 1 1 1 24
mg/kg 10 20 40 80 80

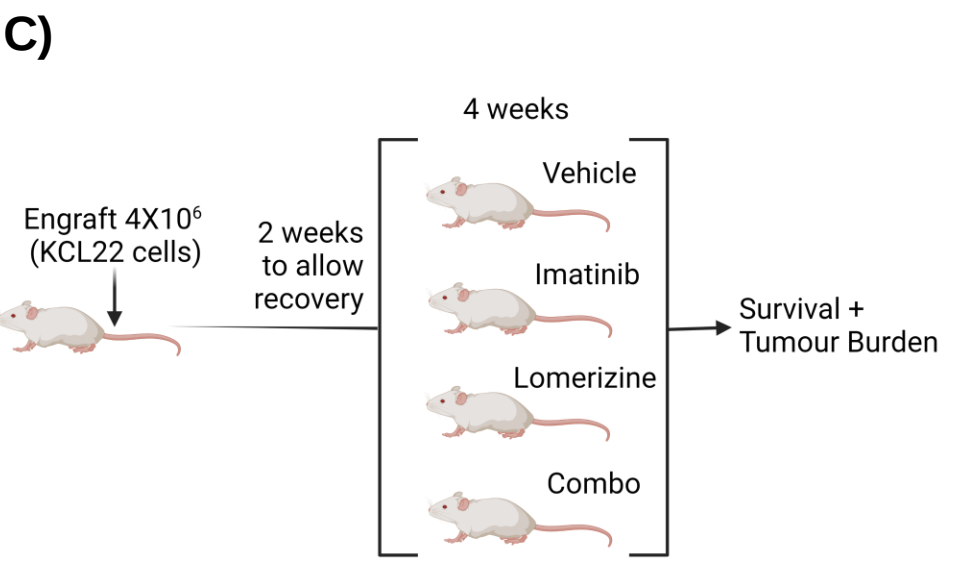
C)
4 weeks
Engraft 4X10⁶ (KCL22 cells)
2 weeks to allow recovery
Vehicle
Imatinib
Lomerizine
Combo
Survival + Tumour Burden

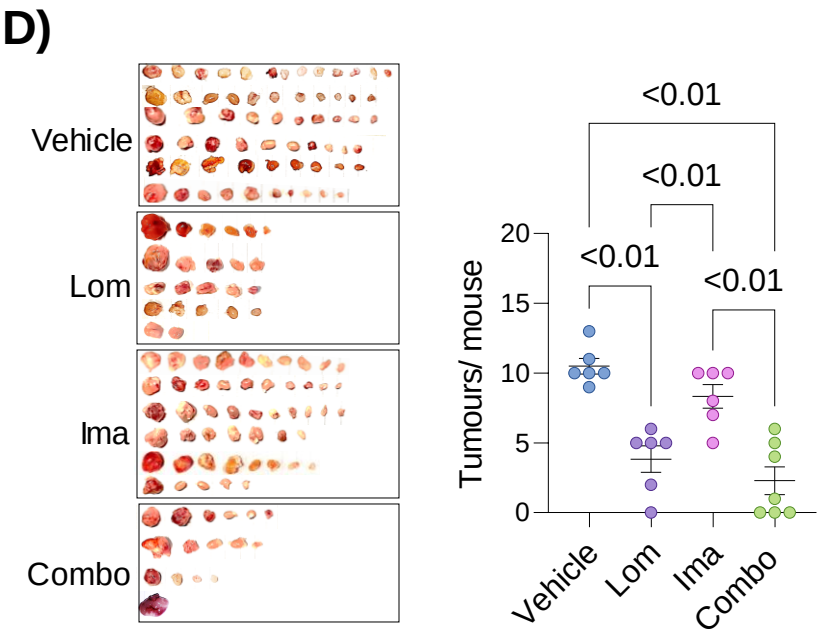
D)
Vehicle
Lom
Ima
Combo
Tumours/ mouse
<0.01
<0.01
<0.01

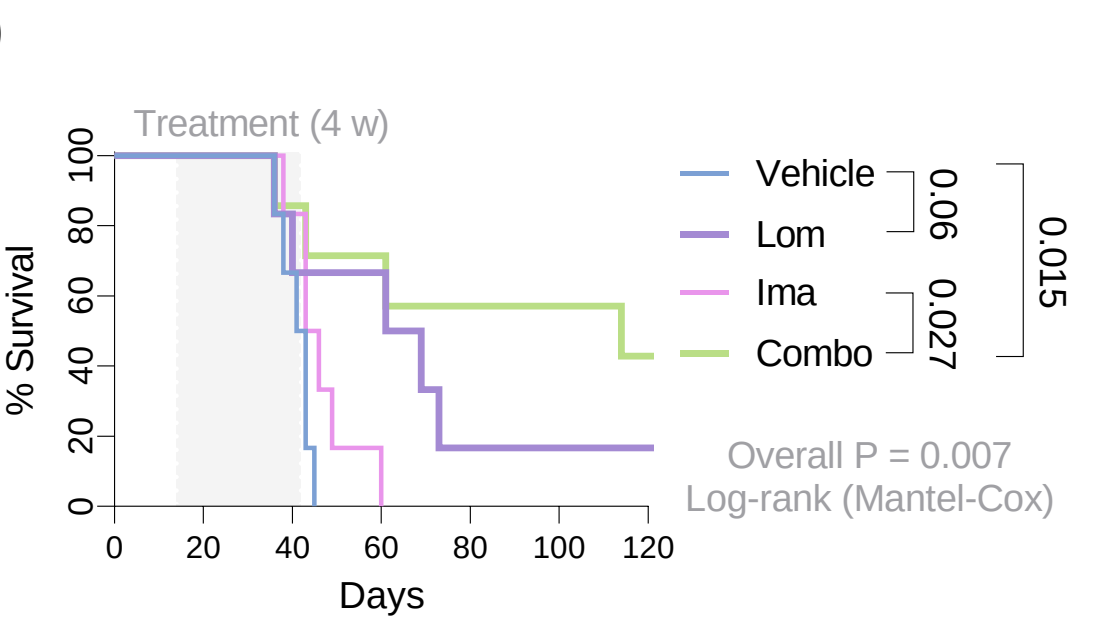
E)
Treatment (4 w)
% Survival
Days
Vehicle
Lom
Ima
Combo
0.06
0.027
0.015
Overall P = 0.007
Log-rank (Mantel-Cox)

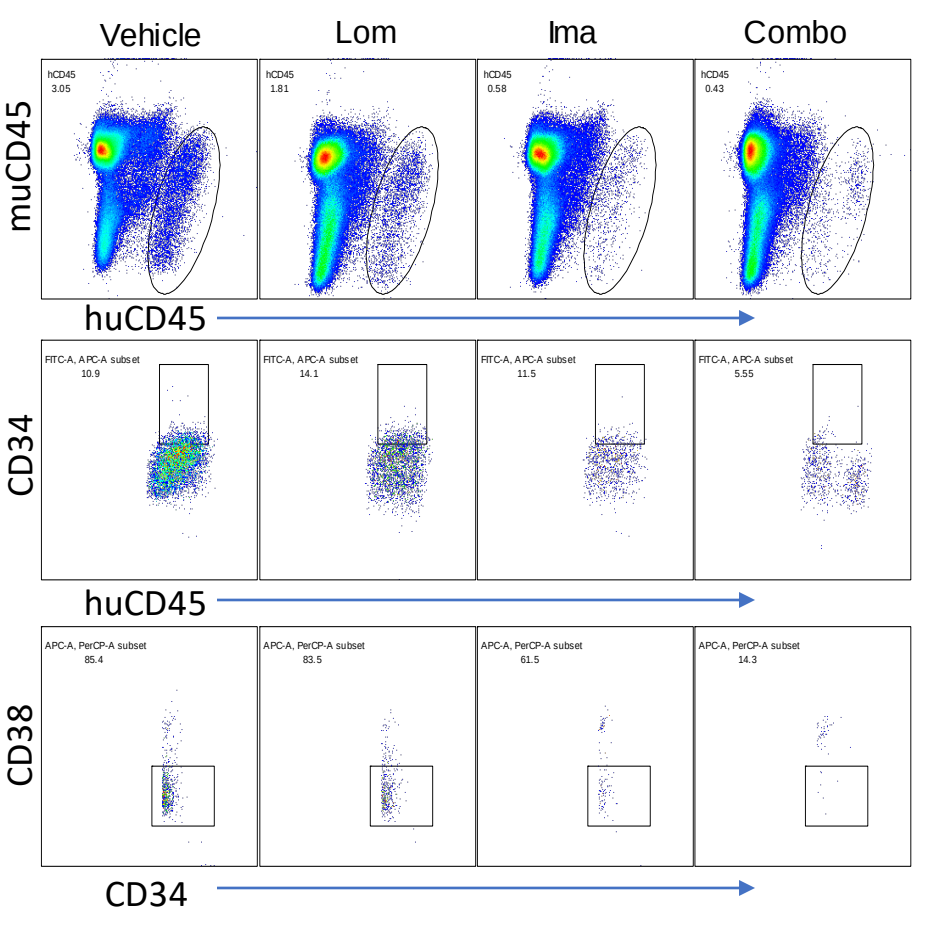
F)
Vehicle
Lom
Ima
Combo
muCD45
huCD45
CD34
huCD45
CD38
CD34

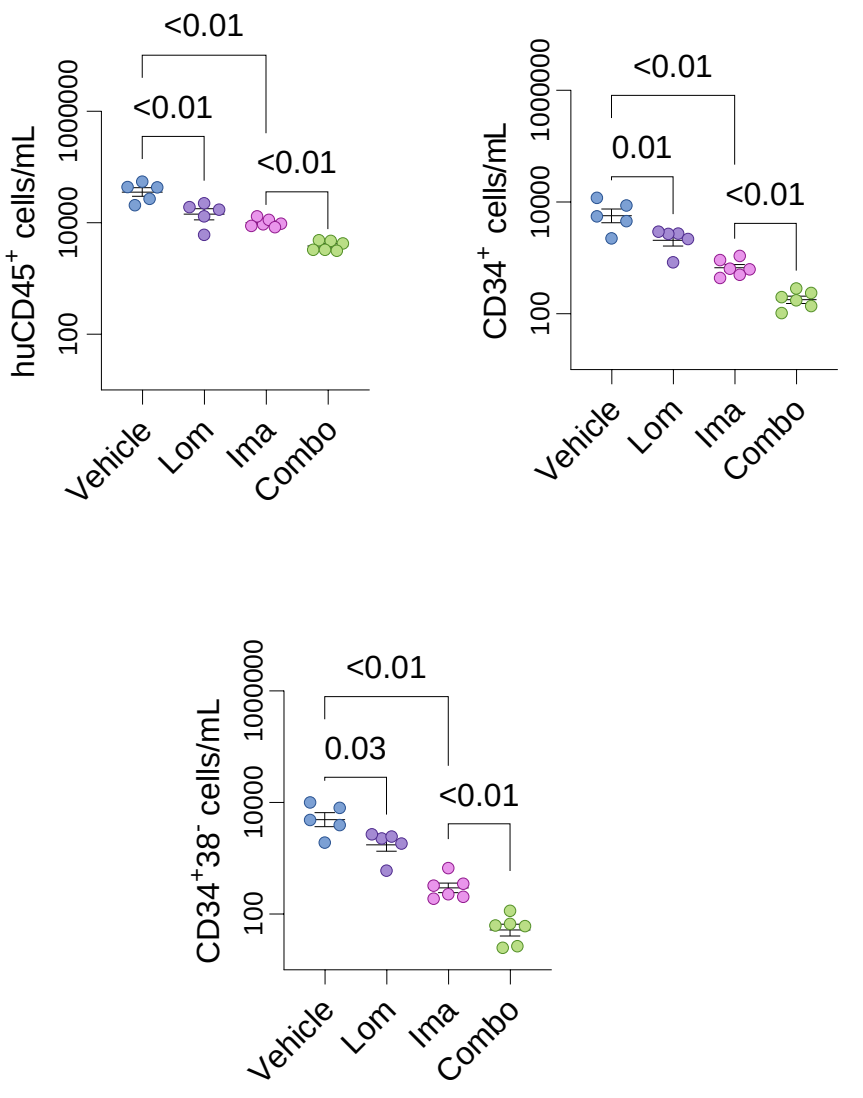
G)
huCD45⁺ cells/mL
<0.01
<0.01
<0.01
CD34⁺ cells/mL
<0.01
0.01
<0.01
CD34⁺38⁻ cells/mL
<0.01
0.03
<0.01
Vehicle
Lom
Ima
Combo

fig. S1

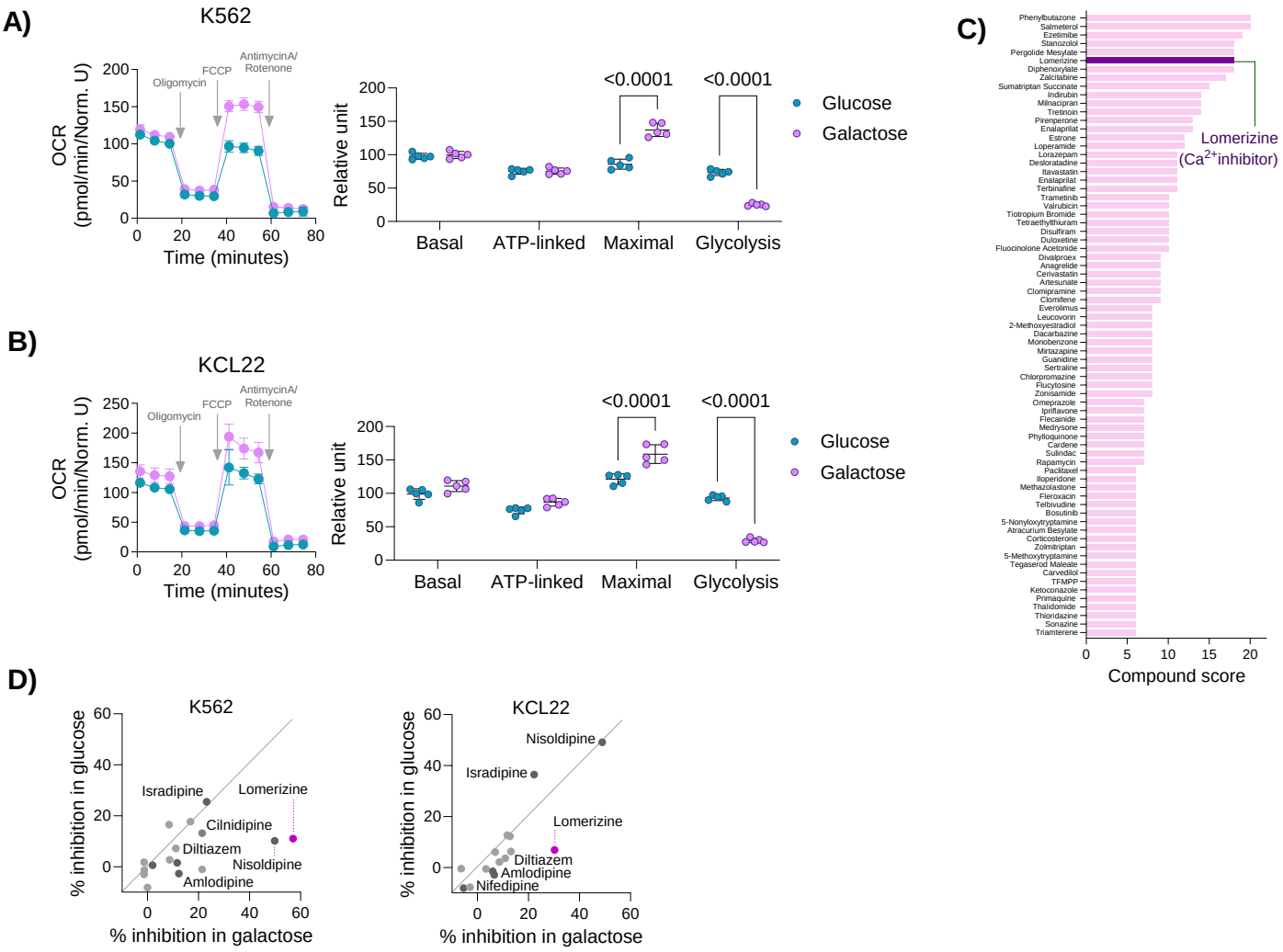

Fig. S1. CML cell lines rely on OXPHOS when cultured in galactose.

(A-B) Representative OCR profile and associated basal, maximal, ATP-linked OCR as well as glycolysis (ECAR) in (A) K562 cells and (B) KCL22 cells cultured in either 11 mM glucose or 11 mM galactose for 24 hours (n=5 wells per condition). Mean ± S.D. *P*. values were calculated using ANOVA and Tukey for multiple comparisons corrections. **(C)** List of the top hits from the screen to identify potential mitochondria respiration inhibitors, highlighting lomerizine as one of the highest scoring compounds. (**D**) Drug screening analysis comprising candidates that are known to have Ca^{2+} channel blocking activity, highlighting lomerizine as an inter-group top hit.

fig. S2

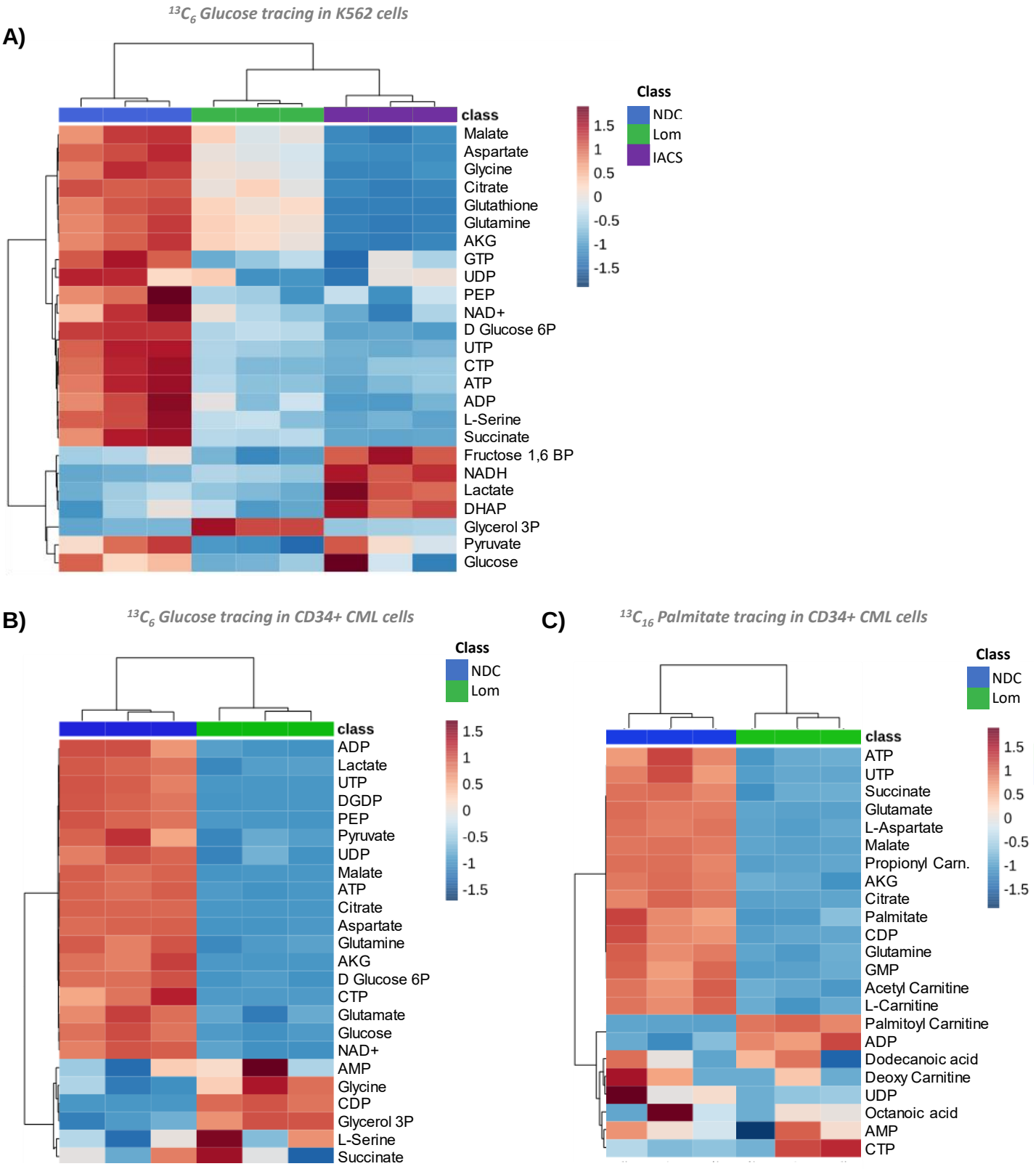
A)
$^{13}C_6$ Glucose tracing in K562 cells
class
Malate
Aspartate
Glycine
Citrate
Glutathione
Glutamine
AKG
GTP
UDP
PEP
NAD+
D Glucose 6P
UTP
CTP
ATP
ADP
L-Serine
Succinate
Fructose 1,6 BP
NADH
Lactate
DHAP
Glycerol 3P
Pyruvate
Glucose
1.5
1
0.5
0
-0.5
-1
-1.5
Class
NDC
Lom
IACS
B)
$^{13}C_6$ Glucose tracing in CD34+ CML cells
class
ADP
Lactate
UTP
DGDP
PEP
Pyruvate
UDP
Malate
ATP
Citrate
Aspartate
Glutamine
AKG
D Glucose 6P
CTP
Glutamate
Glucose
NAD+
AMP
Glycine
CDP
Glycerol 3P
L-Serine
Succinate
1.5
1
0.5
0
-0.5
-1
-1.5
Class
NDC
Lom
C)
$^{13}C_{16}$ Palmitate tracing in CD34+ CML cells
class
ATP
UTP
Succinate
Glutamate
L-Aspartate
Malate
Propionyl Carn.
AKG
Citrate
Palmitate
CDP
Glutamine
GMP
Acetyl Carnitine
L-Carnitine
Palmitoyl Carnitine
ADP
Dodecanoic acid
Deoxy Carnitine
UDP
Octanoic acid
AMP
CTP
1.5
1
0.5
0
-0.5
-1
-1.5
Class
NDC
Lom

Fig. S2. Lomerizine inhibits mitochondrial metabolism in CD34$^+$ CML cells.

(A) Representative heatmap showing $^{13}C_6$ glucose labelling (≥ M+1) into TCA cycle, glycolysis, and relevant metabolites in K562 cells either untreated or treated with 5 μM lomerizine or 20 nM IACS-010759 for 24 hours. **(B-C)** Representative heatmap showing incorporation of labelled carbons (≥ M+1) into TCA cycle and relevant metabolites extracted from (B) $^{13}C_6$ glucose or (C) $^{13}C_{16}$ palmitate in CD34$^+$ CML cells treated with 5 μM lomerizine for 24 hours (n=3 technical replicates per condition using individual CD34$^+$ CML sample). Heatmaps were generated using MetaboAnalyst 5.0 online platform.

fig. S3

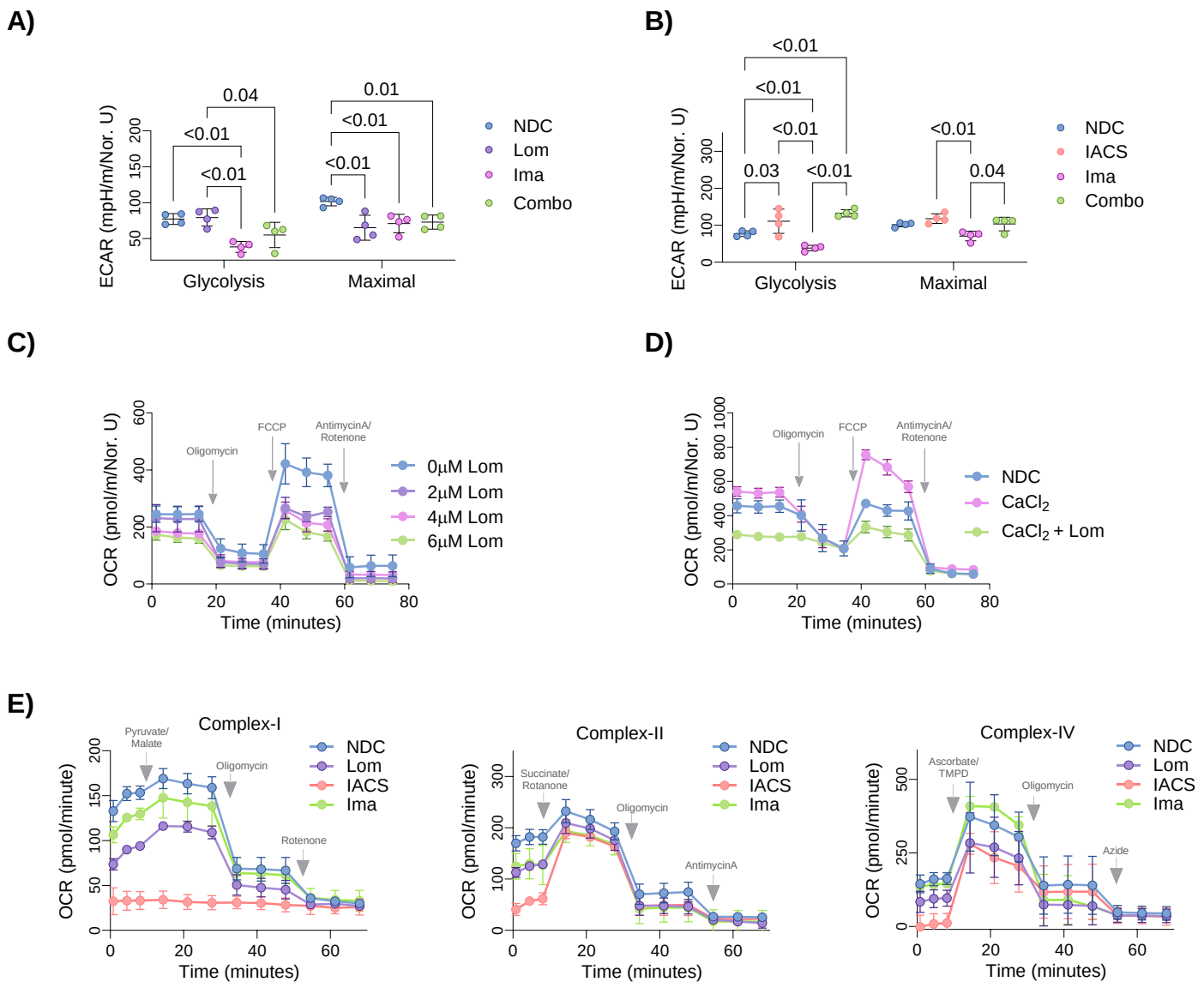

Fig. S3. Lomerizine reduces OCR without impacting individual mitochondrial complexes in CML cells.

A-B) Relative basal and maximal glycolysis (ECAR) in K562 cells treated (A) with or without 5 μM lomerizine, 0.5 μM imatinib and their combination, or (B) with or without 5 nM IACS, 0.5 μM imatinib and their combination for 12 hours (n=4 wells per condition). Means ± SD. *P*. values were calculated using two-way ANOVA and Tukey test was performed to correct for multiple comparisons. **(C)** Representative OCR in KCL22 cells exposed to 0, 2, 4, and 6 μM lomerizine for 60 minutes (n=5 wells per condition). Mean ± SD. **(D)** Representative OCR in K562 cells after exposure to 2 mM $CaCl_2$ or 2 mM $CaCl_2$ + 5 μM lomerizine for 12 hours (n=4 wells per condition). Mean ± SD. **(E)** Measurement of complex I, II, and IV activity of K562 cells in untreated or following 4 hours of exposure to 5 μM lomerizine, 5 nM IACS, 1 μM imatinib (n=4 independent experiments). Means ± SEM.

fig. S4

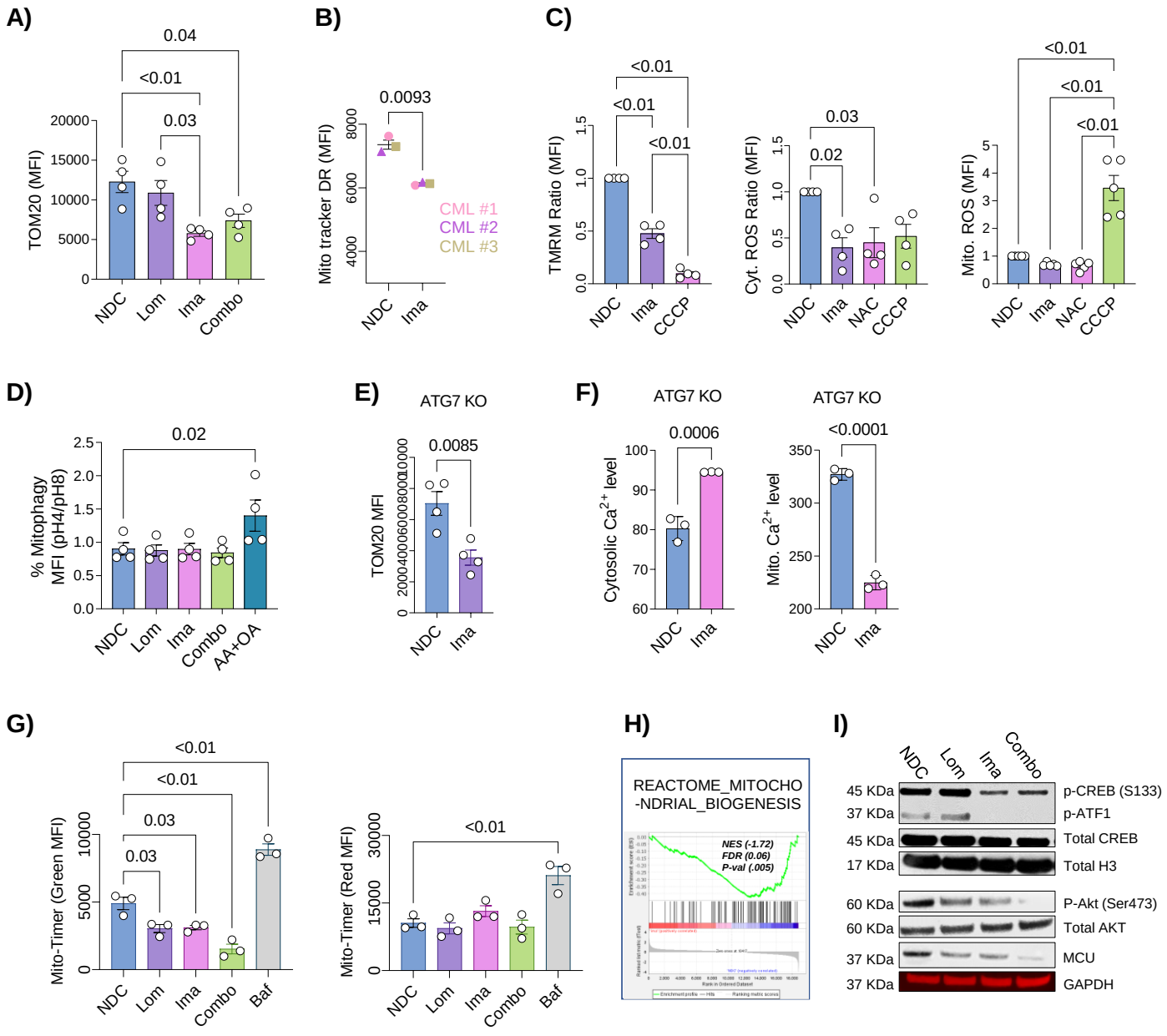
A)
TOM20 (MFI)
0.04
<0.01
0.03
NDC
Lom
Ima
Combo
B)
Mito tracker DR (MFI)
0.0093
CML #1
CML #2
CML #3
NDC
Ima
C)
TMRM Ratio (MFI)
<0.01
<0.01
<0.01
NDC
Ima
CCCP
Cyt. ROS Ratio (MFI)
0.03
0.02
NDC
Ima
NAC
CCCP
Mito. ROS (MFI)
<0.01
<0.01
<0.01
NDC
Ima
NAC
CCCP
D)
% Mitophagy MFI (pH4/pH8)
0.02
NDC
Lom
Ima
Combo
AA+OA
E)
ATG7 KO
TOM20 MFI
0.0085
NDC
Ima
F)
ATG7 KO
Cytosolic Ca2+ level
0.0006
NDC
Ima
ATG7 KO
Mito. Ca2+ level
<0.0001
NDC
Ima
G)
Mito-Timer (Green MFI)
<0.01
<0.01
0.03
0.03
NDC
Lom
Ima
Combo
Baf
Mito-Timer (Red MFI)
<0.01
NDC
Lom
Ima
Combo
Baf
H)
REACTOME_MITOCHO
-NDRIAL_BIOGENESIS
NES (-1.72)
FDR (0.06)
P-val (.005)
I)
NDC
Lom
Ima
Combo
45 KDa
37 KDa
p-CREB (S133)
p-ATF1
45 KDa
17 KDa
Total CREB
Total H3
60 KDa
60 KDa
P-Akt (Ser473)
Total AKT
37 KDa
MCU
37 KDa
GAPDH

Fig. S4. Imatinib decreases mitochondrial Ca^{2+} by inhibiting *de novo* mitochondrial biogenesis.

(A) Relative TOM20 fluorescence intensity demonstrating mitochondrial mass in TOM20 expressing KCL22 cells treated with 10 µM lomerizine, 1 µM imatinib and combination for 24 hours as measured using flow cytometry (n=4 independent experiments). **(B)** Mitochondrial mass in $CD34^+$ CML cells treated with or without 1 µM imatinib for 24 hours, following staining with Mito tracker deep red (n=3 individual CML samples). Means ± SEM. *P*. values were calculated using Student's t-test. **(C)** Mitochondrial membrane potential, cytosolic and mitochondrial oxidative stress in K562 cells in untreated or after exposure to 1 µM imatinib K562 cells for 72 hours. 10 µM CCCP and 100 mM n-acetyl cysteine were used as controls (n=4 independent experiments). **(D)** Mito-mKeima (acidic pH fluorescence/neutral pH fluorescence) ratio illustrating amount of mitophagy in Mito-mKeima expressing KCL22 cells untreated or treated with 10 µM lomerizine, 1 µM imatinib and combination, or 10 µM antimycin A and oligomycin (AA+OA) for 24 hours (n=4 independent experiments). **(E)** TOM20 fluorescence in TOM20 overexpressing K562 ATG7 KO cells treated with or without 1 µM imatinib for 24 hours (n=4 independent experiments). **(F)** Ca^{2+} content in response to stimulation of cells with 3 µM ionomycin in K562 ATG7 KO cells treated with or without 1 µM imatinib for 24 hours (n=3 independent wells from individual experiment). **(G)** MitoTimer bimodal green and red fluorescence illustrating "young" and mature mitochondria content in Mito-timer expressing K562 cells. Cells were pulsed twice with 2 µg/mL doxycycline for 8 hours before and after treatment with 10 µM lomerizine, 1 µM imatinib and combination, or 100 nM bafilomycin for 40 hours (n=3 independent experiments). **(H)** Representative GSEA of Mitochondrial Biogenesis Reactome from the E-MTAB-2594 dataset, comparing imatinib treated versus untreated $CD34^+CD38^-$ CML cells. **(I)** Western blot illustrating amount of total and phosphorylated proteins of lysates extracted from K562 cells untreated or treated with 10 µM lomerizine, 1 µM imatinib or the combination for 10 hours. Means ± SEM. *P*. values were calculated using ANOVA and Tukey test was performed for multiple comparisons (A, C, D, G). (B, E) Means ± SEM. *P*. value was calculated using Student's t-test.

fig. S5

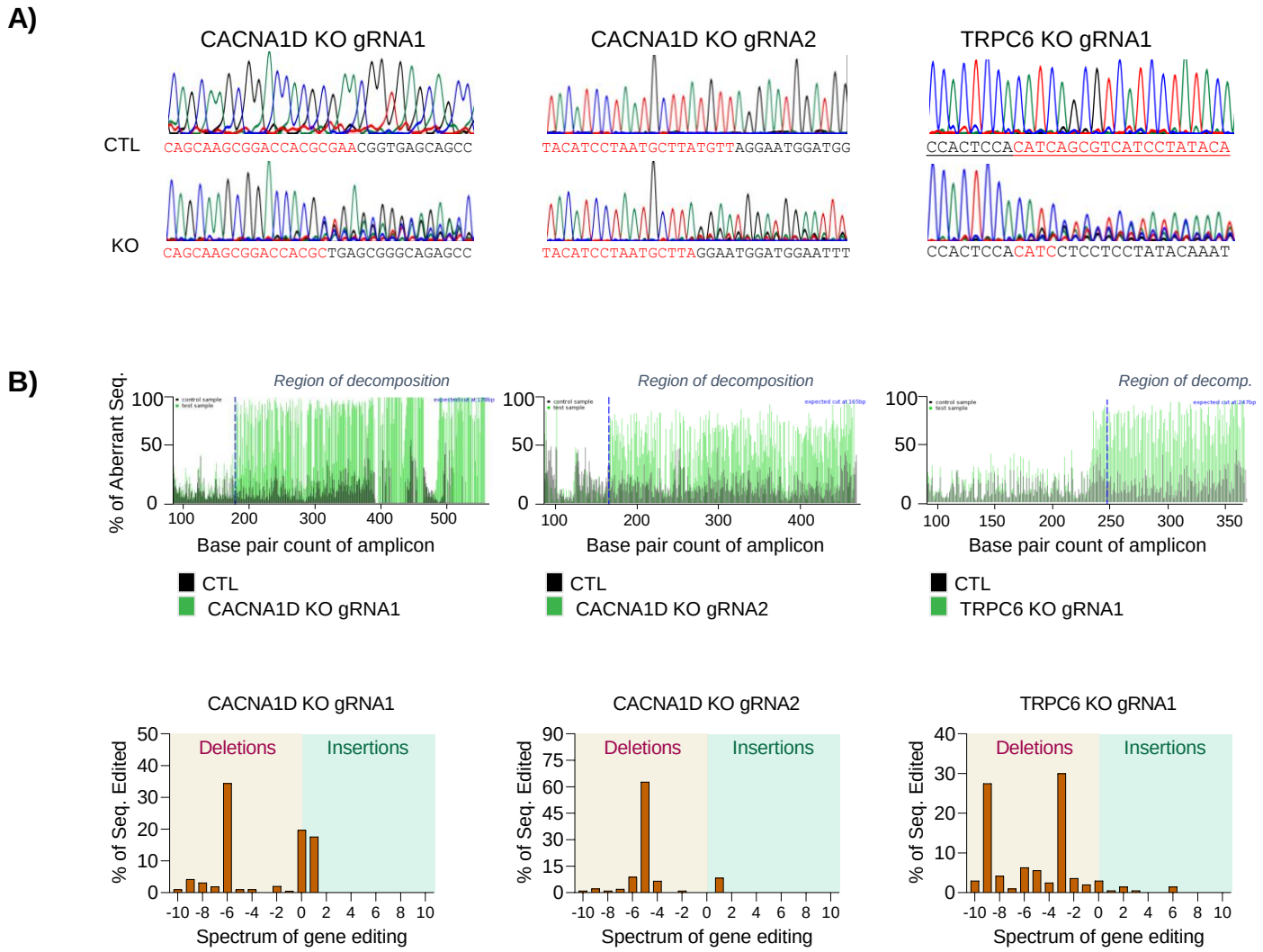

Fig. S5. Verification of CACNA1D and TRPC6 CRISPR Cas9 gene deletion.

(A) Sanger sequencing of genomic DNA extracted from control (CTL), two different CACNA1D KO cells, and TRPC6 KO K562 cells using primers that flanks relevant gRNAs. Peaks was visualised by Chromas software. **(B)** Area of aberrant decomposition (green bars) within the whole amplicon as compared to the standard sequence (black line). Data was analysed by Tide online platform. Further genetic deletion validation analyses show that the editing in genomic DNA occurs through nucleotide deletions rather than nucleotide insertions.

fig. S6

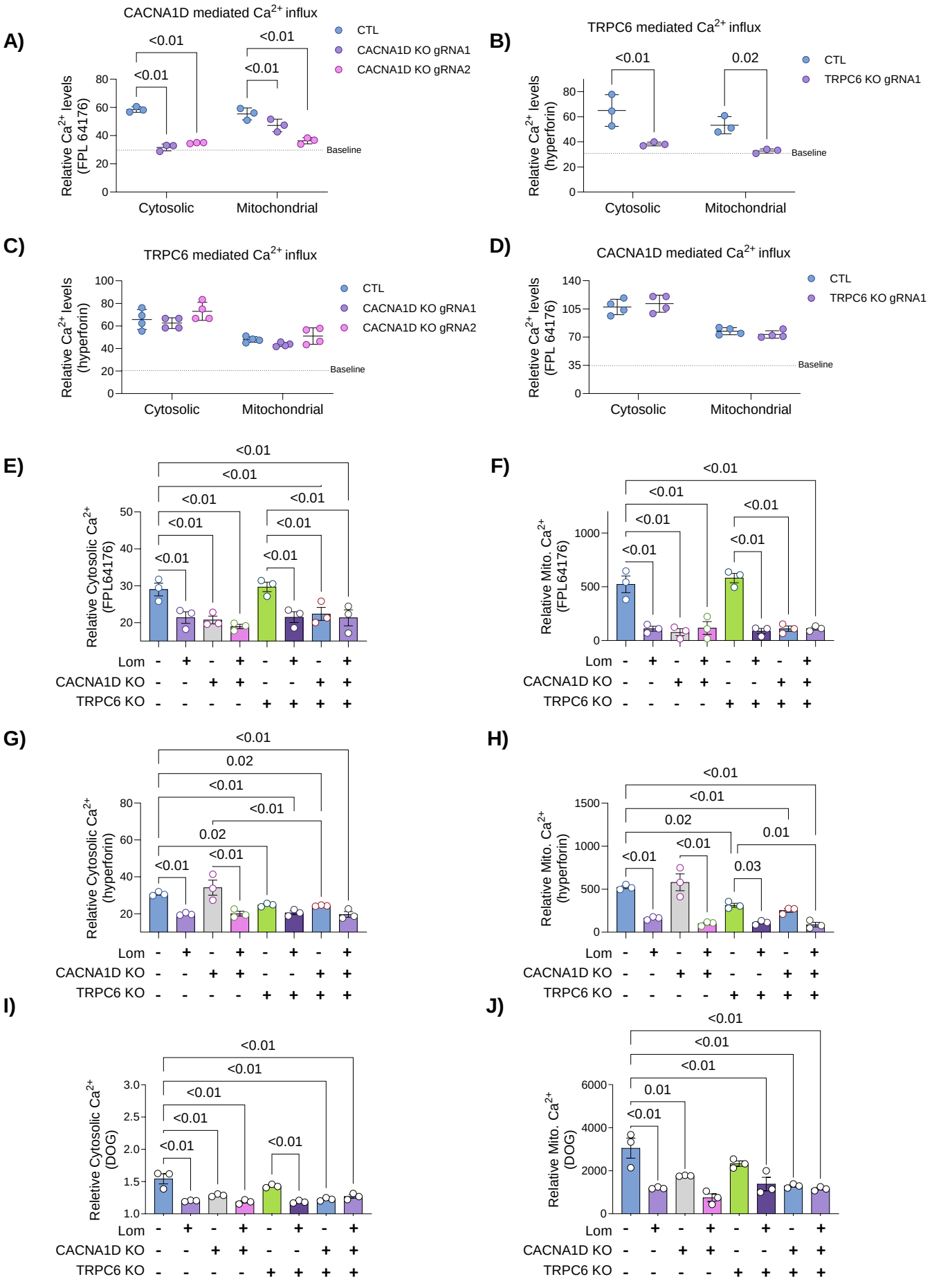
A)
CACNA1D mediated Ca2+ influx
Relative Ca2+ levels (FPL 64176)
CTL
CACNA1D KO gRNA1
CACNA1D KO gRNA2
Baseline
Cytosolic
Mitochondrial
B)
TRPC6 mediated Ca2+ influx
Relative Ca2+ levels (hyperforin)
CTL
TRPC6 KO gRNA1
C)
TRPC6 mediated Ca2+ influx
CACNA1D KO gRNA1
CACNA1D KO gRNA2
D)
CACNA1D mediated Ca2+ influx
E)
Relative Cytosolic Ca2+ (FPL64176)
F)
Relative Mito. Ca2+ (FPL64176)
G)
Relative Cytosolic Ca2+ (hyperforin)
H)
Relative Mito. Ca2+ (hyperforin)
I)
Reletive Cytosolic Ca2+ (DOG)
J)
Relative Mito. Ca2+ (DOG)
Lom
CACNA1D KO
TRPC6 KO

Fig. S6. Lomerizine targets CACNA1D and TRPC6.

(A-D) Mitochondrial and cytosolic Ca^{2+} content in CACNA1D KO K562 cells in response to stimulation with FPL6417 (A) or in response to hyperforin stimulation (C), or in TRPC6 KO K562 cells in response to FPL6417 (B) or hyperforin (D) stimulation (n=3-4 independent experiments). Dotted lines represent arbitrary basal Ca^{2+} content. Means ± SD. and *P*. values were calculated using one-way ANOVA and Tukey for multiple comparisons correction. (E-J) Relative cytosolic and mitochondrial Ca^{2+} content in response to (E, F) 25 µM FPL64176, (G, H) 25 µM hyperforin or (I, J) 25 µM DOG stimulation, in control, CACNA1D KO, TRPC6 KO, or double KO K562 cells ± 20 µM lomerizine for 24 hours (n= 3 independent experiments). Means ± SEM. *P*. values were calculated using one-way ANOVA and Tukey tests.

fig. S7

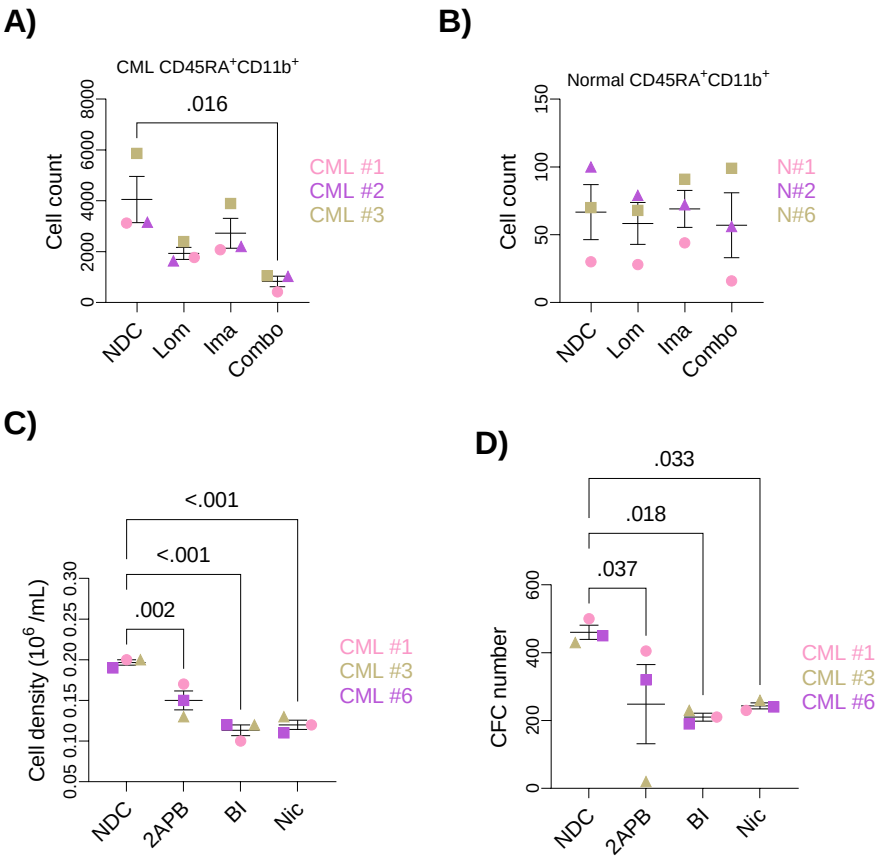

Fig. S7. Ca^{2+} dysregulation affects primitive CML cells *ex vivo*.

(**A-B**) Counts of $CD45RA^+CD11b^+$ cells / $10x10^4$ live $CD34^+$ CML or non-CML cells (n=3 independent CML or non-CML individuals). **(C-D)** $CD34^+$ CML were left untreated or treated with 5 µM BI, 2APB and 10 µM for nicardipine for 3 days (n=3 individual CML samples). (C) Cell density (D) and CFC potential is shown. Means ± SEM. *P*. values were calculated using one-way ANOVA test and Tukey test for multiple comparisons correction.

fig. S8

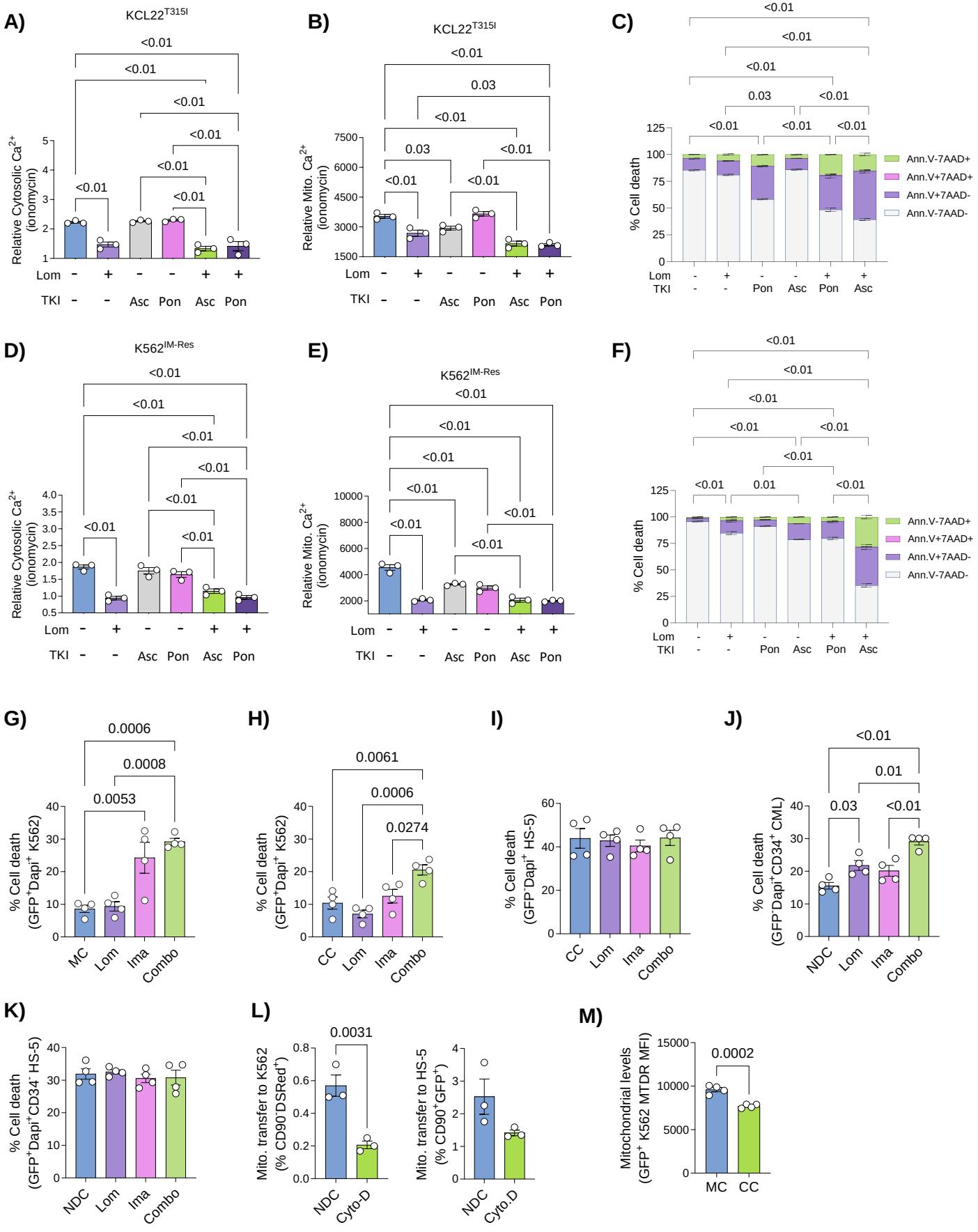
A)
KCL22T315I
Relative Cytosolic Ca2+ (ionomycin)
B)
KCL22T315I
Relative Mito. Ca2+ (ionomycin)
C)
% Cell death
Ann.V-7AAD+
Ann.V+7AAD+
Ann.V+7AAD-
Ann.V-7AAD-
Lom
TKI
Pon
Asc
D)
K562IM-Res
E)
K562IM-Res
F)
G)
% Cell death (GFP+Dapi+ K562)
MC
Lom
Ima
Combo
H)
CC
I)
% Cell death (GFP-Dapi+ HS-5)
J)
% Cell death (GFP-Dapi+CD34+ CML)
NDC
K)
% Cell death (GFP+Dapi+CD34- HS-5)
L)
Mito. transfer to K562 (% CD90-DSRed+)
Cyto-D
Mito. transfer to HS-5 (% CD90+GFP+)
M)
Mitochondrial levels (GFP+ K562 MTDR MFI)

Fig. S8. Lomerizine enhances ponatinib and asciminib effect on TKI-resistant CML cells *in vitro*.

(A-E) Relative cytosolic and mitochondrial Ca^{2+} content in response to 2.5 µM ionomycin in (A-B) $KCL22^{T315I}$, and (D-E) $K562^{Im\text{-}Res}$ cells (n= 3 independent experiments). Means ± SEM. *P*. values were calculated using Student's t-test. **(C, F)** Apoptosis amount in (C) $KCL22^{T315I}$, and (F) $K562^{Im\text{-}Res}$ cells s with or without 10 µM lomerizine, TKI (100 nM ponatinib or 10 nM asciminib), or their combination for 72 hours (n=3 independent experiments). Means ± SEM. P. values were calculated using one-way ANOVA and Tukey tests on live cell fraction. Cells were stained with 5 µM APC-annexin-V and 2 µM Dapi for 15 minutes before quantifying using flow cytometry. **(G-I)** Amount of cell death in Tom20-GFP expressing K562 cells in (G) monoculture or (H) cocultured with HS-5 cells, or (I) cocultured HS-5 cells, following 10 µM lomerizine,1 µM imatinib, or the combination for 48 hours (n≥ 3 independent experiments). Means ± SEM. *P*. values were calculated using one-way ANOVA and Tukey tests. **(J-K)** Amount of death in (J) $CD34^+$ CML and (K) HS-5 in coculture after 48 hours treatment with 10 µM lomerizine, 1 µM imatinib or the combination (n=3 individual $CD34^+$ CML samples). Means ± SEM. *P*. values were calculated using one-way ANOVA and Tukey tests. **(L)** Percentage of mitochondrial transfer between Tom20-GFP expressing K562 and DSRed expressing HS-5 after coculturing for 48 hours. HS-5 cells were pre-treated with 100 nM Cytocalacin D as control for 2 hours followed by gentle replacement with fresh media before coculture. Means ± SEM. *P*. values were calculated using Student's t-test. **(M)** Mitochondrial mass in Tom20-GFP expressing K562 cells, monocultured or cocultured with HS-5 cells for 48 hours as measured by staining $1*10^5$ cells with 0.1 µM Mito tracker deep red for 30 minutes (n=4 independent replicates). Means ± SEM. *P*. values were calculated using Student's t-test.

fig. S9

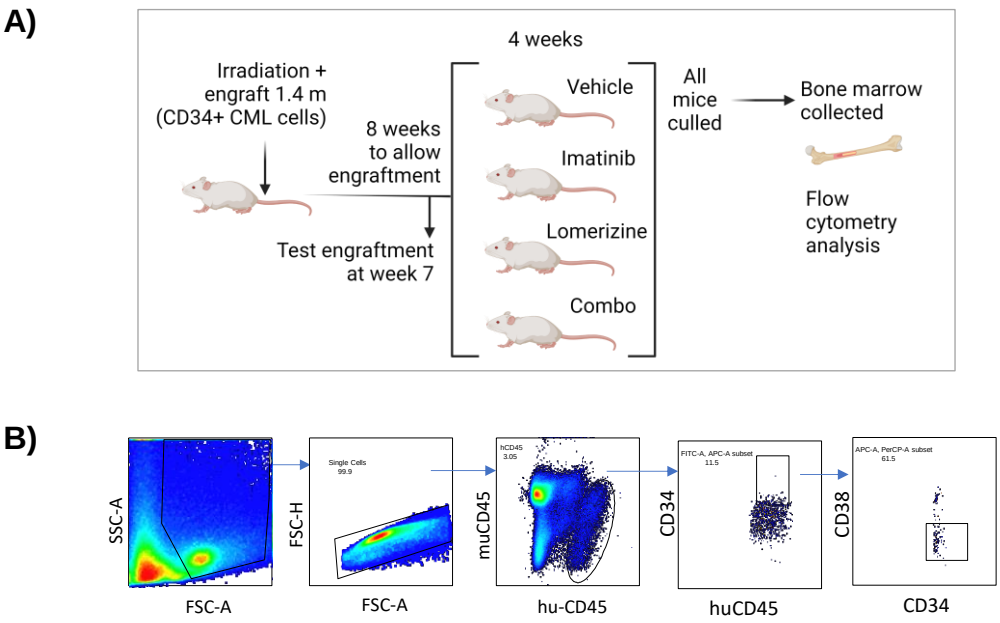

Fig. S9. PDX model approach.

(A) PDX experimental model. Engraftment of $1.3x10^6$ human cells was confirmed 7 weeks after transplantation in the BM. At week 8 post-transplant, mice were divided into four treatment arms (vehicle, lomerizine, imatinib, and a combination of lomerizine and imatinib) and treated for 4 weeks. Mice were sacrificed on the last day of treatment and dissected to collect bones (tibias, femurs, and hip bones), blood, and spleens. Those harvested tissues were then processed and analysed by flow cytometry to measure human $CD45^+$, human $CD34^+$, and human $CD34^+CD38^-$ expression of each mouse. **(B)** Gating strategy for PDX flow cytometry analysis.

fig. S10

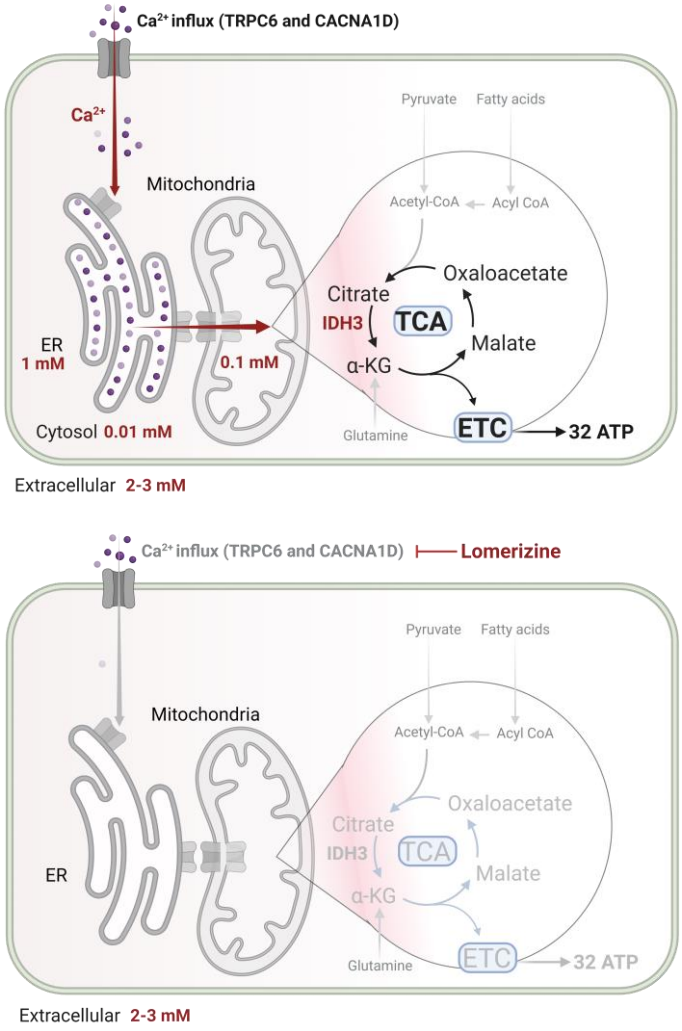

Fig. S10. Model of Ca^2 regulation in CML cells.

Graphical demonstration of Ca^2 regulation in CML cells and how CML LSCs can be targeted through inhibition of Ca^{2+} influx by lomerizine. Most of intracellular Ca^{2+} is stored inside ER sheets, and in turn mitochondria utilise ER Ca^{2+} ions to support metabolism. The extracellular Ca^{2+} influx via CACNA1D and supports mitochondrial dehydrogenase (such as IDH3) activity to drive the TCA cycle in CML cells. Lomerizine treatment inhibits CACNA1D or TRPC6 mediated Ca^{2+} influx, resulting in ER and mitochondrial Ca^{2+} depletion with subsequent mitochondrial metabolism inhibition.

Supplementary Tables

Bank ID	Study ID	Source
nonCML020	Norm#1	Mantle Cell Lymphoma
nonCML029	Norm#2	TCL
nonCML030	Norm#3	Hodgkin
nonCML038	Norm#4	Lymphoma
nonCML042	Norm#5	Lymphoma
nonCML043	Norm#6	Neuroblastoma
nonCML044	Norm#7	Lymphoma
BB190647	Norm#8	Hip BM
BB190773	Norm#9	Hip BM
BB190809	Norm#10	Hip BM
BB190833	Norm#11	Hip BM
BB190898	Norm#12	Hip BM
CML339	CML#1	CP-CML
CML399	CML#2	CP-CML
CML460	CML#3	CP-CML
CML441	CML#4	CP-CML
CML442	CML#5	CP-CML
CML444	CML#6	CP-CML
CML454	CML#7	CP-CML
CML459	CML#8	CP-CML
CML460	CML#9	CP-CML
CML470	CML#10	CP-CML
CML342	CML#11	CP-CML
CML347	CML#12	CP-CML
CML273	CML#13	CP-CML

Table S1: Primary human samples used in this study.

Primer	Type	Guide	Sequence	Melting	GC %
CACNA1D	F	1	GCTGAAGCGAGAATAAGG GC	56.1 ºC	55 %
	R	1	AGGACACTGAACCCGAAT CA	56 ºC	50 %
	F	2	TGGAGGGAAATGCTTATA TGT CT	53.6 ºC	39.1 %
	R	2	GCAGCATCACCAGCCTTAAA	55.9 ºC	50 %
TRPC6	F	1	TCATGAGGCCGTTCAATCCT	56.4 ºC	50 %
	R	1	TCGAGGACCAGCATACAT GT	55.8 ºC	50 %
	F	2	GACTCGGCACCAGATTGAAG	55.8 ºC	55 %
	R	2	AACGATCACTGGGGTCTGAG	56.5 ºC	55 %

Table S2: Primers used for verification of gene editing.

Cell Genotype	Guide DNA sequencing
CACNA1D in CTL	CATCAACGGCAGCAGCAAGCGGACCACGCGAACGGTG
CACNA1D in DKO	CATCAACGGCAGCAGCAAGCGTACGGAGCCGAACCCC
TRPC6 in CTL	TAGCTAGAAGCAAAGCATCCCCAACTCGAGAGAGGTT
TRPC6 in DKO	TAGCTAGAAGCAAAGCATCCCCAACTCGAATAGAAAA

Table S3: Guide sequencing to verify successful gene editing in CACNA1D and TRPC6 DKO K562 cells.